

Measurement of Floc Size and the Influence of Size Distribution on Geotechnical Properties of Oil Sands

Fluid Fine Tailings

By

Jordan A. Elias

A thesis submitted in partial fulfillment of the requirements for the degree of

Master of Science

In

Geoenvironmental Engineering

Department of Civil and Environmental Engineering

University of Alberta

© Jordan A. Elias, 2019

## **ABSTRACT**

Large volumes of fluid fine tailings (FFT) from oil sands mining operations pose difficult engineering challenges because they do not readily dewater and due to their fluid state, require containment. A common approach to reduce FFT volume by water removal is to treat the clay suspension with a coagulant and flocculant to form highly porous aggregates called flocs. This work investigated the effect of increased floc size on geotechnical properties of FFT. A method utilizing a flocculation system and images of flocs was developed to determine floc size distribution of a treated FFT sample. Floc size was measured with image analysis software using images obtained directly after flocculation. Treatment recipes, combining an optimal dose of coagulant and polymer, were designed to give clear release water and highly visible flocs suitable for measurement. Floc size distributions were then determined for each of the optimal treatments. Two of these treatments were further analyzed to assess compressibility, hydraulic conductivity, and vane shear strength. Both compressibility and vane shear strength showed to be sensitive to changes in floc size distribution while hydraulic conductivity did not appear to be largely impacted by floc size.

## **ACKNOWLEDGEMENTS**

I would like to acknowledge Natural Resources Canada Program for Energy Research and Development (PERD) for financial support and would like to thank Dr. Nicholas Beier, Dr. Ward Wilson, Dr. Louis Kabwe and Dr. Kim Kasperski for their support and guidance throughout this project.

## TABLE OF CONTENTS

<b>ABSTRACT</b> .....	<b>II</b>
<b>ACKNOWLEDGEMENTS</b> .....	<b>III</b>
<b>LIST OF TABLES</b> .....	<b>VI</b>
<b>PUBLICATIONS</b> .....	<b>IX</b>
<b>1 INTRODUCTION</b> .....	<b>1</b>
1.1 Objective and scope of thesis.....	2
1.2 Organization of thesis.....	2
<b>2 LITERATURE REVIEW</b> .....	<b>4</b>
2.1 Introduction.....	4
2.2 Geotechnical properties of oil sands fluid fine tailings .....	5
2.3 Floc characterization .....	11
2.4 Previous studies.....	16
2.4.1 Effect of Shear on the Yield Stress and Aggregate Structure of Flocculant-dosed, Concentrated Kaolinite Suspensions .....	17
2.4.2 Geotechnical Behaviour of In-Line Thickened Oil Sands Tailings .....	18
2.4.3 Influence of Dewatering and Desiccation on Microstructure and Vane Strength of Polymer Amended Oil Sand Mature Fine Tailings.....	22
2.4.4 Effect of Pipelining Shear on Consolidation Properties of Oil Sands Fine Tailings.....	24
2.4.5 Effects of Shearing and Shearing Time on Dewatering and Yield Characteristics of Oil Sands Flocculated Fine Tailings .....	25
<b>3 METHODS</b> .....	<b>27</b>
3.1 Material characterization .....	27
3.1.1 Dean Stark extraction .....	27
3.1.2 Particle size distribution .....	28
3.1.2.1 Sieve.....	28
3.1.2.2 SediGraph.....	28
3.1.3 Methylene blue .....	29
3.1.4 Water chemistry.....	29
3.1.5 Mineralogy.....	30
3.1.6 Coagulant properties.....	31
3.2 Tailings treatment .....	32
3.3 Floc measurement.....	37

3.4	Geotechnical properties .....	44
3.4.1	Atterberg limits.....	44
3.4.2	Large strain consolidation .....	45
3.4.3	Hydraulic conductivity .....	47
3.4.4	Vane shear strength .....	47
<b>4</b>	<b>RESULTS.....</b>	<b>48</b>
4.1	Material characterization .....	48
4.1.1	Dean Stark extraction .....	49
4.1.2	Particle size distribution .....	49
4.1.2.1	Sieve.....	49
4.1.2.2	SediGraph.....	49
4.1.3	Methylene blue .....	50
4.1.4	Water chemistry.....	51
4.1.5	Mineralogy.....	51
4.1.6	Coagulant properties.....	54
4.2	Tailings treatment .....	55
4.3	Floc measurement.....	62
4.4	Geotechnical properties .....	66
4.4.1	Atterberg limits.....	66
4.4.2	Large strain consolidation .....	69
4.4.3	Hydraulic conductivity .....	70
4.4.4	Vane shear strength .....	71
<b>5</b>	<b>DISCUSSION .....</b>	<b>74</b>
<b>6</b>	<b>CONCLUSIONS.....</b>	<b>79</b>
6.1	Recommendations for future work.....	80
<b>7</b>	<b>REFERENCES.....</b>	<b>81</b>
<b>8</b>	<b>APPENDIX .....</b>	<b>86</b>

## LIST OF TABLES

Table 2-1 – Common equivalent diameters used for characterizing flocs (taken from Jarvis, Jefferson, and Parsons, 2005).....	15
Table 2-2 – Floc size measurement techniques and measurement ranges.....	16
Table 2-3 – Index test results from measurements of polymer-treated oil sands mature fine tailings (Bajwa and Simms 2013).....	23
Table 3-1 – List of coagulation conditions tested in search of an optimum dosage .....	34
Table 3-2 – Parameter estimates for the fitted normal mixture in Figure 3-6 where $\mu$ and $\sigma$ are the respective mean and standard deviation for each bead size .....	40
Table 4-1 – Tailings characterization .....	48
Table 4-2 – Pore water chemistry for as-received FFT .....	51
Table 4-3 – Tailings mineral quantification using XRD methods .....	53
Table 4-4 – FFT clay content by different measurement methods .....	53
Table 4-5 – Water chemistry for coagulants dissolved in deionized water.....	54
Table 4-6 – Water chemistry for FFT coagulated with K-alum ( $\text{Al}^{3+}$ ) .....	59
Table 4-7 – Water chemistry for FFT coagulated with gypsum ( $\text{Ca}^{2+}$ ) .....	60
Table 4-8 – Water chemistry for FFT coagulated with magnesium chloride ( $\text{Mg}^{2+}$ ).....	61
Table 4-9 – Floc size distribution summary for FFT-1 treated with either K-alum (FFT-1/Al) or gypsum (FFT-1/Ca) and flocculated with A3338 at two different mixing speeds where $D_{xx}$ is the floc diameter for which xx percentage are smaller than .....	64
Table 4-10 – Large strain consolidation test on FFT-1 coagulated with K-Alum and flocculated at mixing speed 350 RPM (un-sheared) .....	72
Table 4-11 - Large strain consolidation test on FFT-1 coagulated with K-Alum and flocculated at mixing speed 900 RPM (sheared).....	72
Table 4-12 – Large strain consolidation test results from ILTT non-sheared from Jeeravipoolvarn (2010) .....	73
Table 4-13 – Large strain consolidation test results from ILTT sheared from Jeeravipoolvarn (2010) .....	73

List of figures	
Figure 2-1 – Hydraulic conductivity of Syncrude lime non-segregated tailings (Suthaker 1995) .....	7
Figure 2-2 – Hydraulic conductivity as a function of void ratio for various oil sands tailings materials (Jeeravipoolvarn 2005) .....	8
Figure 2-3 – Undrained shear strength ( $S_u$ ) of oil sands tailings as a function of solids content (Beier et al. 2013) .....	9
Figure 2-4 – Shear strength and solids content of oil sands fine tailings (laboratory and field shear strength measurements, mostly by vane) (McKenna et al. 2016).....	10
Figure 2-5 - Variation in mass median floc size for kaolin clay suspensions (3-wt% solids) during continuous addition of non-ionic polyacrylamide for 1 min. and continued agitation at 1000 rpm (Ray and Hogg 1987) .....	12
Figure 2-6 – Size frequency distributions showing the effect of shear energy input on aggregate size distribution for concentrated suspensions prepared with 100 g/tonne Magnafloc® LT27AG at pH 8.5 where ‘Kaolinite’ indicates the size distribution of an 8-wt% solids kaolinite suspension prior to flocculant addition (Neelakantan et al. 2018). CL = chord length. ....	17
Figure 2-7 – Effect of pH on floc size distribution at shear energy input of $E=300 \text{ kJ/m}^3$ (Neelakantan et al. 2018) .....	18
Figure 2-8 – Comparison of particle size distributions for sheared in-line thickened tailings (ILTT) (Jeeravipoolvarn 2010) .....	20
Figure 2-9 – Hydraulic conductivity comparison of laboratory non-sheared ILTT, sheared ILTT, and COF (Jeeravipoolvarn 2010) .....	21
Figure 2-10 – Compressibility comparison of laboratory non-sheared ILTT and sheared ILTT (Jeeravipoolvarn 2010) .....	21
Figure 2-11 – Undrained shear strength comparison of laboratory non-sheared ILTT, sheared ILTT and COF (Jeeravipoolvarn 2010).....	22
Figure 2-12 – Particle agglomerate size distribution for polymer amended FFT for different polymer concentrations (Bajwa and Simms 2013) .....	23
Figure 2-13 – Vane shear comparisons for ILTT (Jeeravipoolvarn et al. 2014).....	25
Figure 2-14 – Effect of shearing at 63 s-1 for a residence time corresponding to transport distance of 10 km on 7-day water release of MFT samples flocculated with a) polymer-A, b) polymer-B, and c) polymer-C (Derakhshandeh et al. 2016).....	26
Figure 3-1 – Example of diffraction pattern obtained from X-ray diffraction analysis.....	31
Figure 3-2 – Plot of capillary suction time (CST) of treated FFT as a function of coagulant dosage and lines showing how optimum dosage is graphically determined .....	33
Figure 3-3 – Capillary suction testing schematic (left) and apparatus (right).....	36
Figure 3-4 – Setup for testing bead measurement.....	39
Figure 3-5 – Picture of beads settling through water (left) and after image processing (right) (red=4.5 mm, yellow=3.0 mm) .....	39
Figure 3-6 – Histogram and continuous fit curve for data obtained from image analysis of nine photographs of two different testing bead diameters .....	40
Figure 3-7 – Picture of flocculation setup .....	42
Figure 3-8 – Process map of fluid fine tailings flocculation setup .....	43
Figure 3-9 – Large strain consolidation cell with tailings sample .....	46
Figure 4-1 – Particle size distribution of FFT Dean-Stark solids (<45- $\mu\text{m}$ ) by SediGraph .....	50

Figure 4-2 – Jade output XRD spectra for FFT-1 .....	52
Figure 4-3 - Jade output XRD spectra for FFT-2 .....	52
Figure 4-4 – Capillary suction time for different K-alum ( $Al^{3+}$ ) dosages for FFT-1 and FFT-2 where the error bars represent the standard deviation of multiple CST measurements .....	55
Figure 4-5 – Capillary suction time for different gypsum ( $Ca^{2+}$ ) dosages for FFT-1 and FFT-2 where the error bars represent the standard deviation of multiple CST measurements .....	56
Figure 4-6 – Capillary suction time for different magnesium chloride ( $Mg^{2+}$ ) dosages for FFT-1 and FFT-2 where the error bars represent the standard deviation of multiple CST measurements .....	57
Figure 4-7 – Photos of flocs throughout image analysis process (1) raw image, (2) image after brightness adjustment and floc identification, (3) image of flocs surrounded by black border identifying flocs to be counted and sized .....	63
Figure 4-8 – Floc size distribution for above image (Figure 4-7) .....	63
Figure 4-9 – Floc size distribution for FFT-1 treated with either K-alum (FFT-1/Al) or gypsum (FFT-1/Ca) and flocculated with A3338 at two different mixing speeds .....	64
Figure 4-10 - Floc size distribution for FFT-1 treated with K-alum and flocculated with A3338 at two different mixing speeds compared to ILTT non-sheared and sheared samples by Jeeravipoolvarn (2010) .....	65
Figure 4-11 – Undrained shear strength as a function of moisture content ( $M_{water}/M_{solids}$ ) with liquid limit measured using fall cone for FFT-1 untreated and treated samples .....	67
Figure 4-12 – Undrained shear strength as a function of solids content using fall cone for FFT-1 untreated and treated samples .....	67
Figure 4-13 – Shear strength and solids content of oil sands fine tailings from McKenna et al. 2016 with strength data overlay from this project .....	68
Figure 4-14 – Compressibility of FFT-1 coagulated with K-Alum and flocculated using two different mixing speeds compared to ILTT (Jeeravipoolvarn 2010) .....	69
Figure 4-15 – Hydraulic conductivity of FFT-1 coagulated with K-Alum and flocculated using two different mixing speeds compared to ILTT (Jeeravipoolvarn 2010) .....	70
Figure 4-16 – Vane shear strength versus effective stress for FFT-1 coagulated with K-Alum and flocculated using two different mixing speeds compared to ILTT (Jeeravipoolvarn 2010) .....	71
Figure 8-1 – Activity diagram showing aluminum species in aqueous and solid phases as a function of pH at 25°C .....	86
Figure 8-2 - Activity diagram showing aluminum species in aqueous and solid phases as a function of pH at 50°C .....	87

## **PUBLICATIONS**

Elias, J. and Beier, N.A. 2017. Effect of floc size on geotechnical properties of oil sands fluid fine tailings: Experimental study. Proceedings of the 2017 Tailings & Mine Waste Conference, Banff, AB: November 5-8, 2017.

## 1 INTRODUCTION

Oil sands fluid fine tailings (FFT) are an aqueous suspension consisting primarily of dispersed fine mineral particles along with residual bitumen and soluble inorganic salts and organics (Kasperski 1992). The solids content of this liquid suspension ranges from 2-wt% solids up to the liquid limit (OSTC 2012). Extraction of bitumen from oil sands leaves water, bitumen, and coarse and fine particles as the main by-products that report to tailings streams. Although, both coarse and fine particles report to tailings streams, the fine particles remain suspended in water in tailings ponds. Due to the clay and water chemistry of the fine tailings fraction, the particles remain suspended for many years. Large volumes of FFT pose difficult engineering challenges because they do not readily dewater and due to their fluid state, require containment. One closure goal for FFT is to convert the fluid tailings into a soil-like material having a low water content and adequate geotechnical strength to sustain dry landscape reclamation efforts. By chemically amending fine tailings, large amounts of water can be removed which allows the tailings to transform into a suitable material for reclamation.

Dewatering of FFT can be done by a variety of methods and have been thoroughly discussed previously (BGC Engineering Inc. 2010). Available technologies for dewatering include physical/mechanical processes, natural processes, chemical/biological amendment, mixtures/co-disposal, and permanent storage in water capped deposits (BGC Engineering Inc. 2010). Treatment for dewatering is not limited to one technology area and in many cases chemical amendment is necessary to have sufficient dewatering in a timely manner. Chemical amendment includes the addition of coagulants and/or flocculants and both aid in increasing hydraulic conductivity to aid in faster dewatering (BGC Engineering Inc. 2010). A porous aggregate known as a floc is formed from smaller particles (Jarvis et al. 2005b) whether it is formed by coagulation, flocculant addition, or by natural processes. Flocculation effectiveness is strongly dependent on floc characteristics such as strength, size, shape, and structure (Liang et al. 2015). Neelakantan et al. (2018) studied the effect of different polymers and pH values on yield stress and floc size of kaolinite. Work regarding the effect of floc size on oil sands tailings properties was carried out by Jeeravipoolvarn (2010) where it was found that shearing to reduce floc size had little to no effect on compressibility. Bajwa and Simms (2013) found that increases in polymer dosages led to increased average floc size and liquidity index but did not provide benefits to dewatering through desiccation. Jeeravipoolvarn et al. (2014) found that with in-line thickened tailings, shear causing floc breakage reduced both permeability and vane shear

strength. Derakhshandeh et al. (2016) investigated the effect of pipeline shear on flocculated FFT with particular interest in yield stress and tailings dewatering.

## 1.1 Objective and scope of thesis

The goal of this research is to determine if increasing the average floc size of chemically amended FFT will positively affect the geotechnical properties of the resulting soil-like material. Geotechnical properties of interest in this research are compressibility, hydraulic conductivity, and vane shear strength. By understanding differences in geotechnical properties as a function of floc size, it will be known if controlling floc size in tailings treatment is important for tailings reclamation work. This newfound knowledge may present treatment techniques that can deliver a tailings material suitable for reclamation in a reduced timeframe.

A research program was developed to first create a floc-size measurement system for determining floc size of treated FFT. Treatment conditions with different mixing speeds and coagulants were then investigated to determine recipes for creating flocculated tailings suitable for floc size measurement. Finally, floc size measurements were completed on samples with optimal treatment recipes and then subjected to geotechnical testing.

The specific research objectives were:

1. Develop method to characterize floc size distribution;
2. Develop treatment process to create flocculated tailings suitable for floc measurement;
3. Evaluate impact of treatment process on floc size;
4. Evaluate floc size impact on geotechnical behavior including compressibility, hydraulic conductivity, and vane shear strength.

## 1.2 Organization of thesis

This thesis is organized into seven chapters. Chapter 1 introduces the research topic and describes the scope of this thesis including specific research objectives. Chapter 2 is a review from literature of oil sands tailings geotechnical properties, floc characterization, and related previous studies. Chapter 3 describes the methods used in the body of work including standard methods and those developed specifically for this project. Presented in Chapter 4 are the results of material characterization, floc measurement,

tailings recipe development, and geotechnical properties. Chapter 5 provides a discussion of results and findings. Chapter 6 provides a brief conclusion of this body of research, implications of these findings on the current state of tailings treatment and suggestions for future work.

## 2 LITERATURE REVIEW

### 2.1 Introduction

A large amount of work has been undertaken to characterize oil sands tailings and develop efficient techniques for tailings dewatering. One of the main goals is the removal of water to create a soil-like material having sufficient strength to support dry landscape reclamation.

Many technologies exist for dewatering tailings and a comprehensive list with descriptions of these technologies was summarized by BGC in 2010 for the Oil Sands Research and Information Network (OSRIN) in *Oil Sands Tailings Technology Review* (BGC Engineering Inc. 2010). BGC reviewed 34 oil sands tailings treatment technologies that were divided into five groups: (1) physical/mechanical processes, (2) natural processes, (3) chemical/biological amendments, (4) mixtures/co-disposal, and (5) permanent storage. Each of the dewatering technologies were described in detail in the report including viability, knowledge gaps, and relevant references.

In 2012, the Consortium of Tailings Management Consultants (CTMC) prepared the Oil Sands Tailings Technology Development Roadmap (Tailings Roadmap) for Alberta Innovates Energy and Environment Solutions (AI-EES) and the Oil Sands Tailings Consortium (OSTC) (Sobkowicz 2012). The Tailings Roadmap was intended to recognise potential technologies for oil sands tailings treatment and to provide direction to government and industry on the commercialization of pertinent technologies (Sobkowicz 2012). Through the Tailings Roadmap development, 549 technologies were identified then screened down to 101 unique technologies (Sobkowicz 2010). The 101 unique technologies are discussed in detail in the Tailings Roadmap and are categorized into the following groups: (1) mining, (2) extraction, (3) tailings processing, (4) deposition & capping, (5) water treatment, and (6) reclamation. The Tailings Roadmap is comprised of five volumes, the first of which provides a summary of all project work (Consortium of Tailings Management Consultants, (CTMC) 2012). The various components of the Tailings Roadmap were presented at the International Oil Sands Tailings Conference in 2012.

Of the available oil sands tailings treatment technologies, many require or benefit from the addition of flocculants and coagulants. One of the important knowledge gaps noted includes a better understanding of the role of chemical additives in modifying tailings properties (BGC Engineering Inc. 2010). Beier et al. (2013) discuss the impact of flocculants on the shear strength of oil sands fine tailings. With flocculant addition, shear strength increases can be expected but flocculated tailings may exhibit sensitive behaviour

that may require subsequent remediation (Beier et al. 2013). Requirements have been set by the Alberta Energy Regulator (AER) for managing fluid tailings volumes in Directive 085. In conjunction with Directive 085, the Tailings Management Framework (TMF) stipulates that fluid tailings need to be ready to reclaim ten years after the end of mine life of each project. With these regulations and pressure to reduce the environmental impact of oil sands mining operations, there is a need for continual improvement of tailings treatment techniques to produce ready to reclaim material. To assess treatment techniques in anticipation of reclamation, geotechnical characterization is needed. Following is a review of geotechnical properties of oil sands tailings, floc characterization, and a review of previous studies pertinent to this body of work.

## 2.2 Geotechnical properties of oil sands fluid fine tailings

A review of geotechnical properties of oil sands tailings was written for the Energy Innovation Program in 2017 as part of the report titled *Improving Tailings and Reclamation Technologies to Create Stable and Sustainable Forest Landscapes in the Mineable Oil Sands Region: Towards the Development of Self-Healing Landscapes*. A version of that review is included as part of this section of the literature review.

Fluid fine tailings (FFT) are a liquid suspension of oil sands fines ranging in solids content from 2-wt% solids content and up to the liquid limit (OSTC 2012). Mature fine tailings (MFT) are FFT with low sand content and greater than 30-wt% solids (Fine Tailings Fundamentals Consortium, (FTFC) 1995, OSTC 2012).

MFT properties vary markedly and can change after being subjected to dewatering treatments. MFT solids content ranges from 30-wt% to 60-wt% (Fine Tailings Fundamentals Consortium, (FTFC) 1995) while other properties include (BGC Engineering Inc. 2010):

- Liquid limit (LL) ranging from 40% to 75% water content (ratio of the weight of water to the weight of solids);
- Plastic limit (PL) ranging from 10% to 20% water content;
- Hydraulic conductivity (k) ranging from  $1 \times 10^{-6}$  m/s to  $1 \times 10^{-9}$  m/s;
- Undrained shear strength ( $S_u$ ) below 1-kPa (fluid).

As stated above, the Atterberg limits for fine tailings vary depending on tailings properties. The addition of flocculants can change the Atterberg limits and push the liquid limit up to 100% and the plasticity index (PI) to 73% (Beier et al. 2013). The PI represents the range of water content where the soil behaves

plastically and is simply defined as the difference between liquid and plastic limits (ASTM International 2017a).

$$PI = LL - PL$$

Hydraulic conductivity is controlled by the fines/water ratio (Jeeravipoolvarn 2005). Treatments, which can include addition of coagulant, flocculant, or even sand or overburden, affect the geotechnical properties of the resulting material. For example, the addition of lime may decrease hydraulic conductivity as shown in Figure 2-1 (Suthaker 1995). The hydraulic conductivity of lime-treated non-segregating tailings (NST) is about half to a full order of magnitude lower than untreated fine tailings. A more comprehensive summary of hydraulic conductivity in Figure 2-2 shows the relationship between hydraulic conductivity and void ratio for a variety of oil sands tailings having undergone different treatments. It is evident from these, and other results, that the hydraulic conductivity of a deposit is influenced by numerous variables including clay content, mineralogy, and water chemistry (Jeeravipoolvarn 2005, Beier et al. 2013).

Undrained shear strength of fluid fine tailings is low due to the high water content but is increased by water removal and chemical amendments. Beier et al. (2013) provides a summary of the effects of flocculant addition on shear strength. In particular, how increases in solids content affects the undrained shear strength for different tailings and treatments (Figure 2-3). More recently, McKenna et al. (2016) compiled shear strength measurements for oil sands fine tailings from a number of sources, and treated in a number of ways, which are presented in Figure 2-4. The data in Figure 2-4 show a relationship between peak undrained shear strength and density albeit with a range of one to two orders of magnitude (McKenna et al. 2016). Tailings with low density that are treated with coagulants, flocculants, or cements will have higher shear strength than untreated tailings (McKenna et al. 2016).

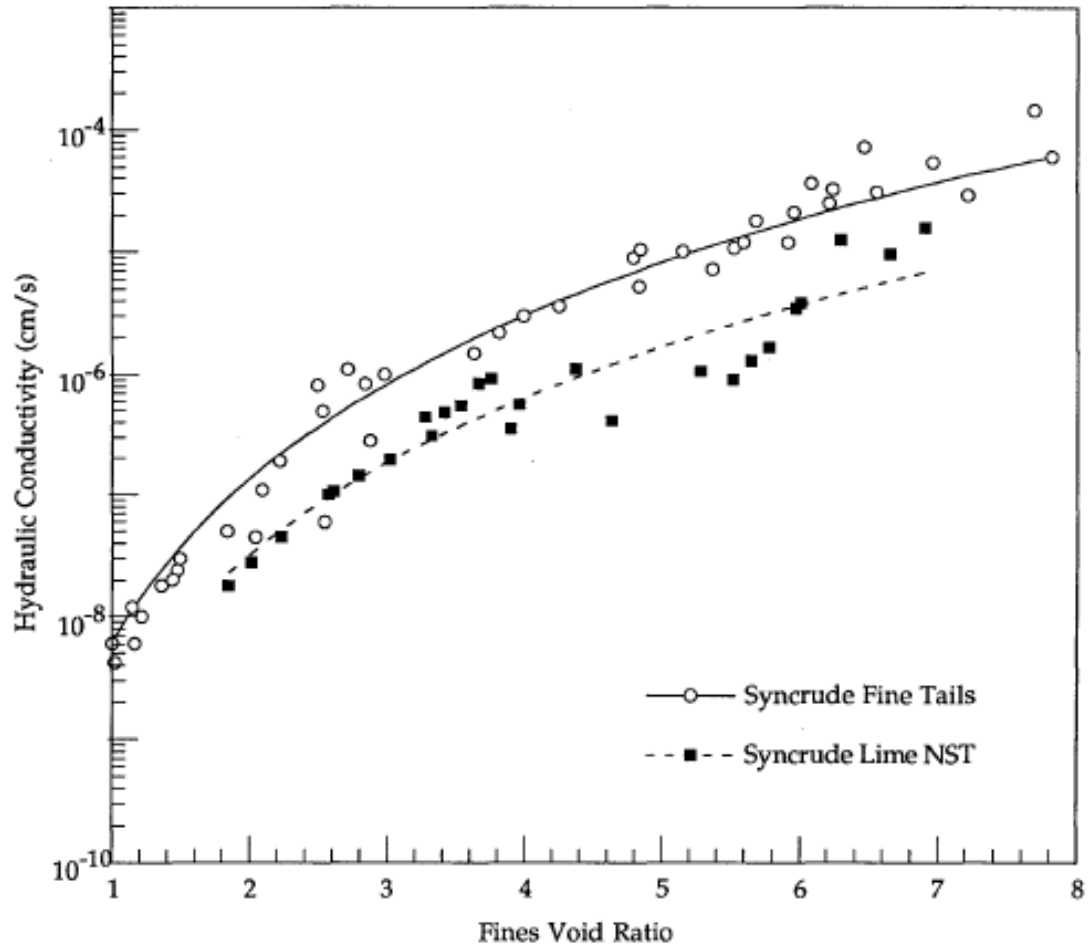


Figure 2-1 – Hydraulic conductivity of Syncrude lime non-segregated tailings (Suthaker 1995)

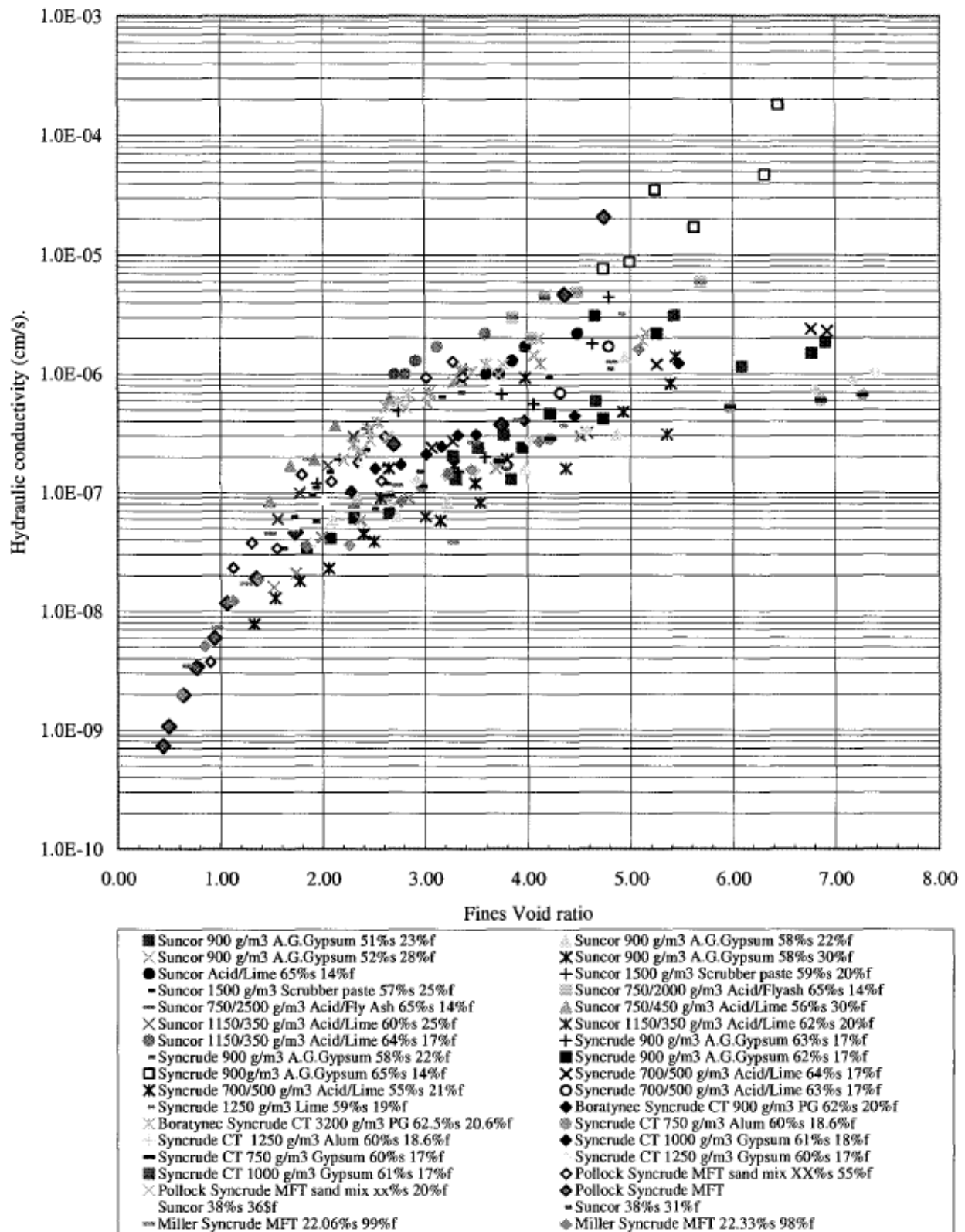


Figure 2-2 – Hydraulic conductivity as a function of void ratio for various oil sands tailings materials (Jeeravipoolvarn 2005)

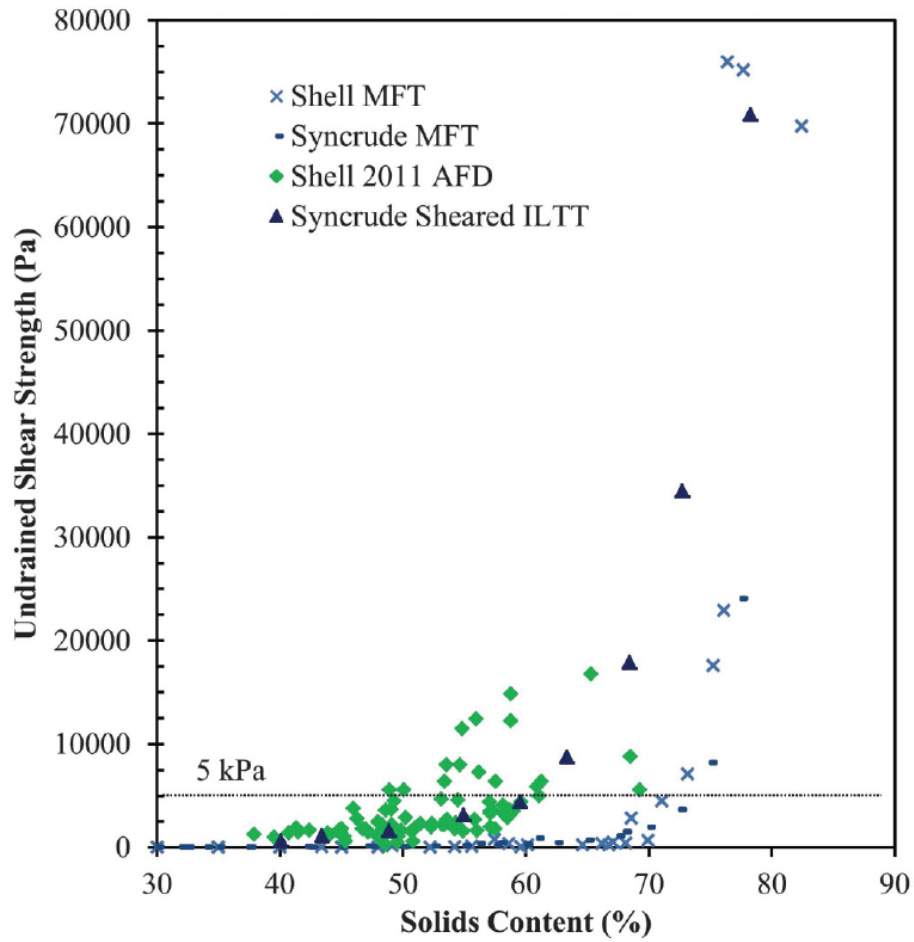


Figure 2-3 – Undrained shear strength ( $S_u$ ) of oil sands tailings as a function of solids content (Beier et al. 2013)

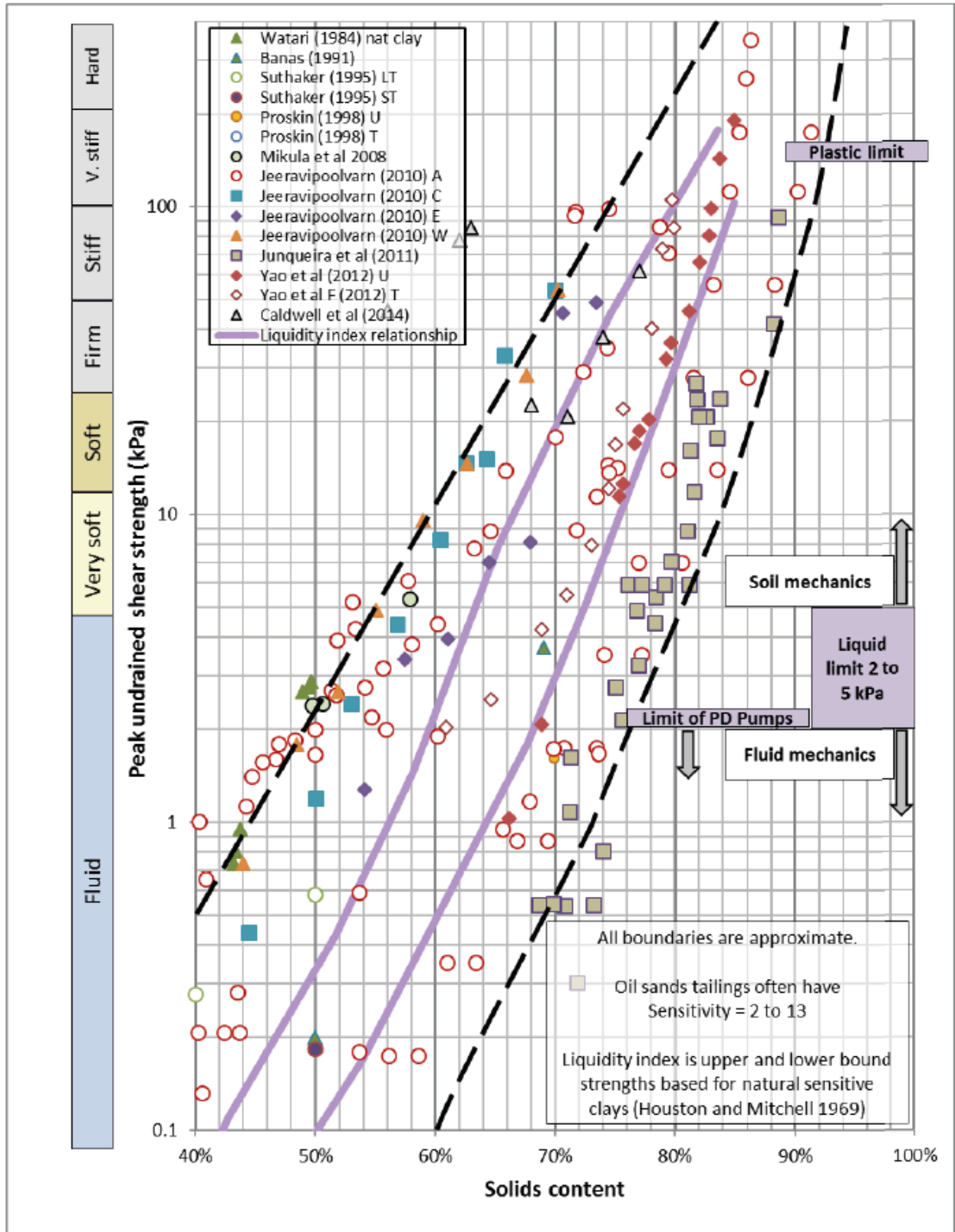


Figure 2-4 – Shear strength and solids content of oil sands fine tailings (laboratory and field shear strength measurements, mostly by vane) (McKenna et al. 2016)

### 2.3 Floc characterization

To describe floc characterization, it is important to define coagulation and flocculation, especially since the term coagulation is sometimes used interchangeably with flocculation.

Coagulation is the formation of aggregated particles driven by changes in colloid chemistry (Jarvis et al. 2005b). Coagulation is achieved by reducing the double layer thickness on the surface of the suspended particles, which allows the particles to come into close contact with each other to form bigger particles (Jarvis et al. 2005a). This reduction / neutralization of the particle's surface charge allows particles to agglomerate due to attractive Van der Waals' forces (Leung 2016). Thus, coagulants can be added to neutralize charges on particles that are kept in suspension by electrical repulsion (Leung 2016). Coagulation in this body of work refers to the initial step in a flocculation process where dispersed particles are destabilized allowing them to form aggregates.

Flocculation is the aggregation of fine suspended particles typically done to aid in solid-liquid separation processes (Hogg 2005). It has also been described as "the process of transferring coagulated colloids into contact with each other to form larger aggregates" (Jarvis et al. 2005a). The three usual steps in coagulation and flocculation are (1) destabilization of suspended particles, (2) floc formation and growth, and (3) floc degradation due to shear (Jeeravipoolvarn 2010). Note that aggregates formed by either coagulation with metal salts or flocculation with polymer flocculant are both referred to as flocs.

Particles can be flocculated in the suspension by use of polymers whose molecular chains attract and wrap up fine particles to form larger agglomerates known as flocs (Leung 2016). Floc size, density, and structure strongly depend on the strength of particle-particle interactions, particle concentration, and mixing conditions (Addai-Mensah and Prestidge 2005). Figure 2-5 shows that flocculation of kaolin clay suspension leads to increases in median floc size with mixing during polymer addition but decreases in floc size with continued mixing after polymer addition. The zone of constant floc size in Figure 2-5 is presumed to be a balance between floc breakage and re-agglomeration (Ray and Hogg 1987).

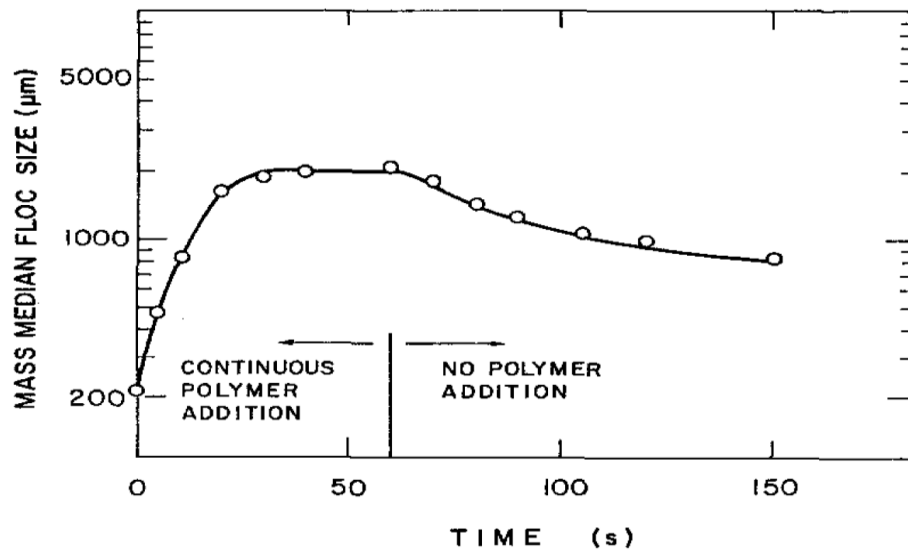


Figure 2-5 - Variation in mass median floc size for kaolin clay suspensions (3-wt% solids) during continuous addition of non-ionic polyacrylamide for 1 min. and continued agitation at 1000 rpm (Ray and Hogg 1987)

In general, a floc is a porous aggregate formed from smaller particles (Jarvis et al. 2005b) whether it is formed by natural processes, coagulation, or polymer flocculant addition. Flocculation is utilized in industrial solid-liquid separation processes such as water treatment and chemical and mineral processing (Jarvis et al. 2005b). Flocculation is used to speed up particle settling and dewatering or even to increase mineral concentrate recovery in mining processes (Liang et al. 2015). Flocculation effectiveness is strongly dependent on floc characteristics such as floc strength, size, shape, and structure (Liang et al. 2015). Similar characterization techniques can be applied whether they were formed by coagulation alone or in conjunction with polymer flocculation.

A recent study on floc breakage and reformation in treated oil sands FFT found that flocs formed by coagulant addition alone were quite insensitive to shear but flocs generated with polymer flocculant tended to show floc size degradation (Watson et al. 2011).

Several thorough reviews of floc characterization have been done in recent years (Jarvis et al. 2005a, Jarvis et al. 2005b, Liang et al. 2015). This includes a review of floc strength and breakage by Jarvis et al. (2005) and a separate review on floc structure measurements by Jarvis et al. (2005). More recently, Liang et al. (2015) reviewed modern characterization techniques for flocs in mineral processing. These reviews along with supplementary references are used to describe the current state of floc size measurement and characterization.

Floc strength is important in solid-liquid separation since smaller flocs tend to settle more slowly compared to larger flocs of similar density (Jarvis et al. 2005a). Larger flocs broken into smaller flocs results in flocs with increased resistance to breakage (Liang et al. 2015) and these smaller flocs generally tend to be stronger than larger flocs (Jarvis et al. 2005a). For alum-kaolin flocs, smaller flocs generally have lower removal efficiencies (Wang et al. 2011) meaning smaller flocs are more likely to remain in suspension. Floc strength is essentially the energy required to break flocs but there is difficulty in quantifying this energy (Jarvis et al. 2005a). Floc strength can be described by shear resistance capacity or by direct measurement of interaction forces (Liang et al. 2015). Steady-state floc size at a given shear rate can give an indication of floc strength (Jarvis et al. 2005a). A common approach to measuring floc strength is to measure observed changes in floc size at different applied hydrodynamic shear rates; typically, using impeller-based systems (Jarvis et al. 2005a). Shear is usually described in terms of the average velocity gradient and includes an energy dissipation term and kinematic viscosity (Camp and Stein 1943). Although floc strength is most commonly determined using applied shear, other more advanced techniques are available and are described in Jarvis et al. (2005).

Floc strength comes from the relationship between average floc size and average velocity gradient assessed over a range of velocity gradients (Jarvis et al. 2005a). In general, flocs generated by polymer addition show increases in floc strength with increased polymer dosage with the exception of biological flocs which show the opposite trend (Jarvis et al. 2005a). Some empirical conclusions have been drawn saying that large flocs tend to have more branches and so are weaker while spherical shaped flocs have greater resistance to breakage (Liang et al. 2015). Francois (1987) found that increasing aluminum coagulant dosage also increased floc strength (Francois 1987). In fact, it may be possible to optimize coagulant dosage based on floc strength (Jarvis et al. 2005a). The coagulated floc structure is influenced by pH, shear conditions, types of coagulants, and colloid particles (Wang et al. 2011).

The irregular shapes and sizes of flocs make them difficult to measure and because of this, there is a multitude of techniques employed to characterize floc size and shape. The delicate nature of flocs adds to the complexity of measurement protocols (Jarvis et al. 2005b). A variety of in situ and ex situ methods exist for measuring floc size and include:

- Light scattering, ex situ
- Light transmission, ex situ
- Microscopy, ex situ
- Dynamic image analysis (DIA), ex situ

- Photography and video using image analysis software, in situ
- Focused beam reflectance measurement (FBRM), in situ
- Particle vision measurement (PVM), in situ

Since floc shape is irregular, the size is typically represented by an equivalent diameter (Jarvis et al. 2005b). There are many equivalent diameters (perimeter diameter, projected area diameter, Stoke's diameter, Feret's diameter, etc.), summarized in Table 2-1, so it is important to be consistent when comparing different floc measurements (Jarvis et al. 2005b). Measurement results depend greatly on orientation of the floc, so it is critical to average a number of measurements (Jarvis et al. 2005b). It is important to ensure that the number of flocs measured is high enough to have a statistically reliable distribution; for example, the (now obsolete) British Standard for microscope counting recommended that a minimum of 625 particles need to be analyzed to have a statistically reliable size distribution (BS3406, 1963) (Jarvis et al. 2005b).

Transfer of flocs to a measurement system from a mixing vessel is problematic since the volume is being continually reduced and so the velocity gradients will change as a function of time, which is why continuous loop testing is favoured (Jarvis et al. 2005a). However, inclusion of the measurement system in the mixing vessel will change the shear profile of the system, which will affect the equilibrium floc size (Jarvis et al. 2005a). A limitation of a recirculation experiment to monitor floc growth and breakage was that the effect of pumping on floc size could not be quantified but this can be overcome by using a continuous process (Biggs and Lant 2000). A recirculation system continually pumps flocs from a vessel through a measurement system then deposits the flocs back to the original vessel. A continuous process does employ recirculation and only uses newly generated flocs. Photographic methods are beneficial in that the measurement technique does not influence floc size, however extra care is needed to get photographs suitable for image processing (Jarvis et al. 2005a). Image analysis is considered to give results closest to actual sizes (Liang et al. 2015). Dynamic image analysis (DIA) is an automated image capture and analysis system, which is beneficial because of the large number of particles that can be more easily assessed (Liang et al. 2015).

Table 2-1 – Common equivalent diameters used for characterizing flocs (taken from Jarvis, Jefferson, and Parsons, 2005)

Floc Diameter	Description	Diagram	Equation for Calculation
<i>Perimeter diameter, <math>d_c</math></i>	The diameter of a circle with the same perimeter ( $P$ ) as the measured particle.		$d_c = \frac{P}{\pi}$
<i>Projected area diameter1, <math>d_a</math></i>	The diameter of a circle with the same projected cross-section area ( $A$ ) as the floc measured in a stable orientation.		$d = 2 \sqrt{\frac{A}{\pi}}$
<i>Projected area diameter2, <math>d_p</math></i>	The diameter of a circle with the same projected area as the floc measured in a random orientation.		
<i>Surface diameter, <math>d_s</math></i>	The diameter of a sphere having the same surface area ( $S$ ) as the floc.		$d_s = \sqrt{\frac{S}{\pi}}$
<i>Volumetric diameter, <math>d_v</math></i>	The diameter of a circle with the same volume ( $V$ ) as the floc measured.		$d_v = \sqrt[3]{\frac{6V}{\pi}}$
<i>(OR equivalent spherical diameter)</i>			
<i>Surface-volume diameter, <math>d_{sv}</math></i>	The diameter of a sphere with the same surface area to volume ratio as the floc.		$d_{sv} = \frac{d_v^3}{d_s^2}$
<i>Free-falling diameter, <math>d_f</math></i>	The diameter of a sphere having the same density and free-falling speed as the floc in the same fluid at the same density and viscosity.		
<i>Stoke's diameter, <math>d_{st}</math></i>	The diameter of a free falling particle in the laminar flow range (where $Re < 0.2$ ).		$d_{st} = \frac{18\mu v}{\rho_f - \rho}$
<i>Feret's diameter, <math>d_f</math></i>	The (mean) value between pairs of parallel tangents to the projected outline of the particle.		-
<i>Martin's diameter, <math>d_M</math></i>	The length of the chord parallel to a fixed direction which splits the floc projected area into two equal parts.		-
<i>Circumscribing diameter, <math>d_{sc}</math></i>	The diameter of the smallest circle that circumscribes the outline of the projected floc.		-
<i>Inscribing diameter, <math>d_i</math></i>	The diameter of the biggest circle that fits inside the outline of the projected floc.		-

The different floc size measurement techniques and applicable measurement ranges are summarized in Table 2-2.

Table 2-2 – Floc size measurement techniques and measurement ranges

Technique	Measurement size range (µm)
Light scattering	0.1-2000 (Liang et al. 2015)
Light transmission	20-2000 (Jarvis et al. 2005a)
Microscope	0.01-10,000 (Liang et al. 2015)
DIA (Dynamic image analysis)	1-2000 (Liang et al. 2015)
Photography	>30 (Jarvis et al. 2005a)
FBRM (Focused beam reflectance measurement)	1-2000 (Liang et al. 2015)
PVM (Particle vision measurement)	0.5-2000 (Liang et al. 2015)

Floc shapes are quite irregular but can be described by convexity, circularity, roundness, aspect ratio, area fractal dimension, and mass fractal dimension (Liang et al. 2015). Fractal dimension is a way of describing the complex geometry of particle aggregates (Jarvis et al. 2005b). Fractal objects exhibit: “(1) self-similarity and (2) power-law relationship between two variables characterized by a non-integer fractal dimension,  $D_f$ ” (Jarvis et al. 2005b). Examples of fractal dimensions are shown in Equation 2-1 and Equation 2-2 where  $D_f$  is the fractal dimension and  $L$  is the floc equivalent diameter. Fractal dimensions can be found by light scattering, settlement, or image analysis (Jarvis et al. 2005b).

Equation 2-1 – Area fractal dimension

$$A \propto L^{D_f}$$

Equation 2-2 – Mass fractal dimension

$$M \propto L^{D_f}$$

## 2.4 Previous studies

The following studies either involve floc size measurement directly or indirectly by assessing the effect of shear on flocculated tailings. All studies summarized below looked at the effect of floc size reduction or shear on tailings properties. For sheared flocculated tailings samples it is generally understood that floc size is reduced by shearing.

#### 2.4.1 Effect of Shear on the Yield Stress and Aggregate Structure of Flocculant-dosed, Concentrated Kaolinite Suspensions

This study, carried out by Neelakantan, R., et al. (2018), aimed to evaluate the effect of polymer and water chemistry on vane yield stress and floc (aggregate) size. Concentrated kaolinite suspensions were flocculated with two different anionic polymers at two different pH values. Each of the flocculated suspensions were sheared at a number of different shear energies. The resulting particle (floc) size distribution and vane yield stress were determined for each condition. Kaolinite was used in this study as it is one of the most prevalent clay types in mineral tailings and so is commonly used in model studies. Flocculated kaolinite samples were sheared using a concentric cylinder shearing apparatus. Floc sizes were measured using FBRM with addition of a dilution step to battle against instrument fouling issues. As an example of the floc/particle measurements, Figure 2-6 shows the progression of floc/particle size distribution for kaolinite treated with polymer with increases in shear energy. Figure 2-7 shows the effect of pH on floc size distribution, measured as chord length.

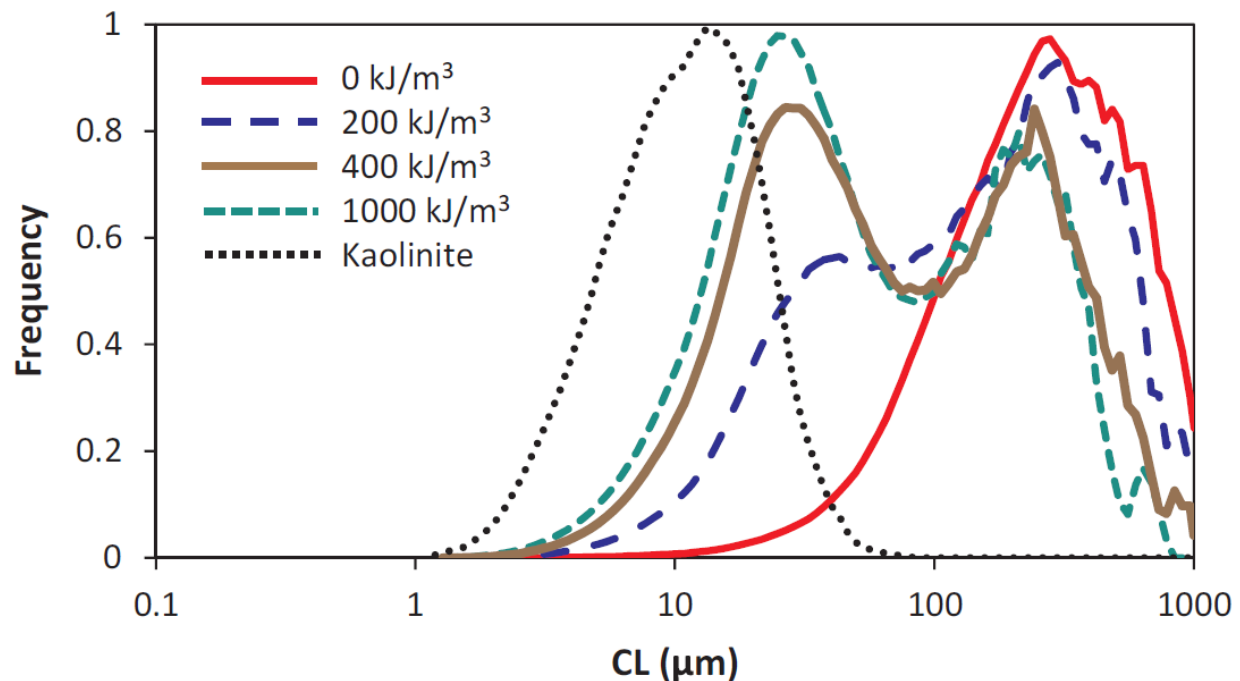


Figure 2-6 – Size frequency distributions showing the effect of shear energy input on aggregate size distribution for concentrated suspensions prepared with 100 g/tonne Magnafloc® LT27AG at pH 8.5 where ‘Kaolinite’ indicates the size distribution of an 8-wt% solids kaolinite suspension prior to flocculant addition (Neelakantan et al. 2018). CL = chord length.

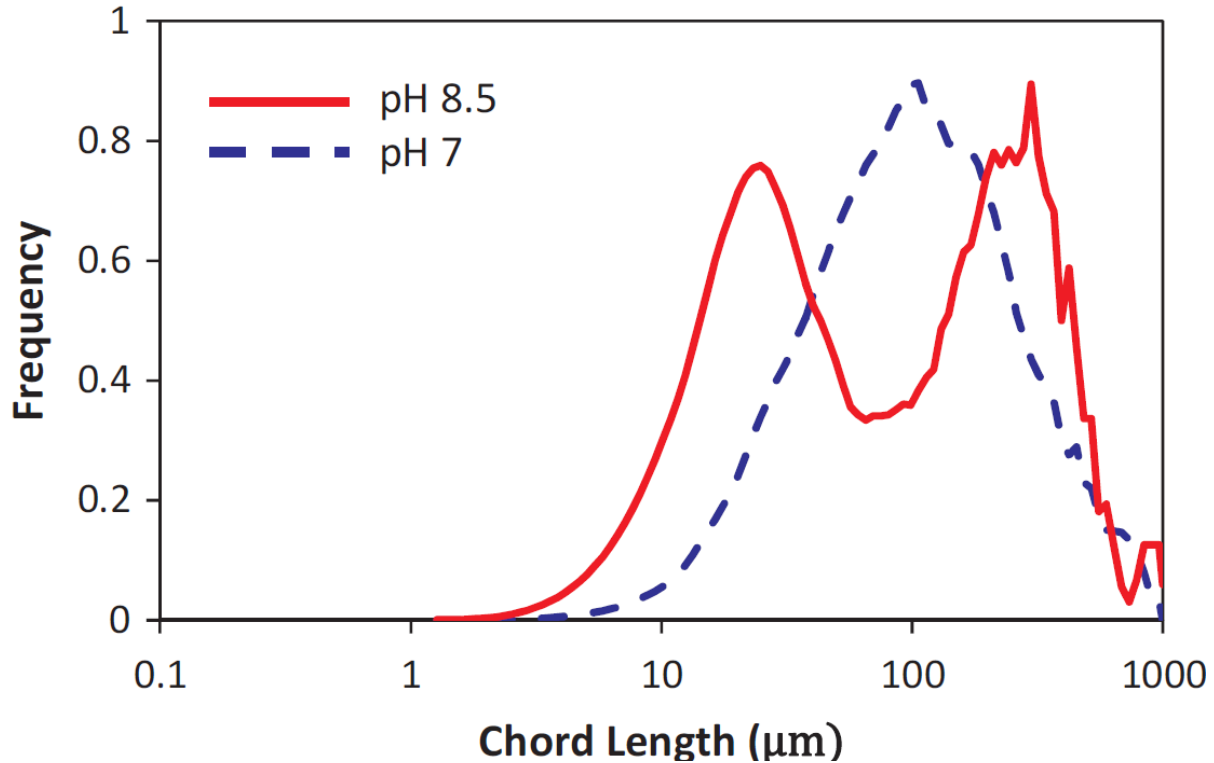


Figure 2-7 – Effect of pH on floc size distribution at shear energy input of  $E=300 \text{ kJ/m}^3$  (Neelakantan et al. 2018)

From this body of work it was found that decreases in yield stress were related to changes in the apparent solids volume fraction resulting from floc breakage and compaction due to shear. Most of the fragmented flocs ranged from 1-100  $\mu\text{m}$  which dominated the rheological behaviour of the suspension. It was also found that pH influences the fragmented floc structure leading to changes in equilibrium yield stress.

#### 2.4.2 Geotechnical Behaviour of In-Line Thickened Oil Sands Tailings

This study was carried out by Jeeravipoolvarn, S. (2010) and involves the geotechnical behaviour of in-line thickened oil sands tailings. In-line thickening is a tailings treatment process where flocculants and coagulants are added in the pipe to aid in dewatering. These additives serve to increase hydraulic conductivity, shear strength, and floc size of thin fine tailings. Thin fine tailings in this study refers to cyclone overflow with a solids content of approximately 8-wt%. The process is designed to improve settling and strength behaviour of thin fine tailings. Early work on the in-line thickening process was done by Syncrude Canada Ltd. to achieve rapid sedimentation and high solids content deposit with high solids capture. The process was not optimized to achieve specific desirable engineering properties such as

hydraulic conductivity, compressibility, and shear strength. Jeeravipoolvarn (2010) compared these engineering properties of in-line thickened tailings (ILTT) where cyclone overflow tailings were treated with anionic and cationic polymer flocculants. The flocculant used was CIBA Magnafloc 6260 at 0.5 g/L and the coagulant was cationic polymer CIBA Magnafloc 368 prepared to 1.0 g/L. Sheared ILTT samples were prepared to represent shear conditions expected from pipelining tailings and then the resulting products characterized. ILTT and sheared ILTT samples were prepared under controlled mixing conditions. To get a full range of sedimentation and consolidation properties three different test results were combined: a hindered sedimentation test, a compressibility standpipe test, and a large strain consolidation test. By combining these results, hydraulic conductivity and compressibility characteristics could be measured over a wide range of void ratios (less than 80 for hydraulic conductivity and 16 and lower for compressibility). Flocs were measured by non-dispersed hydrometer tests and wet sieve tests. Shearing ILTT substantially reduced the floc size, shifting the fines fraction ( $-45 \mu\text{m}$ ) from 5% up to 77%. Floc sizes for non-sheared ILTT were all less than 0.9 mm while sheared ILTT flocs were less than 0.3 mm. For comparison, the particle size and floc size distributions for cyclone overflow and ILTT are shown in Figure 2-8. From this figure, it is clear that flocculation is effective at increasing the apparent particle size (floc size) and that by shearing the ILTT the floc size is reduced. Hydraulic conductivity for cyclone overflow and ILTT is shown in Figure 2-9 over a wide range of void ratios. Hydraulic conductivity for each of the three samples is quite different at high void ratios but are very similar at low void ratios. Shearing ILTT reduced the hydraulic conductivity by several orders of magnitude at high void ratios. However, shearing ILTT had little to no effect on compressibility at void ratio less than 5, but had marginal effects at void ratio greater than 7.5 (Figure 2-10). In-line thickening increased the undrained shear strength of cyclone overflow and shearing the ILTT reduced its undrained shear strength, as shown in Figure 2-11. It was found that shearing damaged floc structures, but not so much as to return the treated tailings back to its original state. The effects of shearing predominate at higher void ratios while at lower void ratios the only notable change is the small reduction in undrained shear strength.

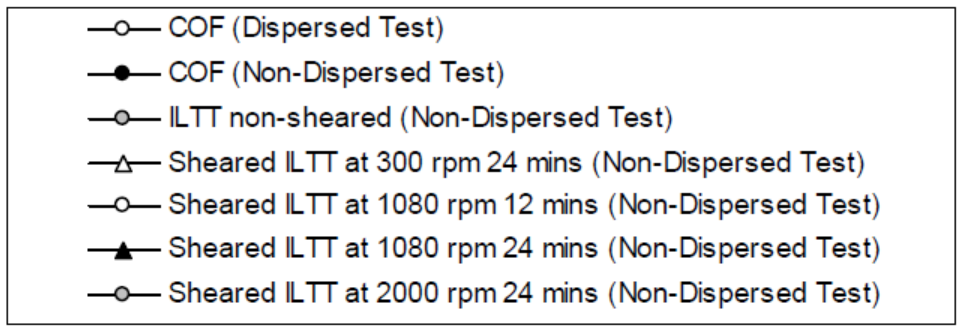
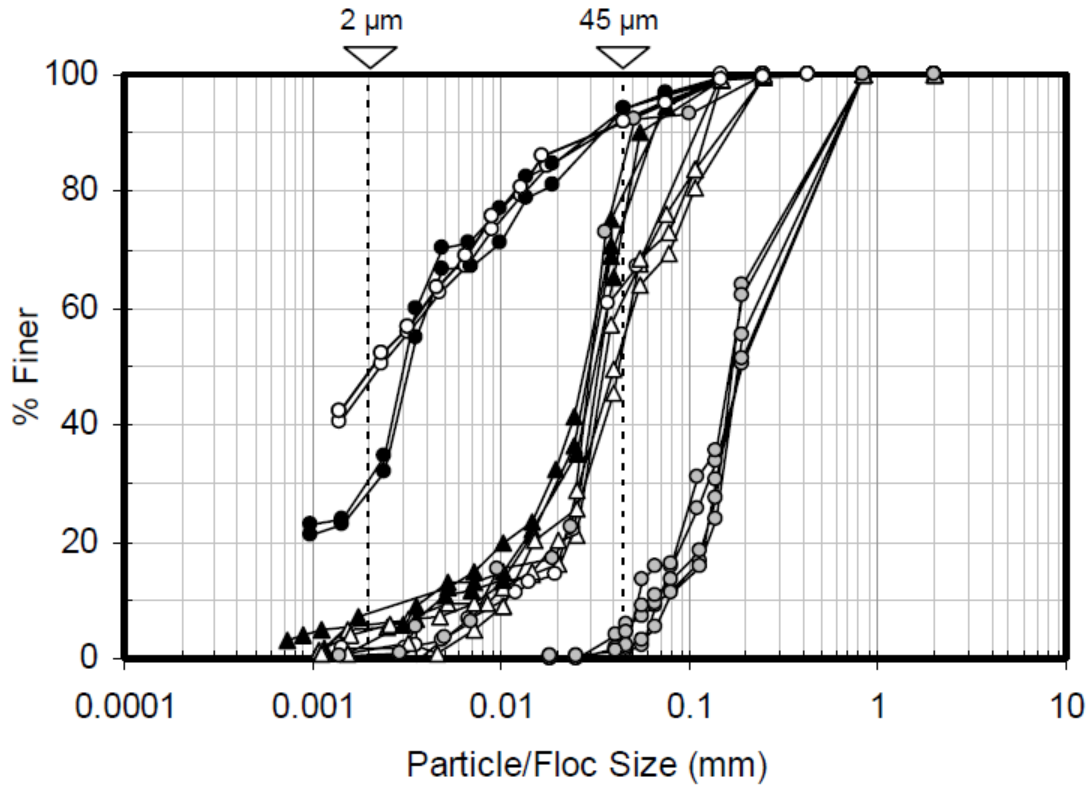


Figure 2-8 – Comparison of particle size distributions for sheared in-line thickened tailings (ILTT) (Jeeravipoolvarn 2010)

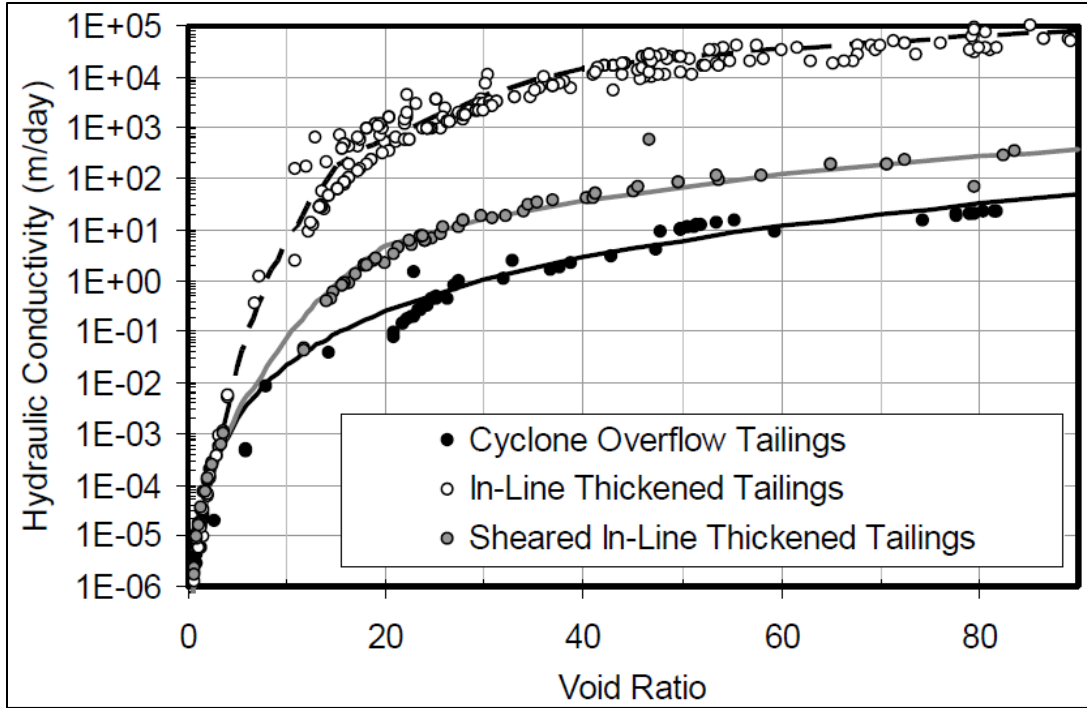


Figure 2-9 – Hydraulic conductivity comparison of laboratory non-sheared ILTT, sheared ILTT, and COF (Jeeravipoolvarn 2010)

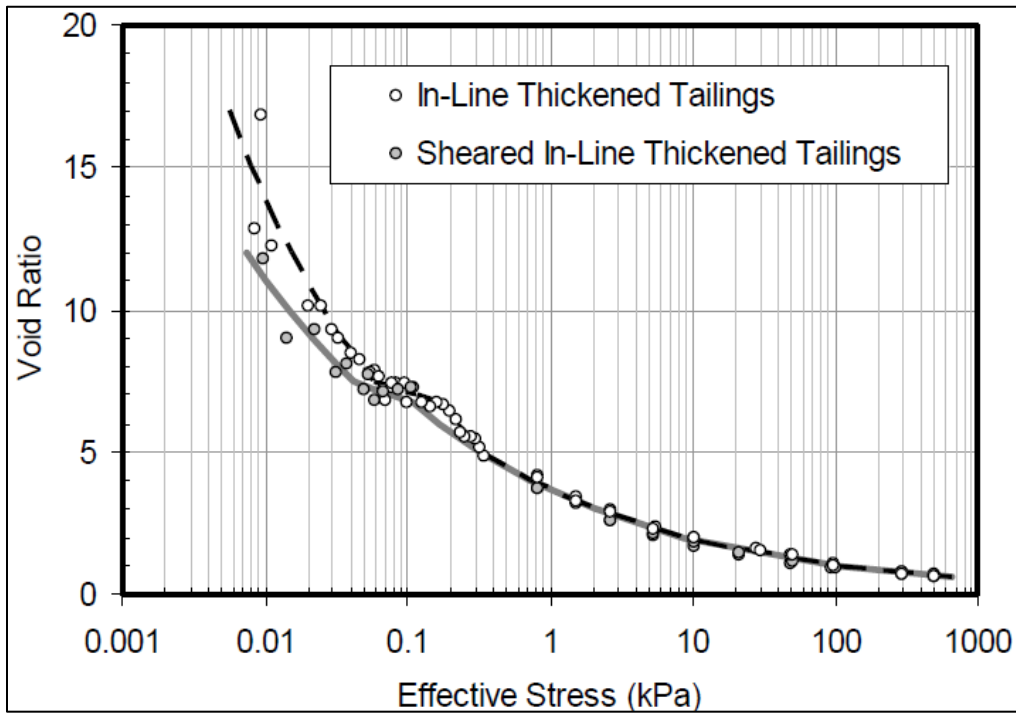


Figure 2-10 – Compressibility comparison of laboratory non-sheared ILTT and sheared ILTT (Jeeravipoolvarn 2010)

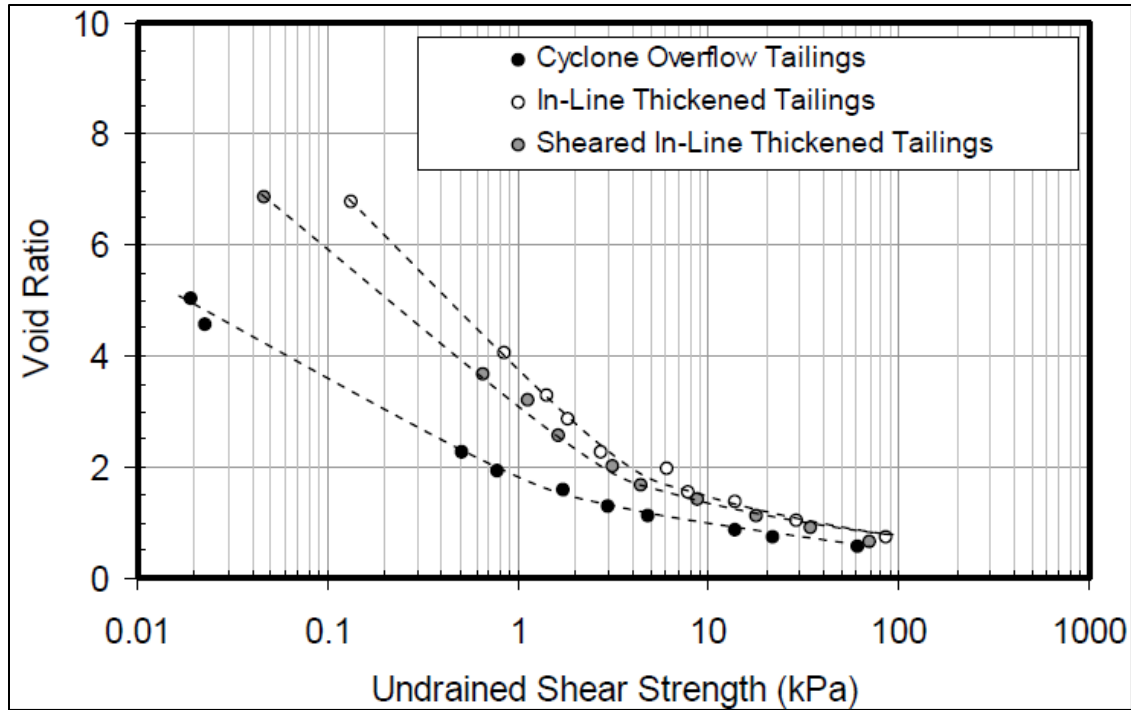


Figure 2-11 – Undrained shear strength comparison of laboratory non-sheared ILTT, sheared ILTT and COF (Jeeravipoolvarn 2010)

#### 2.4.3 Influence of Dewatering and Desiccation on Microstructure and Vane Strength of Polymer Amended Oil Sand Mature Fine Tailings

This paper, by Bajwa, T. and Simms, P. (2013), presents research on the microstructure and undrained shear strength of polymer-flocculated FFT. Of particular relevance to the current body of work is the discussion related to floc size distribution of treated FFT. The paper uses the terminology “apparent grain size distribution” since the measurement technique employed wet sieving and hydrometer for particle size determination. The paper explores the behaviour of polymer-treated FFT using a number of different polymer dosages. Polymer-amended FFT samples were analyzed to determine grain size distribution among other index tests. Samples were also obtained for vane shear strength measurement and scanning electron microscopy (SEM) testing. Results for particle size distribution of polymer amended fine tailings, for each of the polymer dosages, is presented in Figure 2-12. From Figure 2-12 it can be seen that the apparent particle size distribution is influenced by the polymer dosage. Index test results for these samples are presented below in Table 2-3. The apparent particle size data has been converted to a sand-to-fines ratio (+ 45  $\mu\text{m}$  / -45  $\mu\text{m}$ ) which allows for simple comparison of size data.

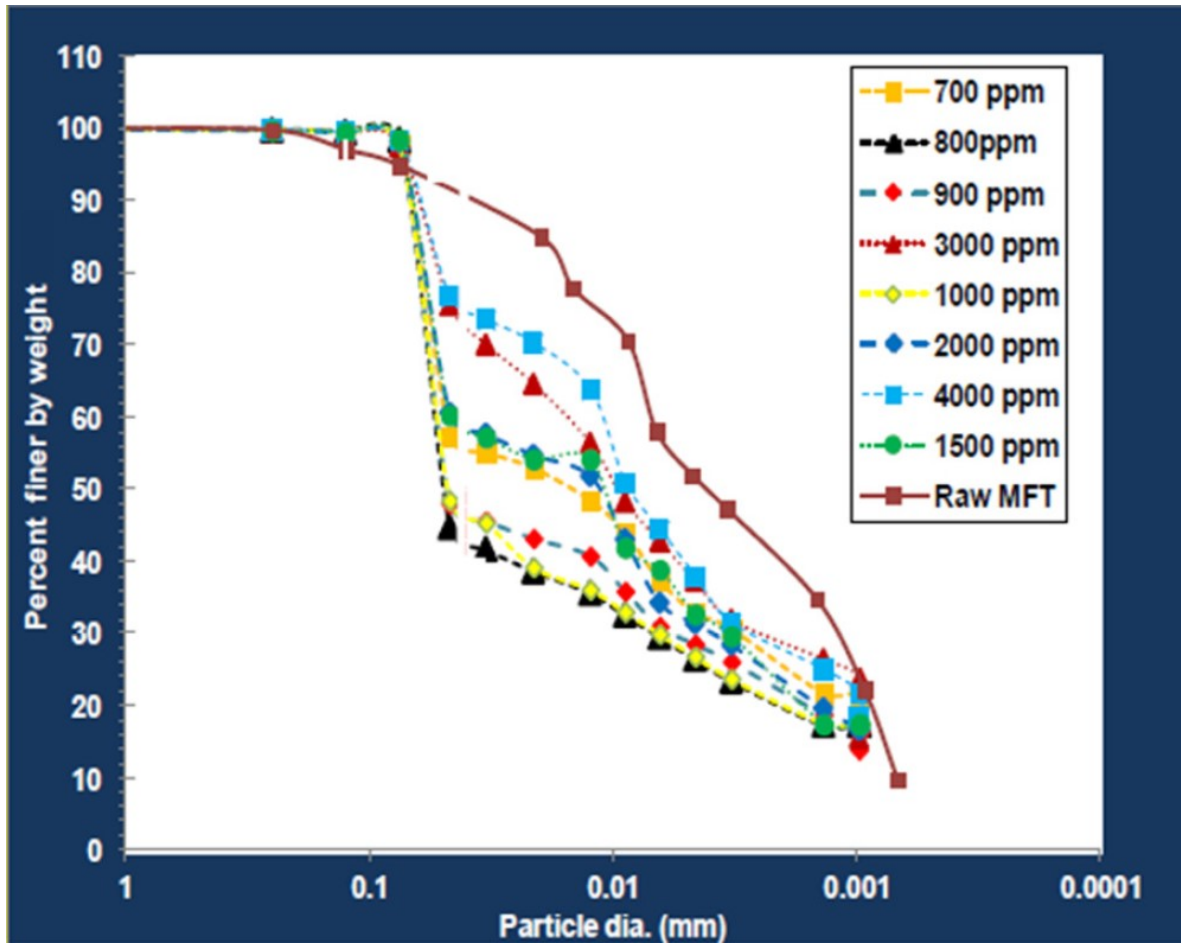


Figure 2-12 – Particle agglomerate size distribution for polymer amended FFT for different polymer concentrations (Bajwa and Simms 2013)

Table 2-3 – Index test results from measurements of polymer-treated oil sands mature fine tailings (Bajwa and Simms 2013)

Characteristics	Polymer amended mature fine tailings								
	0	700	800	900	1000	1500	2000	3000	4000
Concentrations (ppm)	0	700	800	900	1000	1500	2000	3000	4000
Liquid limit (%)	45	77	82	-	81	78	73	70	70
Plastic limit (%)	19	43	43	-	43	43	43	43	43
Plasticity index	26	34	39	-	38	35	30	27	27
Liquidity index	4.65	2.85	2.49	-	2.55	2.77	3.23	3.59	3.59
Sand-to-fines ratio (SFR)	0.1	0.7	1.3	1.17	1.17	0.72	0.72	0.45	0.4

The use of polymer to flocculate oil sands fine tailings has the effect of increasing the apparent particle size in addition to decreasing the liquidity index. The sand-to-fines ratio is the highest for tailings samples treated with between 800 and 1000 ppm flocculant. Results of other index testing revealed increases in specific gravity and liquidity index but there does not appear to be any notable impact of dosage on vane shear strength. SEM images of the polymer treated samples clearly showed pore spaces and flocs but assessment of flocculation was inconsistent with characterization data because the micrographs showing good flocculation did not correlate to the best flocculation assessed using the sand-to-fines measurement. This study was successful at determining floc sizes in a manner that allows comparison of results and showed that increasing the polymer dosage beyond the optimum, for this tailings sample, did not improve dewatering. The paper by Jeeravipoolvarn et al. (2014) is similar to the work already discuss with sheared and non-sheared ILTT but focuses on lower void ratios from 0 to 6. The major finding in the paper is that the greatest impact of shear on ILTT is the slight reduction in shear strength at lower void ratios. The reduction of shear strength due to shearing is not consistent with what was found in this current body of work.

#### 2.4.4 Effect of Pipelining Shear on Consolidation Properties of Oil Sands Fine Tailings

This conference paper, by Jeeravipoolvarn et al. (2014), is based on work performed for Jeeravipoolvarn (2010) summarized above but with some additional comparisons of engineering properties. The premise is the same as above where ILTT was sheared causing floc breakage. Comparisons of compressibility, hydraulic conductivity, and vane shear strength were presented. Comparisons in this study are only for lower void ratio range (0 to 6) and compression only up to 10 kPa. This study found that shearing ILTT increased the compressibility when compared to non-sheared ILTT. Hydraulic conductivity for sheared ILTT was lower at higher void ratios which means that although sheared ILTT will compress more than non-sheared ILTT, it will take longer. Overall, it was found that the greatest impact on ILTT due to shearing was the reduction in shear strength at a given void ratio (Figure 2-13). This means that sheared ILTT will have to undergo more consolidation than non-sheared ILTT to meet a similar shear strength.

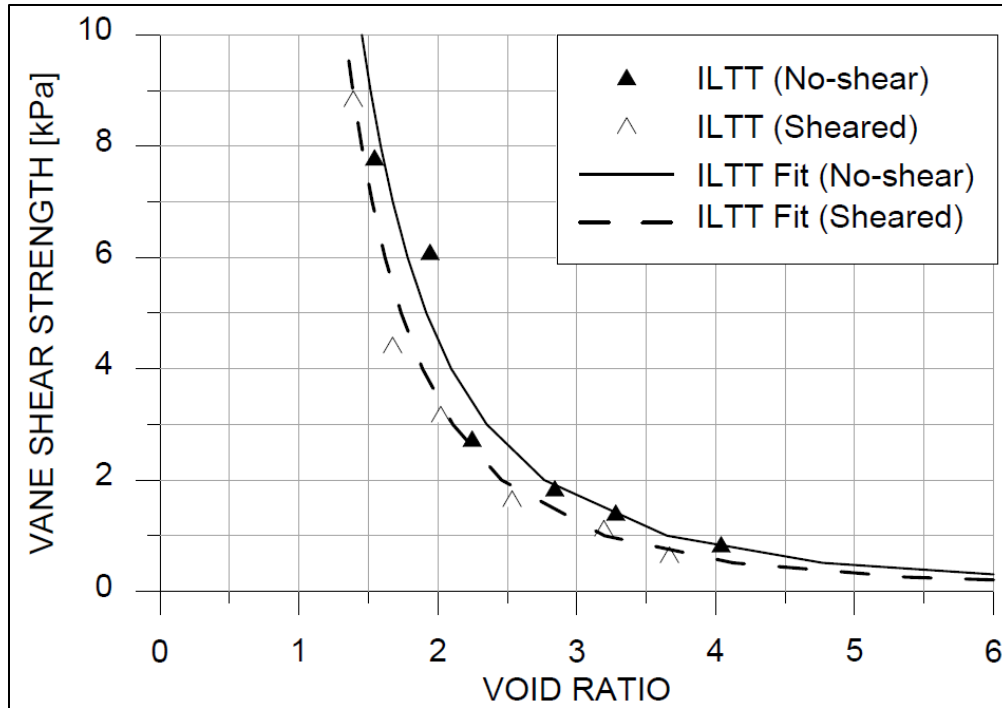


Figure 2-13 – Vane shear comparisons for ILTT (Jeeravipoolvarn et al. 2014)

#### 2.4.5 Effects of Shearing and Shearing Time on Dewatering and Yield Characteristics of Oil Sands Flocculated Fine Tailings

This study, by Derakhshandeh et al. (2016), focused on the effect of pipeline shear on dewatering and yield characteristics of flocculated mature fine tailings (MFT). Testing involved flocculation of MFT with three different polymers using in-line flocculation with dynamic mixing. To model pipeline shear, a Couette device was used for controlled shearing of the flocculated tailings. Shearing was adjusted to represent different pipeline transport distances ranging from 100 m to 10 km. Dewatering was assessed using capillary suction time (CST), permeability index (PI), and water release tests. Yield characteristics were assessed by measuring peak yield stress. It was found that shearing of flocculated MFT had marginal effects on initial dewatering, but overall shear increased the rate of dewatering. It was also concluded that there was a reduction in yield stress of the flocculated slurry due to shear. The effect of pipeline shear had only a slight negative impact on initial dewatering while the long-term dewatering of sheared samples was greater than for non-sheared. Figure 2-14 shows the long-term dewatering trends for both sheared and non-sheared flocculated tailings samples. For each of the polymers tested the common trend is that the sheared samples released more water over the 7-day test duration. This shows that although shear can compromise initial dewatering, there is a net benefit to water release over time.

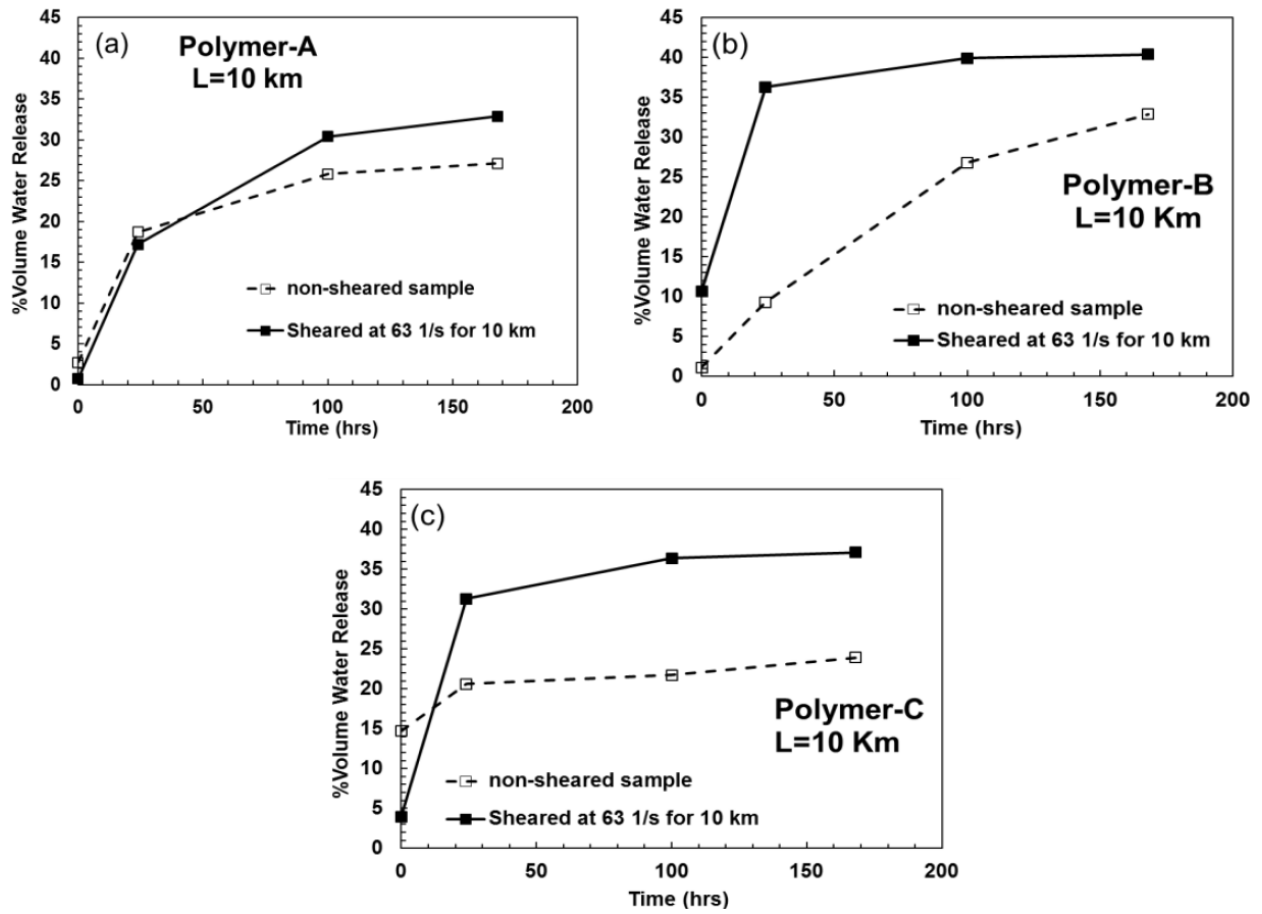


Figure 2-14 – Effect of shearing at 63 s<sup>-1</sup> for a residence time corresponding to transport distance of 10 km on 7-day water release of MFT samples flocculated with a) polymer-A, b) polymer-B, and c) polymer-C (Derakhshandeh et al. 2016)

### 3 CHARACTERIZATION TECHNIQUES AND TEST PROCEDURES

This chapter describes the methods used for initial tailings characterization and experimental techniques for floc measurement, tailings treatment, and geotechnical testing. Included are industry standard methods as well as techniques developed specifically for this project.

#### 3.1 Material characterization

Two oil sands FFT samples were used for initial coagulant screening, one of which was selected for flocculation studies. Both FFT samples were analyzed to determine composition (bitumen, solids, and water), particle size distribution, clay content, water chemistry, and mineralogy.

The Dean-Stark extraction procedure was used to quantify the main constituents of FFT (bitumen, mineral, and water). Particle size distribution (PSD) determination was done using a combination of wet sieve, for the coarse fraction, and a gravity sedimentation technique for fine particles. Clay content analysis utilized methylene blue titration. Water chemistry analysis includes major ions, alkalinity, conductivity, and pH. Mineral characterization of solids from Dean-Stark extraction used the X-ray diffraction (XRD) method.

Potassium alum, gypsum, and magnesium chloride were assessed as coagulation aides prior to flocculation. The flocculant used was a solution of a high molecular weight anionic branched polyacrylamide (SNF A3338) prepared to a concentration of 0.4-wt% with tap water.

##### 3.1.1 Dean Stark extraction

To quantify the bitumen, solids, and water content of the tailings samples the Dean-Stark extraction procedure was used (COSIA 2016). This procedure was also used to acquire solids for particle size analyses and clay characterization. Bitumen and water were extracted from the tailings sample using a modified Soxhlet extractor apparatus. The extraction works by heating toluene to allow its vapours to wash over the tailings sample held in a thimble, which separates bitumen and water from the solids. Tailings solids remain in a thimble while water is condensed in a water trap. Bitumen is collected together with toluene in the boiling flask then further analyzed to determine total bitumen quantity in the tailings sample.

### 3.1.2 Particle size distribution

Particle size distribution of tailings samples used solids from Dean-Stark extraction. Coarse particles were screened using a sieve method while fine particles were characterized using a SediGraph apparatus, which uses an X-ray sedimentation technique.

#### 3.1.2.1 Sieve

Distribution of particle sizes greater 45- $\mu\text{m}$  were characterized by sieve analysis using a wet test method (ASTM International 2017b). For this method a No. 200 mesh is used to determine the fraction of particles finer than 75- $\mu\text{m}$  but for this research a No. 325 mesh sieve was used. For oil sands tailings, fine particles are defined as those that are finer than 45- $\mu\text{m}$ . For this reason, the ASTM procedure was modified to account for this difference in fines definitions in order to be consistent with the oil sands industry definition. The No. 325 sieve corresponds to a 45- $\mu\text{m}$  opening and is commonly the only sieve used when analyzing particle size of fluid fine tailings. This is because most particles are less than 45- $\mu\text{m}$  and finer particles are processed using the sedimentation technique with the SediGraph instrument.

Solids from Dean Stark extraction were mixed thoroughly with tap water to disperse particles then quantitatively added to the No. 325 sieve. The sieve with solids was placed in a Ro-Tap<sup>®</sup> machine and connected to tap water. The test was completed by continuously shaking and tapping the sieves while flushing with water to remove all fines. The test was deemed complete when the flush water was absent of suspended solids. Solids remaining on the sieve were dried and weighed to determine the fraction of particles greater than 45- $\mu\text{m}$ . Fine solids that passed through the sieve were retained for subsequent analysis with the SediGraph instrument.

#### 3.1.2.2 SediGraph

SediGraph is a particle size analyzer that uses settling rates in conjunction with Stokes' law to determine particles sizes. To employ Stokes' law for this method, the particles are assumed to be solid and spherical with particle density and fluid properties being known. Particles settle under the influence of gravity and settling rates are determined by measuring X-ray transmission. Solids used for this method were from Dean Stark extraction since solids must be free of hydrocarbon contaminants before being placed in the instrument. Solids were dispersed using a 0.05% w/v sodium hexametaphosphate (Calgon) solution and

a combination of heat, mixing, and sonication. Once the solids were dispersed, the sample was transferred to the Micrometrics SediGraph III 5120 for analysis. An auto-sampler was used to mix and re-suspend solids for analysis. The system computer uses settling rates, X-ray absorption data, and particle and fluid properties to determine the particle size distribution of solids that passed through the No. 325 sieve.

### 3.1.3 Methylene blue

The procedure used was that as reported by Omotoso and Morin (Omotoso and Morin 2008). Solids were diluted with de-ionized water then combined with 1M NaHCO<sub>3</sub> so that the resulting NaHCO<sub>3</sub> concentration was 0.015M. NaOH was added to adjust the pH to between 8 and 11 to promote particle repulsion and hence dispersion (Currie et al. 2014). After adequate dispersion, the suspension was acidified by adding 10% v/v H<sub>2</sub>SO<sub>4</sub> to drop the pH to between 2.5 and 3.8. This adjustment is required to ensure (1) amorphous Fe<sub>2</sub>O<sub>3</sub> is positively charged and does not adsorb methylene blue and (2) methylene blue interacts solely with the clays (Currie et al. 2014). Following this sample preparation procedure, the methylene blue titration was carried out until the saturation point was reached. The saturation point is realized when aliquots placed on Whatman 43 filter paper produce a blue halo around the solids. The titration end-point is used to calculate a methylene blue index (MBI) and clay content.

### 3.1.4 Water chemistry

Samples for water chemistry were centrifuged and filtered to remove solids prior to analyses. Cation concentrations (Ca<sup>2+</sup>, Na<sup>+</sup>, K<sup>+</sup>, Mg<sup>2+</sup>, Al<sup>3+/2+</sup>) were measured using inductively coupled plasma optical emission spectrometry (ICP-OES) on a Varian Vista-PRO™ CCD Simultaneous ICP-OES. Anion concentrations (SO<sub>4</sub><sup>2-</sup> and Cl<sup>-</sup>) were determined by ion chromatography on a Dionex ICS-3000. Alkalinity (HCO<sub>3</sub><sup>-</sup> and CO<sub>3</sub><sup>2-</sup>) and pH were measured using PC-Titrate™ Alkalinity Auto-titrator by Mandel. Conductivity was determined using conductivity probe InLab® 731 by Mettler Toledo. Measured species are reported in mg/L. Sodium adsorption ratio (SAR) was calculated from the measured cation concentrations using Equation 3-1 where concentrations are in mol/L. SAR is the ratio of Na<sup>+</sup> to divalent ion concentrations, and is typically used for evaluating soil solutions or irrigation waters (Essington 2004). For use of SAR in oil sands it has been generalized that fine tailings with a SAR exceeding 20 are likely to be dispersed while a SAR less than 5 presents a more flocculated structure (Miller 2010). For FFT

coagulation experiments, discussed later, the SAR is determined from water chemistry of coagulated FFT samples treated with a number of dosages of  $Al^{3+}$ ,  $Ca^{2+}$ , and  $Mg^{2+}$ .

Equation 3-1 – Sodium adsorption ratio

$$SAR = \frac{[Na^+]}{\sqrt{Ca^{2+} + Mg^{2+}}}$$

### 3.1.5 Mineralogy

The mineralogical composition of the two FFT samples was evaluated using X-ray diffraction analysis. A homogenous sample of Dean-Stark solids was processed in a micronizing mill using quartz pellets and methanol. Micronizing was done to reduce the particle size to less than 5  $\mu m$ . The sample was then dried at 100°C for two hours to evaporate the methanol. The dried sample was then treated with Vertrel XF fluid in a mixing mill vessel and processed to obtain spherical particles with an average diameter of 2 to 5  $\mu m$ . This procedure is necessary to avoid preferred orientation during XRD analysis.

X-ray diffraction analyses were completed using a Rigaku D/MAX Rapid-II rotating anode powder diffractometer fitted with an imaging plate detector, using  $CrK\alpha$  radiation. Diffraction data were obtained from angle of incidence spanning 5° to 150° 2 $\theta$ . The measured diffraction pattern was converted to a two-dimensional plot of intensity vs 2 $\theta$  plot by 2DP™ data processing software. The two-dimensional plot was retained for the mineral identification processes. An example of the diffraction pattern is shown in Figure 3-1.

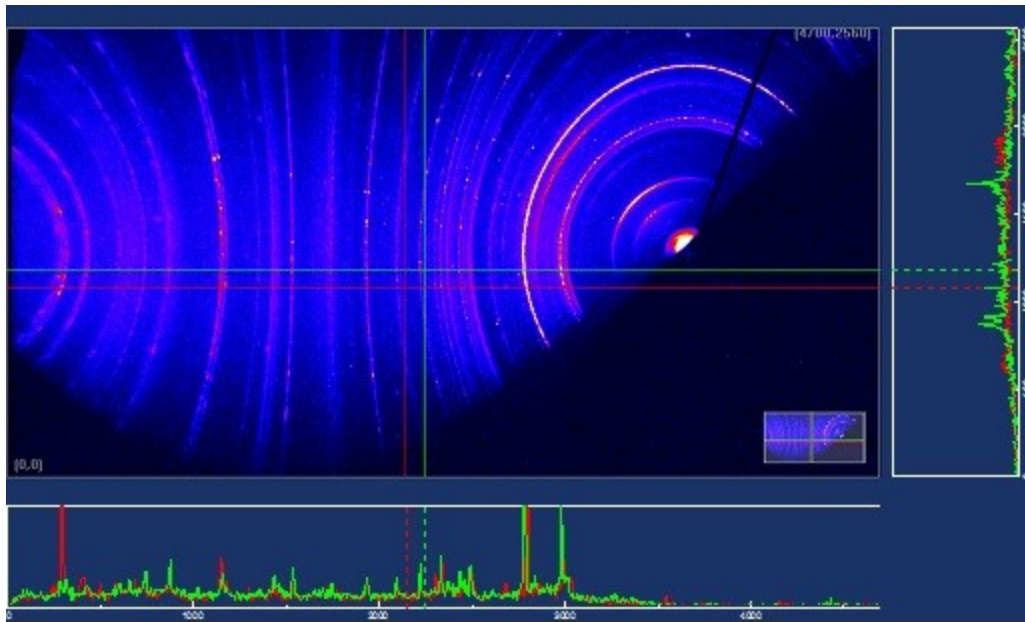


Figure 3-1 – Example of diffraction pattern obtained from X-ray diffraction analysis

Oil sands tailings mineralogy typically consists of quartz and clays with the main clay components being kaolinite and illite (Kasperski 1992, Kaminsky et al. 2009). Minor phases present include carbonates and titanium oxides. Major phases were identified using the mineral identification software Jade™. Minor phases were mostly identified manually since the identification software has trouble with quantities of less than 10%. Manual identification was done by matching observable peaks with literature values and comparing results to minerals typically found in oil sands tailings. Mineral solids were quantified with AutoQuan™ using Rietveld analysis. The Rietveld method uses crystallographic constraints to constrain peak positions and intensities so this technique is only suitable for materials with known structures. For oil sands tailings mineralogy the Rietveld technique is suitable since the primary constituents have known structures.

### 3.1.6 Coagulant properties

Three different inorganic salts were assessed for their applicability as coagulant aides. They were aluminum potassium sulfate dodecahydrate (K-alum), calcium sulfate dihydrate (gypsum), and magnesium chloride hexahydrate (magnesium chloride). The choice of coagulant candidates was based on the desire to assess coagulation effectiveness of inorganic salts having different multivalent cations.

Additionally, these coagulants are the highest three in the lyotropic series  $\text{Al}^{3+} > \text{Ca}^{2+} > \text{Mg}^{2+}$ . Coagulant chemical formulae are:  $\text{AlK}(\text{SO}_4)_2 \cdot 12\text{H}_2\text{O}$ ,  $\text{CaSO}_4 \cdot 2\text{H}_2\text{O}$ , and  $\text{MgCl}_2 \cdot 6\text{H}_2\text{O}$ .

### 3.2 Tailings treatment

The goal of the tailings treatment portion of this research is twofold. First, treatment is required to enhance solid-liquid separation, so this separation must be evident from selected treatment recipes. Second, high contrast images are required for accurate floc analysis, so clear release water and well-defined flocs must be developed. To meet the treatment requirements, it is possible to vary several parameters including FFT solids content, mixing energy, and chemical types and dosages. From previous experience, treatment of FFT with the selected polymer flocculant without coagulant yields slightly turbid release water so both coagulant and flocculant were used in this project. The use of sufficient coagulant helps decrease the amount of suspended fine solids which effectively reduces turbidity of release water. The methodology for developing suitable treatment recipes was as follows:

- Select chemicals for treatment aids from among three different coagulants (K-alum, gypsum, magnesium chloride) and a single flocculant (A3338);
  - Although many polymer flocculants are available for FFT treatment, A3338 was the only flocculant selected for this body of work because it is widely used for oil sands tailings treatment;
- Assess performance of each coagulant over a range of dosages for each of the two FFT samples using capillary suction time as a performance indicator;
- Determine optimum coagulant dosages for studying flocculation;
- Determine optimum flocculant dosage by visually observing overdosed or underdosed conditions where overdosed FFT will exhibit stringy, excess polymer and underdosed FFT will lack the appearance of a flocculated structure and there will not be clear release water.

Capillary suction time (CST) is a key test to assess sludge dewaterability (Fitria et al. 2014). The CST apparatus provides a quick and simple way to determine the effects of different chemical agents and dosages (Scholz 2005). To carry out a CST test the slurry is poured into a small tube sitting on a piece of filter paper. Water from the slurry is pulled into the filter paper by capillary suction. The rate that water is pulled to the filter paper is defined as the capillary suction time with units of seconds per centimeter. Timing of the rate of water movement is automated by use of two sets of electrodes triggered by water

contact to start and stop timing. CST represents the rate of water extraction from slurry so low values indicate good dewaterability while high values represent poor dewaterability. Therefore, CST testing is useful to assess coagulation because CST values decrease with increased coagulation. With the use of CST, it is possible to determine optimum coagulant dosages based on the trend of decreasing CST with increasing coagulant dosage. For this body of work the optimum coagulant dosage is selected by bisecting the angle formed by two tangents to the extremities of the CST-dosage curve (see Figure 3-2 for example). Working with two FFT samples, three coagulants, and multiple dosages, 34 different conditions (Table 3-1) were tested in search for the optimum coagulant dosage for each inorganic salt. Although coagulant was used in the tailings treatment recipe to minimize turbidity, turbidity was not measured and did not play a part in determining the optimum coagulant dosage.

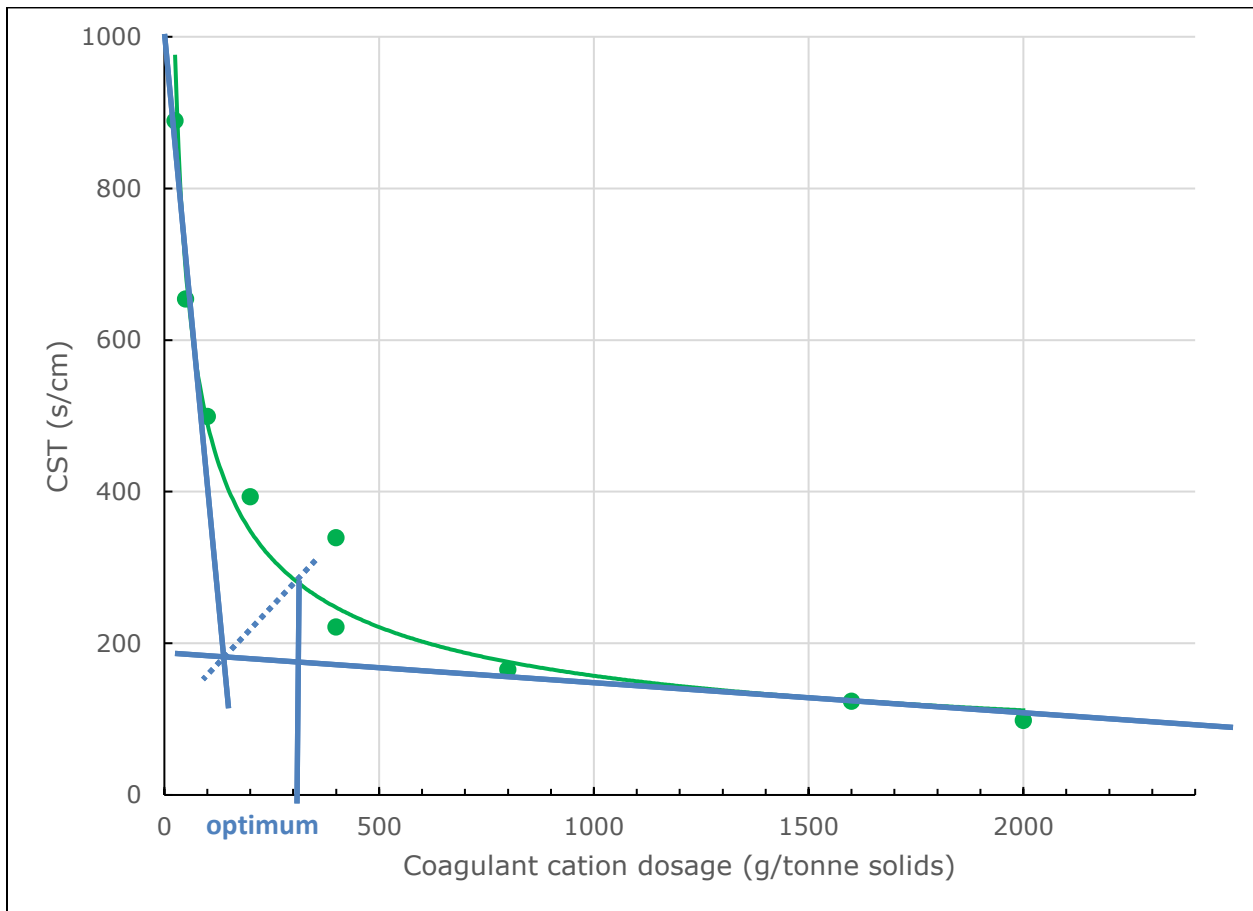


Figure 3-2 – Plot of capillary suction time (CST) of treated FFT as a function of coagulant dosage and lines showing how optimum dosage is graphically determined

Table 3-1 – List of coagulation conditions tested in search of an optimum dosage

FFT	Cation	M <sup>n+</sup> dosage (g/tonne of solids)
FFT-1	Al <sup>3+</sup>	40
FFT-1	Al <sup>3+</sup>	160
FFT-1	Al <sup>3+</sup>	160
FFT-1	Al <sup>3+</sup>	320
FFT-1	Al <sup>3+</sup>	480
FFT-1	Al <sup>3+</sup>	480
FFT-1	Al <sup>3+</sup>	480
FFT-1	Al <sup>3+</sup>	960
FFT-1	Al <sup>3+</sup>	1920
FFT-1	Ca <sup>2+</sup>	25
FFT-1	Ca <sup>2+</sup>	50
FFT-1	Ca <sup>2+</sup>	100
FFT-1	Ca <sup>2+</sup>	200
FFT-1	Ca <sup>2+</sup>	400
FFT-1	Ca <sup>2+</sup>	400
FFT-1	Ca <sup>2+</sup>	800
FFT-1	Ca <sup>2+</sup>	1600
FFT-1	Ca <sup>2+</sup>	2000
FFT-1	Mg <sup>2+</sup>	100
FFT-1	Mg <sup>2+</sup>	200
FFT-1	Mg <sup>2+</sup>	400
FFT-1	Mg <sup>2+</sup>	800
FFT-2	Al <sup>3+</sup>	160
FFT-2	Al <sup>3+</sup>	320
FFT-2	Al <sup>3+</sup>	480
FFT-2	Al <sup>3+</sup>	960
FFT-2	Ca <sup>2+</sup>	400

FFT	Cation	M <sup>n+</sup> dosage (g/tonne of solids)
FFT-2	Ca <sup>2+</sup>	800
FFT-2	Ca <sup>2+</sup>	1600
FFT-2	Ca <sup>2+</sup>	2400
FFT-2	Mg <sup>2+</sup>	110
FFT-2	Mg <sup>2+</sup>	206
FFT-2	Mg <sup>2+</sup>	400
FFT-2	Mg <sup>2+</sup>	800

Coagulation testing was done by first diluting FFT samples to 20-wt% solids with tap water (0.30 g/L total dissolved solids including mostly Ca<sup>2+</sup>, Mg<sup>2+</sup>, Na<sup>+</sup>, Cl<sup>-</sup>, and SO<sub>4</sub><sup>2-</sup>). Performing coagulation testing with CST at 20-wt% solids is beneficial because at lower solids content (less than 10-wt% solids) the CST values tend to be too low to easily discern optimum dosages. Conversely, CST testing with high solids content (greater than 30-wt% solids) FFT takes too long and water can begin to evaporate from the filter paper which yields erroneous results.

Diluted FFT was treated in 300-g batches with each of the individual coagulants at varying dosages. Coagulant powder was added to the slurry while continuously mixing. Coagulant was added as a powder rather than a solution in order minimize dilution and maintain the initial solids content around 20-wt% solids. Tailings slurry with coagulant was mixed for at least four hours to allow sufficient time for cation exchange, although much less time is typically required. A brief study was conducted to monitor conductivity of the coagulated FFT to determine how long it would take for major changes to cease. From this it was determined that substantial changes in conductivity presented quickly and that four hours would be more than enough time to coagulation to occur. Following coagulation of FFT, CST testing was carried out (five replicates) for each of the 34 conditions. CST measurements were carried out using a Triton Electronics Type 319 Multi-CST with five single radius test heads and Whatman® number 4 filter paper, pictured in Figure 3-3. The remaining sample was used for water chemistry analysis to determine major ions, conductivity, and pH.



Figure 3-3 – Capillary suction testing schematic (left) and apparatus (right)

CST test results for each FFT sample and coagulant were plotted and analyzed to determine the optimum coagulant dosage. Analysis to determine optimum coagulant dosage is described above and pictured in Figure 3-2. The optimum dosages were used for tailings treatment prior to flocculation. Flocculation of coagulated FFT required further dilution to 10-wt% solids to better distinguish the flocs. Flocculation testing involved increasing polymer addition until solid-liquid separation and a clearly-defined floc structure were observed. Suitable polymer dosages gave clear floc formation and clear release water. Care was taken not to overdose the FFT, which would lead to excess polymer in the sample. Excess polymer is detected by touching the surface of the release water to check for the presence of stringy polymer.

Initially, the intent was to see which of the three different coagulants would perform best but after the coagulation assessment magnesium chloride was removed as an option because it did not appear to offer any substantial benefit. The exclusion of magnesium chloride also served to limit coagulants to those already used in industry which include gypsum and alum (Sedgwick and Fair 2014). The two recipes

selected for the flocculation study used FFT-1, either gypsum or potassium alum as the coagulant, and A3338 polymer for the flocculant.

### 3.3 Floc measurement

Many techniques exist for measuring flocs, as described in Chapter 2; photography with image analysis was selected as the measurement technique for this project. This technique minimizes disturbance of flocs and allows measurement of macroscopic flocs, which were expected for this project. Selection of this technique was beneficial because of its simplicity and that it could be carried out without additional equipment modification or procurement. This measurement technique is well suited for the laboratory environment and could possibly be used for higher flow rates as long as flocs are distinguishable from the transporting fluid. A requirement of this measurement technique is images of high quality and high contrast. This can be achieved with a high-resolution camera and use of a treatment recipe that gives low turbidity release water. Low turbidity release water is required for recycling of process water and allows high visual contrast between flocs and water.

With the floc measurement technique selected, it was necessary to develop a procedure specific to the materials and equipment available for this project.

This phase made use of the following equipment:

- Glass tank (30 cm tall, 50 cm wide, 5 cm deep)
- Digital camera (Canon™ EOS 60D DSLR)
- Testing beads (3.0 mm and 4.5 mm)
  - Cole-Parmer® mixer testing beads, acetate, yellow, 3.0 mm
  - Cole-Parmer® mixer testing beads, acetate, red, 4.5 mm
- Image analysis software (AxioVision™ 4.8)

The glass tank was filled with tap water for use as a settling medium. The digital camera was positioned to capture images of testing beads as they settled through the water (Figure 3-4). Testing bead sizes were selected to be in the range of expected floc sizes. Testing beads were slowly deposited into the water-filled tank with a number of images being captured during deposition. Images were analyzed using AxioVision™ to determine both the number of beads and average diameter of each. Image processing involved multiple steps including application of scaling (pixel to millimeter conversion) and several image

corrections and enhancements prior to measurement of particles captured in the image. Each image captured had to be analyzed individually but image corrections made for the first image of each test could be carried over to subsequent images. This permitted a slight degree of automation.

Image corrections and enhancements include:

- Brightness, contrast, gamma value
- Sigma (reduces noise in image)
- Shading correction
- Edge enhancement
- Segmentation (selection of objects to be measured)
- Deletion of artifacts
- Object separation (particles identified as one but should be separate)
- Manual addition, deletion, and separation of particles

Figure 3-5 shows an image of testing beads in water before and after image processing. After the initial image was processed, the steps used could be saved for future use in a mostly automated processing procedure. Analysis of each image typically included a final manual step to remove parts of the image where beads appeared to overlap. After processing, the acquired size data was analyzed to see how well the image analysis software could measure the different sized beads. Using JMP® statistical software, the distribution was determined and the histogram with continuous fit curve is presented in Figure 3-6. The fitting parameters for the bimodal distribution of bead sizes is shown in Table 3-2. The standard deviations for each of the bead size distributions are used as the inherent error in this measurement technique. Several issues that had to be addressed to get high-quality images (and thus minimize the error) included: (1) use of appropriate background, (2) minimizing shadows by adjusting brightness and position of lighting, (3) obtaining high-resolution images of moving objects, and (4) use of fast shutter speed to capture moving bodies.

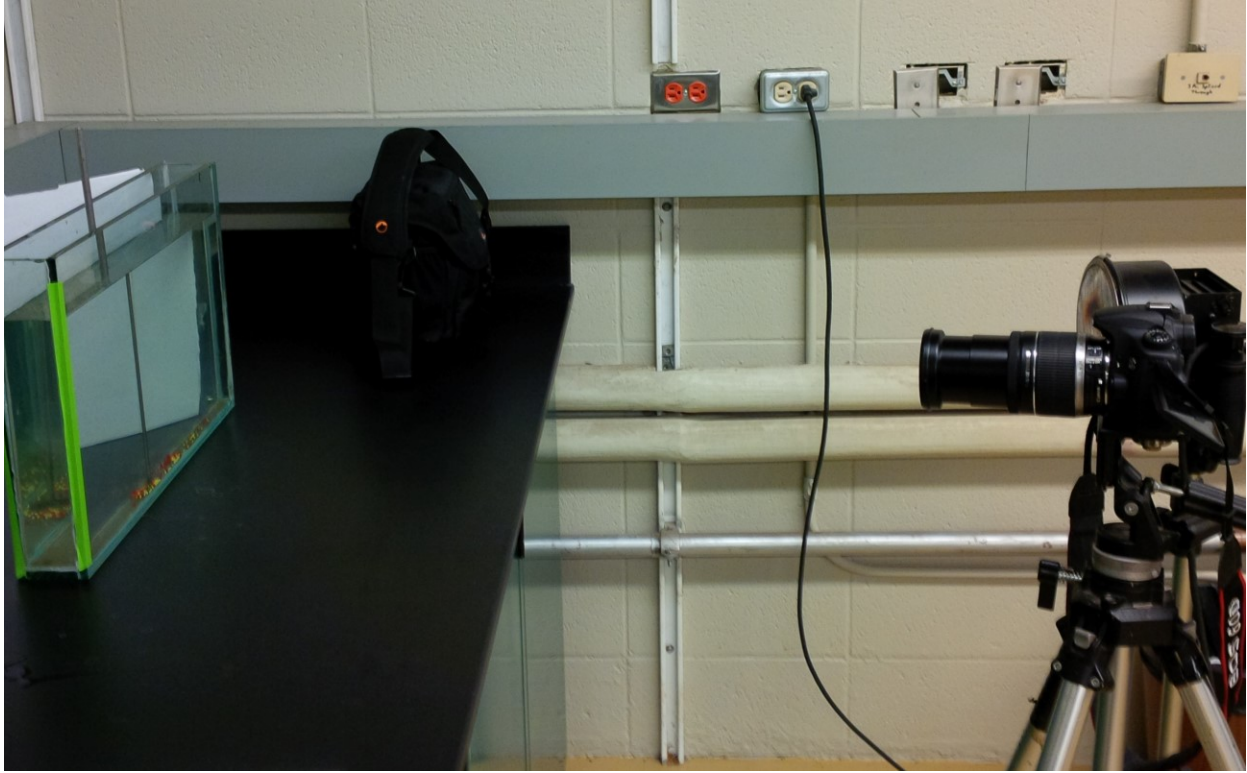


Figure 3-4 – Setup for testing bead measurement

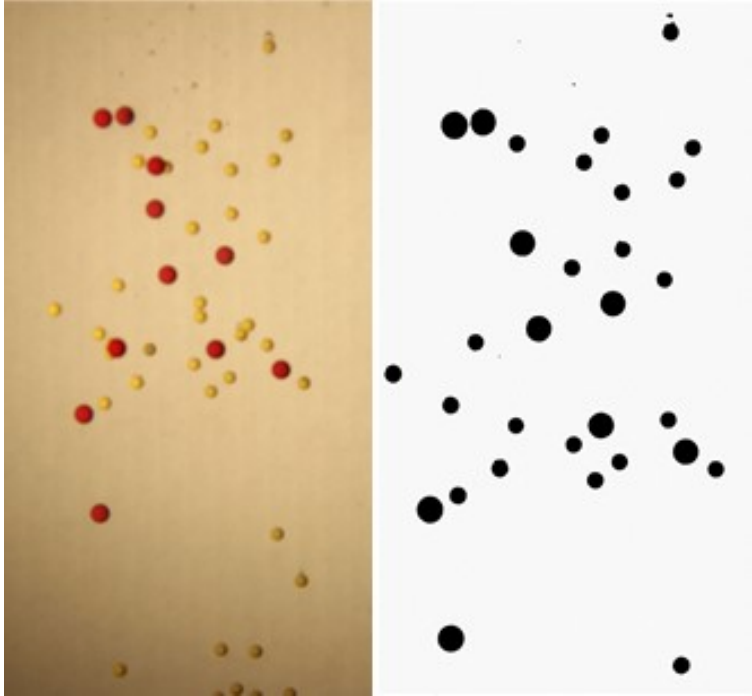


Figure 3-5 – Picture of beads settling through water (left) and after image processing (right) (red=4.5 mm, yellow=3.0 mm)

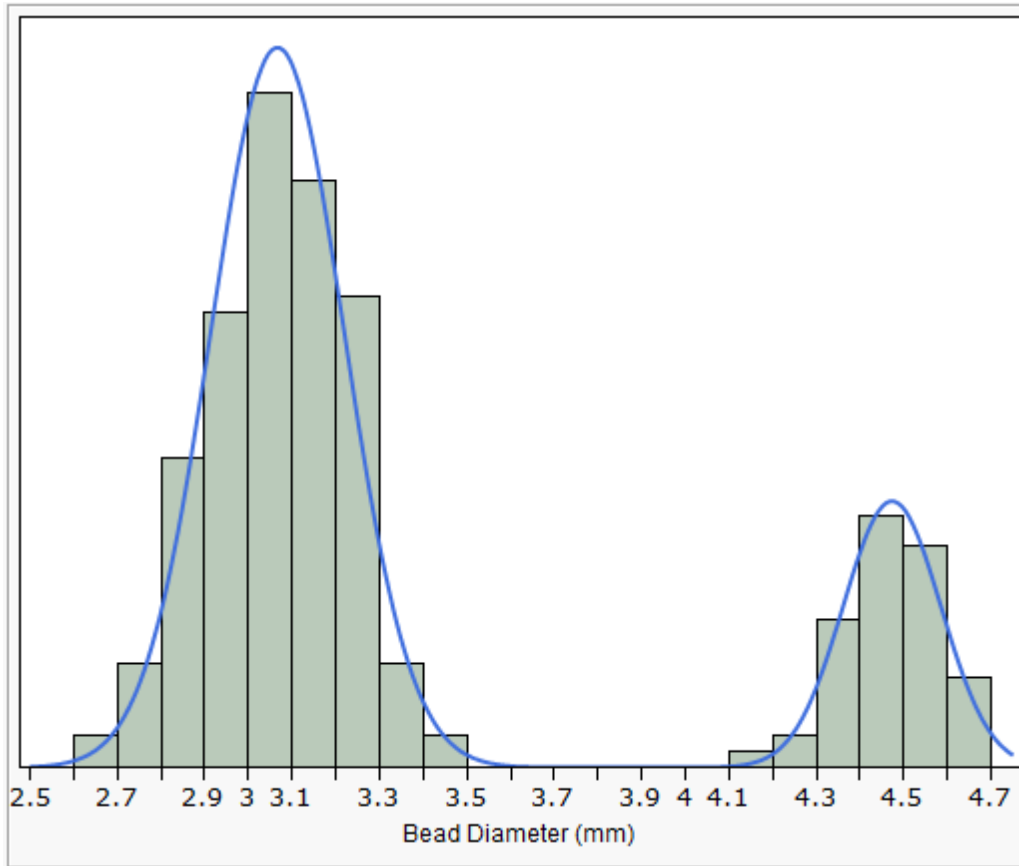


Figure 3-6 – Histogram and continuous fit curve for data obtained from image analysis of nine photographs of two different testing bead diameters

Table 3-2 – Parameter estimates for the fitted normal mixture in Figure 3-6 where  $\mu$  and  $\sigma$  are the respective mean and standard deviation for each bead size

Parameter		Estimate	Lower 95%	Upper 95%
Mean	$\mu_{3mm}$	3.07	3.04	3.09
Mean	$\mu_{4.5mm}$	4.47	4.44	4.50
Standard deviation	$\sigma_{3mm}$	0.15	0.13	0.18
Standard deviation	$\sigma_{4.5mm}$	0.11	0.08	0.15

The testing bead measurements agreed relatively well since the average measurements were close to the 3 mm and 4.5mm values. Although the average diameters of test beads were acceptable, the variance was larger than expected since all the beads should measure either 3 mm or 4.5 mm.

The next step was to extend the measurement method to flocs. The goal of this phase was to have well-flocculated tailings with discernable flocs suitable for image analysis. To be able to employ this measurement technique for flocs it was necessary to develop a deposition system that included in-line polymer dosing and mixing. This system was necessary to have continuous polymer dosing and controlled mixing to promote consistency in floc generation. The system required a deposition tank for floc size measurements. The custom-built deposition tank enabled acquisition of floc images for subsequent analysis and determination of average floc diameter. The deposition system design included a simple sampling system to allow for retrieval of representative samples for geotechnical testing. Four flocculated samples were generated using gypsum and K-alum as coagulants and two different flocculation mixing speeds. The floc size distribution was determined, and samples retained for each of the four test conditions.

Tailings were treated with both coagulant and flocculant. Coagulation treatment was done in batch mode and allowed to mix/interact with FFT for approximately 24-hours. Polymer flocculant was added in line and mixed first using an in-line static mixer then with an in-line dynamic mixer. The dynamic mixing stage of treatment was set up so that treated tailings were deposited into the open top of the vessel, mixed using the agitator, then deposited via spill-over openings into either the deposition tank or sample container. The residence time in the dynamic mixer was approximately 15 seconds. Referring to Figure 3-7 note that the polymer and feed pumps combine coagulated FFT (using K-alum or gypsum) with polymer flocculant at the static in-line mixer. The flocculated FFT mixture was transferred to the dynamic mixer where final floc formation took place. From the dynamic mixer vessel, flocculated material was deposited partially in the deposition tank and the remainder in a sample collection container. The process diagram for this tailings treatment process is detailed in Figure 3-8. The deposition tank is an important step in floc size determination because it provides a stage for image capture of the flocs. Note that the deposition tank was filled with water prior to floc deposition and during process operation. Water in the deposition tank provided a medium through which flocs could settle.

Creation of flocs in FFT needed to be repeatable to ensure a consistent floc size distribution (FSD) for a given tailings treatment so the experimental setup was designed to run with minimum handling to mitigate human error. The dynamic mixer was a benchtop overhead mixer with a Visco Jet®-120 mm impellor and was included to provide extra mixing for improved flocculation and to control floc size. After each test, all images of flocs were analyzed according to the same procedure used for the test beads. Floc

size data from image analysis were converted from a frequency distribution to a mass fraction and plotted as cumulative percent versus average floc-size diameter to obtain the floc size distribution.

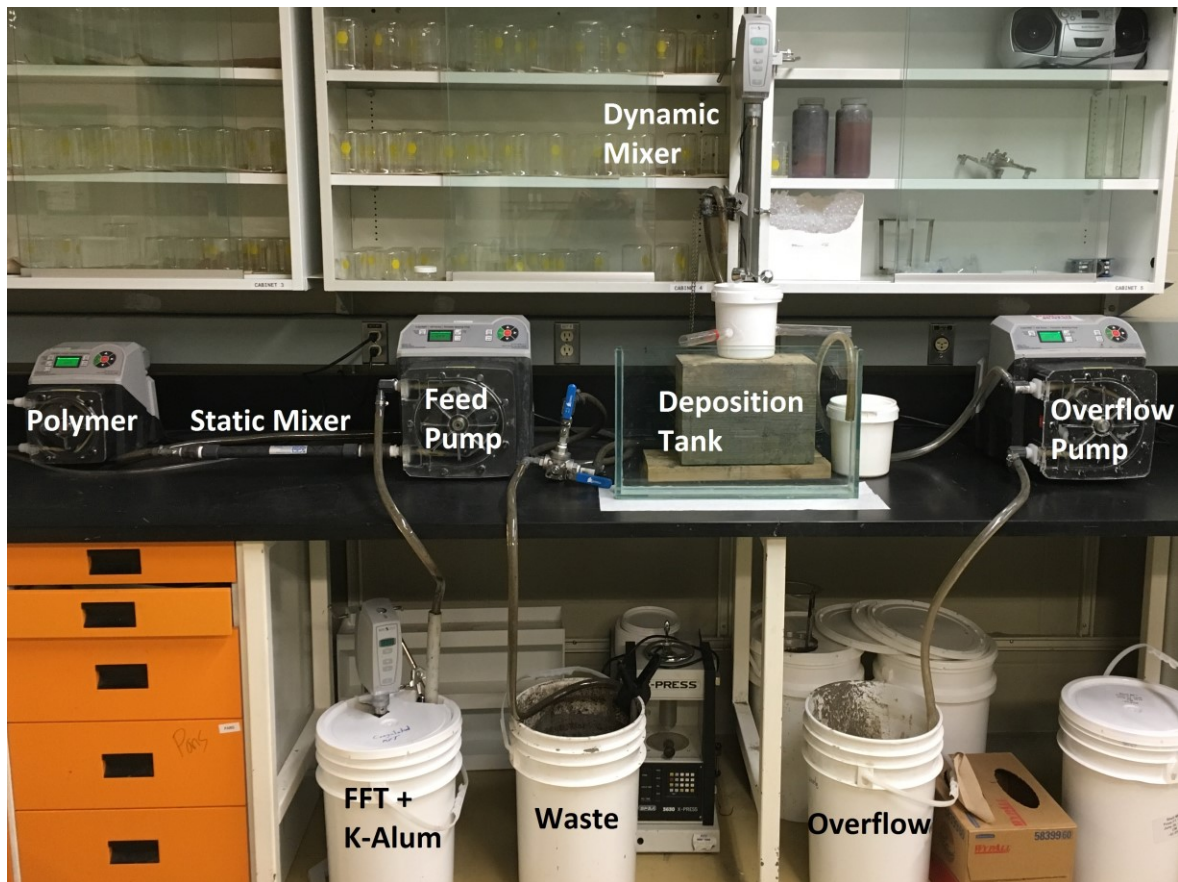


Figure 3-7 – Picture of flocculation setup

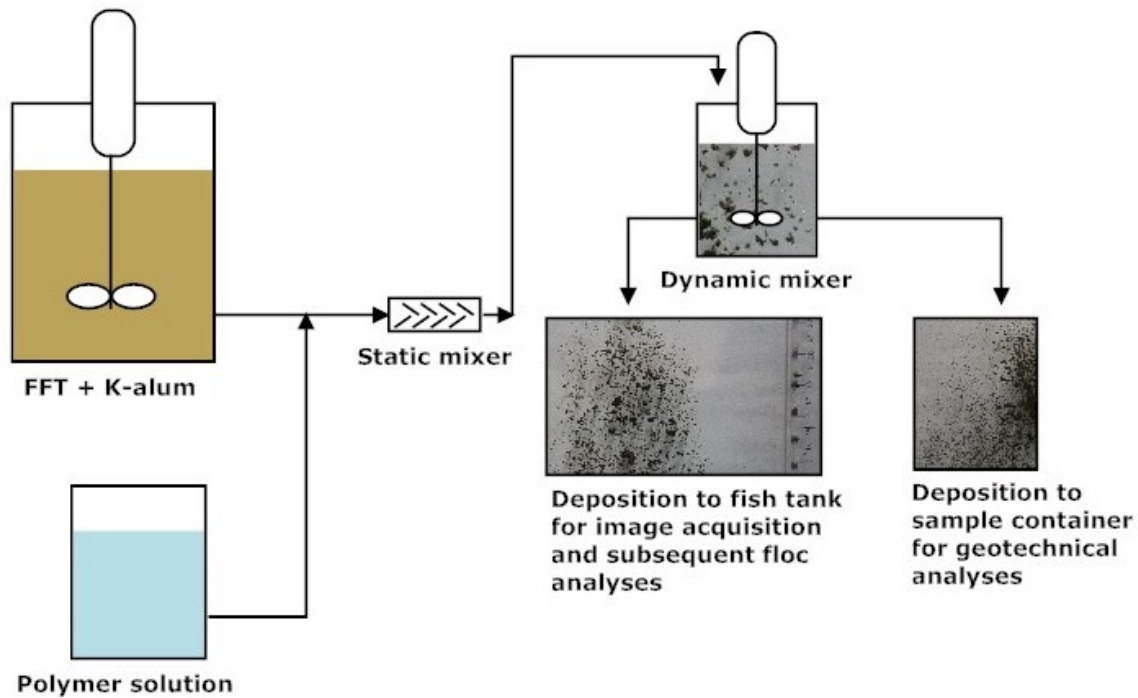


Figure 3-8 – Process map of fluid fine tailings flocculation setup

Determining and developing a suitable floc-size measurement system was a critical component of this project. Out of the many available options for measuring floc size, it was decided to use photography with image analysis. This technique was well suited for measuring large flocs with minimal disturbance since flocs were measured immediately after spilling out of the flocculation vessel. Additionally, samples of flocculated material were collected at the same time as floc image capture to ensure that both sampling and image capture streams had the same amount of mixing. This method had to be optimized to get high-resolution images with minimal interference from shadows and glare. Testing beads were used for the commissioning phase in preparation for actual floc measurements. Flocculation of tailings was done using a continuous flocculation setup to allow for image capture of flocs during creation of samples. Images were analyzed to get floc size distributions for each tailings treatment. The flocculation setup also allowed for representative samples of flocculated tailings to be obtained for further analyses.

### 3.4 Geotechnical properties

After initial testing of coagulant dosages it was decided that, since FFT-1 more closely matched cyclone overflow properties (Jeeravipoolvarn 2010), only FFT-1 would be further tested for geotechnical properties. Comparison of FFT-1, FFT-2, and cyclone overflow characterization are detailed later on in Table 4-1. Oil sands tailings sample FFT-1 was treated with either gypsum or K-alum and A3338 with floc size measurements made during flocculation. Each FFT treatment recipe was mixed with either a low (350-RPM) or high (900-RPM) speed. These mixing speeds were used because below 350 RPM, mixing was insufficient to flocculate the FFT and for mixing speeds greater than 900 RPM too much shear was introduced to the sample and floc measurements could not be made. These mixing speeds are not necessarily representative of field mixing conditions but represent the limits of the laboratory setup. The two samples produced using K-alum as a coagulant were subjected to geotechnical testing in order to observe the effect of different floc sizes on geotechnical properties. Flocculated samples coagulated with gypsum were characterized for floc size distribution but excluded from geotechnical testing since larger flocs were generated using K-alum as the coagulant. Geotechnical characterization included Atterberg limits, compressibility, hydraulic conductivity, and vane shear strength of the consolidated material.

#### 3.4.1 Atterberg limits

FFT-1 was selected for flocculation studies and so only, this sample was assessed to determine liquid and plastic limits. Atterberg limits were determined for FFT-1 untreated and for two samples coagulated with either gypsum or K-alum and flocculated with A3338. Samples generated using the different mixing speeds were not considered since continuous remolding of samples is required for Atterberg limits determinations. Liquid limit was determined using the fall cone test using previously established techniques (Hansbo 1957, Karlsson 1961). As part of the liquid limit determination, the relationship between undrained shear strength and water content was established. Plastic limit was measured according to ASTM D4318 (ASTM International 2017a). The fall cone method for liquid limit determination requires carrying out fall cone tests at different moisture contents. The target for liquid limit determination is to have a 10 mm cone impression with a 60-gram cone having an angle of 60 degrees. Several points around 10 mm cone impression can be used to determine the moisture content corresponding to a 10 mm cone impression. An alternate method requires a 20 mm cone impression with an 80-gram cone having an angle of 30 degrees.

### 3.4.2 Large strain consolidation

The large strain consolidation test was used to obtain compressibility data and hydraulic conductivity as a function of void ratio. Specific relationships obtained by large strain consolidation testing include effective stress-void ratio and void ratio-hydraulic conductivity. These relationships are used in finite strain consolidation modelling to predict both the rate and amount of settlement under a range of expected loads (Scott et al. 2008). Samples analyzed in this part of the project were collected during the floc measurement phase. Four samples were collected: those treated with two different coagulants at two mixing speeds, but only the two samples coagulated with K-alum were subjected to large strain consolidation testing since larger flocs were generated with this recipe. These two samples were allowed to dewater in their respective sample containers for approximately one month, after which they were decanted and transferred to the large strain consolidation cells. Decanted water was retained and used to water-cap each sample and to make up for evaporative losses throughout testing. The two samples were subjected to multi-step loading with thirteen load steps including the initial self-weight load. Starting after the self-weight load, each subsequent load was doubled up to the maximum load of 800 kPa. Application of each load was maintained until excess pore pressure dissipated and primary consolidation was complete according to displacement-time data.

The general procedure for large strain consolidation testing was as follows:

1. Prepare approximately 2 L of sample for placement into large strain consolidation cell (Figure 3-9)
2. Decant release water then subsample for water content determination
3. Prepare test cell by placing filter paper over porous stone in cell then saturate both filter paper and porous stone with process water
4. Drain water used for saturation through ports in base of cell to fill lines with process water
5. Carefully transfer a known mass of sample to the test cell and record initial height of sample
6. Add process water to cover the sample up to the overflow port on the test cell
7. Allow sample to consolidate under self-weight until settlement ceases and excess pore pressure dissipates
  - Note that pore pressure for this step was measured using a manometer tube while subsequent pore pressure measurements were monitored using sensors and logged with a data logger

8. After consolidation is complete the hydraulic conductivity is measured
9. Install load piston as the first load increment after self-weight and allow to consolidate then measure hydraulic conductivity
10. Continue to increase the load increments and measure hydraulic conductivity after consolidation is complete. Load increments are increased by a factor of two each time until the final load of 800 kPa with vane shear strength measurements made after hydraulic conductivity determination
11. After the final consolidation step the hydraulic conductivity is measured then the test is disassembled with samples collected for solids content determination

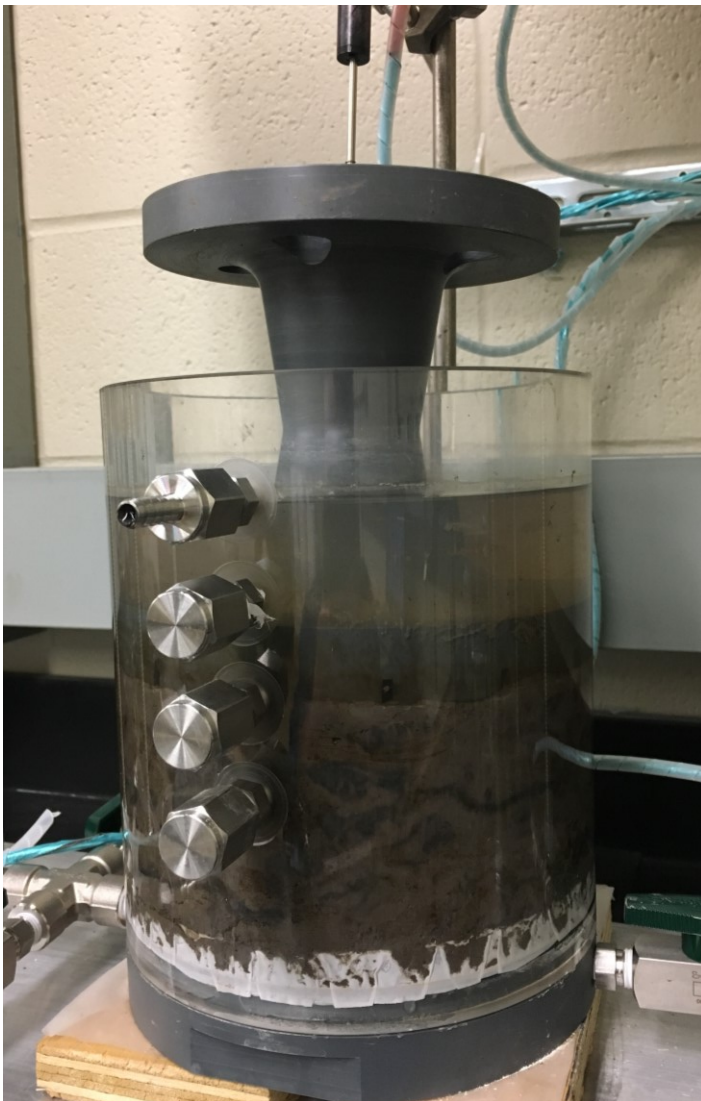


Figure 3-9 – Large strain consolidation cell with tailings sample

### 3.4.3 Hydraulic conductivity

As part of the large strain consolidation test the hydraulic conductivity was measured. The measurement was carried out at the end of each load step before application of subsequent loads. Hydraulic conductivity was measured using a constant head procedure with upward flow through the loaded sample. The hydraulic gradient was kept to a minimum to ensure seepage forces did not exceed the applied stress, which could cause further consolidation. Each test was monitored for at least one hour or until steady flow could be realized by the observation of several consistent measurements.

### 3.4.4 Vane shear strength

After consolidation was complete for each load, starting at approximately 10 kPa applied load, the vane shear strength was measured according to standard methods using a rotational speed of 60 deg/min (ASTM International 2016). To accomplish this measurement, the sample was unloaded and water was carefully decanted. After sufficient water removal, the vane shear strength was measured. Measurements were made using a laboratory vane apparatus VJT5300 made by VJ Tech Ltd. This vane apparatus makes measurements based on application of torsional load with one of four calibrated springs to a small vane (12.7 mm x 12.7 mm). Vane shear strength is calculated using Equation 3-2 and Equation 3-3 where  $\tau_v$  is the vane shear strength of the soil (in kPa),  $M$  (N·mm) is the mathematical product of the spring calibration factor and the maximum angular rotation in degrees, and  $K$  (mm<sup>3</sup>) is a constant that depends on the dimensions of the vane. The constant,  $K$ , is calculated according to Equation 3-3 where  $H$  and  $D$  are the vane height and diameter respectively.

Equation 3-2 – Vane shear strength calculation

$$\tau_v = \frac{1000M}{K}$$

Equation 3-3 – Constant used for vane shear strength calculation

$$K = \pi D^2 \left( \frac{H}{2} + \frac{D}{6} \right)$$

## 4 CHARACTERIZATION DATA AND EXPERIMENTAL RESULTS

Presented in this chapter are the results from material characterization, tailings treatment study, floc measurement data, and geotechnical properties of treated FFT.

### 4.1 Material characterization

Following is the presentation of results from material characterization. A comparison of both FFT samples to cyclone overflow from Jeeravipoolvarn (2010) is presented since further comparisons on floc size and geotechnical properties will be made throughout this study. Although FFT-1 was ultimately selected for flocculation and geotechnical testing it was important to characterize FFT-2 and carry out coagulation testing to see if there was any major differences in the performance of coagulants between FFT-1 and FFT-2. An overview of characterization results and comparison to cyclone overflow is shown in Table 4-1. Underlined values are those that were used to compare FFT-1 to cyclone O/F and which solidified the decision to eliminate FFT-2 from the flocculation portion of the study.

Table 4-1 – Tailings characterization

	Composition (wt%)		
	FFT 1 – as received	FFT 2 – as received	Cyclone O/F (Jeeravipoolvarn 2010)
Kaolin in mineral solids	<u>32.4</u>	16.4	<u>45.5</u>
Illite in mineral solids	22.2	16.7	4.5
Quartz in mineral solids	36.0	60.1	41.0
< 45- $\mu$ m in mineral solids	<u>96.1</u>	74.3	<u>94</u>
SFR	0.04	0.35	0.06
Clay in mineral solids	74.1	57.9	-
Bitumen in FFT	<u>4.3</u>	3.6	<u>3.3</u>
Water in FFT	54.3	52.2	-
Mineral solids in FFT	39.9	43.3	29.4

Notes: Clay wt% was determined by methylene blue index testing. Fines fraction (<45- $\mu$ m) was determined using Sedigraph for FFT samples and by hydrometer for cyclone O/F. Mineral solids content

is the 'as-received' value which was subsequently diluted to 20-wt% for coagulant testing and ~10-wt% solids for flocculation.

#### 4.1.1 Dean Stark extraction

Results of Dean Stark analysis are summarized in Table 4-1 as the bitumen, water, and mineral solids in FFT. Dean Stark analysis for each FFT gave similar bitumen, water, and mineral fractions. Bitumen content for cyclone overflow is also presented but complete Dean Stark results were not available from this reference.

#### 4.1.2 Particle size distribution

Sieve analysis was used to quantify and remove solids greater than 45- $\mu\text{m}$  for both FFT-1 and FFT-2 samples with solids finer than 45- $\mu\text{m}$  characterized using SediGraph. Cyclone O/F from Jeeravipoolvarn (2010) was sieved to characterize the 45- $\mu\text{m}$  solids with the fine particles passing 45- $\mu\text{m}$  characterized using hydrometer.

##### 4.1.2.1 Sieve

Results of sieve analysis are summarized in Table 4-1 as the fraction of mineral solids less than 45- $\mu\text{m}$  and the sand-to-fines (SFR). SFR for FFT-1 and FFT-2 are 0.04 and 0.35 respectively.

##### 4.1.2.2 SediGraph

Mineral solids finer than 45- $\mu\text{m}$  were analyzed using SediGraph and results are presented in Figure 4-1. Figure 4-1 includes Sedigraph data for both FFT-1 and FFT-2 samples along with reference lines for both 2- $\mu\text{m}$  and 45- $\mu\text{m}$ . Although the mineral solids were sieved to remove particles larger than 45- $\mu\text{m}$  there are still particles of this size and larger included in the SediGraph measurement. This may be because some particles passed through the sieve that are not spherical and may be less than 45- $\mu\text{m}$  in two dimensions but larger in the third dimension. Cyclone overflow used by Jeeravipoolvarn (2010) was analyzed using hydrometer and the results from testing of dispersed samples measured 94% fines and 30% clay (< 2-  $\mu\text{m}$ ).

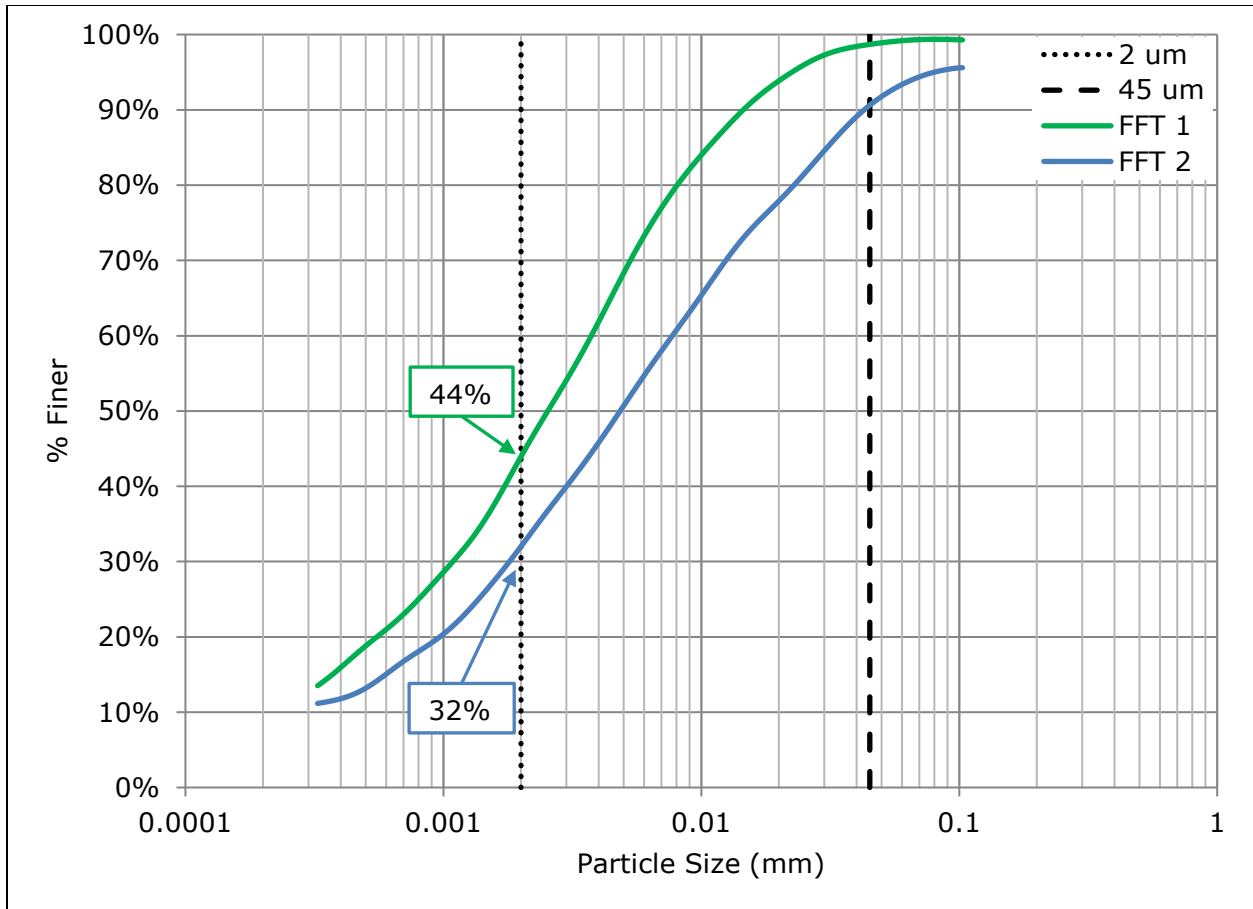


Figure 4-1 – Particle size distribution of FFT Dean-Stark solids (<45- $\mu$ m) by SediGraph

#### 4.1.3 Methylene blue

Clay content by methylene blue is summarized in Table 4-1 for each of the FFT samples. Clay content by methylene blue for cyclone overflow is not presented since results were not available from this reference. Methylene blue testing was done on solids retrieved from Dean & Stark extraction so samples are free of bitumen. Clay content by methylene blue was 74.1-wt% for FFT-1 and 57.9-wt% for FFT-2. The higher clay content of FFT-1 compared to FFT-2 is supported by the XRD analyses discussed in the mineralogy Section 4.1.5.

#### 4.1.4 Water chemistry

Results from water chemistry analyses are shown in Table 4-2. Sodium adsorption ratio (SAR) was calculated and included with the water chemistry data. The most notable differences in water chemistry are the higher ionic strength and SAR of FFT-2 compared to FFT-1. The SAR for both FFT-1 and FFT-2 are 16 and 38 respectively which represents a dispersed structure. Tailings having SAR greater than 7 is indicative of a disperse structure (Miller 2010).

Table 4-2 – Pore water chemistry for as-received FFT

	Conductivity (mS/cm)	Aqueous Ion Concentration (mg/L)									pH	SAR
		Ca <sup>2+</sup>	Na <sup>+</sup>	K <sup>+</sup>	Mg <sup>2+</sup>	Al <sup>3+/2+</sup>	Cl <sup>-</sup>	SO <sub>4</sub> <sup>2-</sup>	HCO <sub>3</sub> <sup>-</sup>	CO <sub>3</sub> <sup>2-</sup>		
FFT-1	1.75	23	378	15	12	0	216	2	750	0	8.08	16
FFT-2	2.93	9	551	7	4	0	222	7	1015	27	8.31	38

#### 4.1.5 Mineralogy

The XRD spectra for FFT-1 and FFT-2 are shown in Figure 4-2 and Figure 4-3 respectively. Quantification results for the two tailings samples are shown in Table 4-3 with major constituents being kaolin, illite, and quartz. Clay content by XRD methods is determined from the summation of kaolin and illite fractions which yielded 54.74-wt% and 33.34-wt% for FFT-1 and FFT-2 respectively. Quartz content measured 35.97-wt% and 60-76-wt% for FFT-1 and FFT-2 respectively. Note that for quantification of minor constituents the uncertainty can be greater than the concentration. Because of this uncertainty, only major constituents were considered when comparing tailings samples for selection for the flocculation portion of this study. Clay content as determined by Sedigraph, methylene blue, and XRD are summarized in Table 4-4. Note that FFT-1 has higher clay content than FFT-2 irrespective of method used for clay determination.

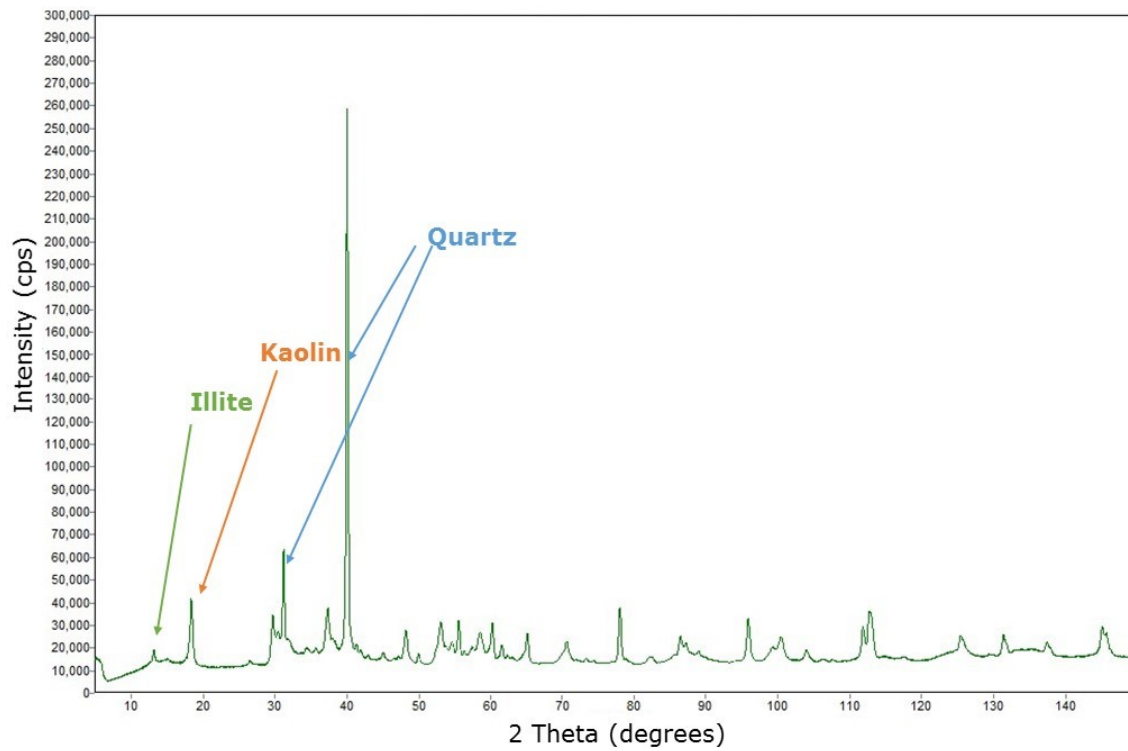


Figure 4-2 – Jade output XRD spectra for FFT-1

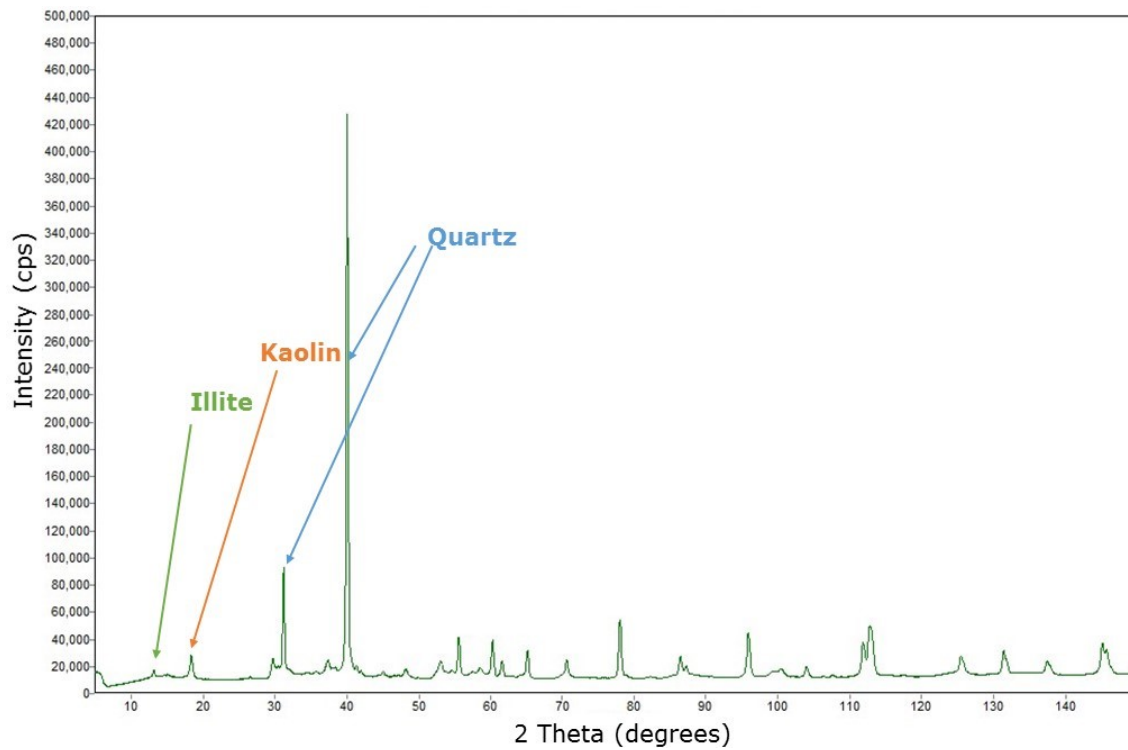


Figure 4-3 - Jade output XRD spectra for FFT-2

Table 4-3 – Tailings mineral quantification using XRD methods

		FFT-1		FFT-2	
		%Conc. w/w	%Uncertainty	%Conc. w/w	%Uncertainty
Clays	Kaolin	32.44	1.7	16.43	1.6
	Illite	22.24	1.6	16.71	1.7
	Chlorite	0.07	0.3	0.20	0.3
Carbonates	Calcite (CaCO <sub>3</sub> )	0.53	0.3	0.59	0.3
	Siderite (FeCO <sub>3</sub> )	4.06	0.5	2.09	0.5
Titanium oxides (TiO <sub>2</sub> )	Anatase	3.21	0.7	2.12	0.7
	Rutile	0.14	0.2	0.07	0.2
Feldspars	Microcline	-	-	0.94	0.6
	Pyrite (FeS <sub>2</sub> )	1.25	0.2	0.07	0.1
	Zircon	0.12	0.1	0.03	0.1
	Quartz (SiO <sub>2</sub> )	35.97	1.1	60.76	1.4
Total %Clay		54.74	-	33.34	-

Table 4-4 – FFT clay content by different measurement methods

	FFT-1	FFT-2
Measurement Technique	%Conc. w/w	
Sedigraph	44%	32%
Methylene Blue	74%	58%
XRD	55%	33%

#### 4.1.6 Coagulant properties

To check the purity of the coagulants each one was dissolved in deionized water at a known concentration then compared to water chemistry results (Table 4-5). Considering the low relative percent difference between predicted and measured values, the accuracy of sample preparation and water chemistry analysis it is safe to assume a coagulant purity of 100% for the purpose of dosage calculations in this study.

Table 4-5 – Water chemistry for coagulants dissolved in deionized water

Aqueous Ion Concentration (mg/L)									
Coagulant / <u>predicted concentration</u>	Ca <sup>2+</sup>	Na <sup>+</sup>	K <sup>+</sup>	Mg <sup>2+</sup>	Al <sup>3+/2+</sup>	Cl <sup>-</sup>	SO <sub>4</sub> <sup>2-</sup>	pH	Relative percent difference
K-Alum									
( <u>132</u> mg/L Al <sup>3+</sup> )	5	0	200	1	<u>138</u>	3	931	3.74	4.3%
Gypsum									
( <u>407</u> mg/L Ca <sup>2+</sup> )	<u>435</u>	0	0	0	0	3	966	6.05	6.7%
Magnesium chloride									
( <u>297</u> mg/L Mg <sup>2+</sup> )	13	4	9	<u>313</u>	0	867	7	6.25	5.2%

## 4.2 Tailings treatment

To optimize coagulation of FFT, both of the tailings samples were treated with one of three coagulants at a number of dosages then assessed using the CST test. Each coagulation test consisted of measuring the CST value five times which was then used to calculate the standard deviation for further use as error bars in the following three figures.

For each condition, samples were retained for water chemistry analysis to determine conductivity, pH, and ions of interest.

Presented in Figure 4-4 is the response of capillary suction time to increases in K-alum dosage tested on FFT-1 and FFT-2. Optimum dosages were found using the technique described in Section 3.2 and are labeled on the plot.

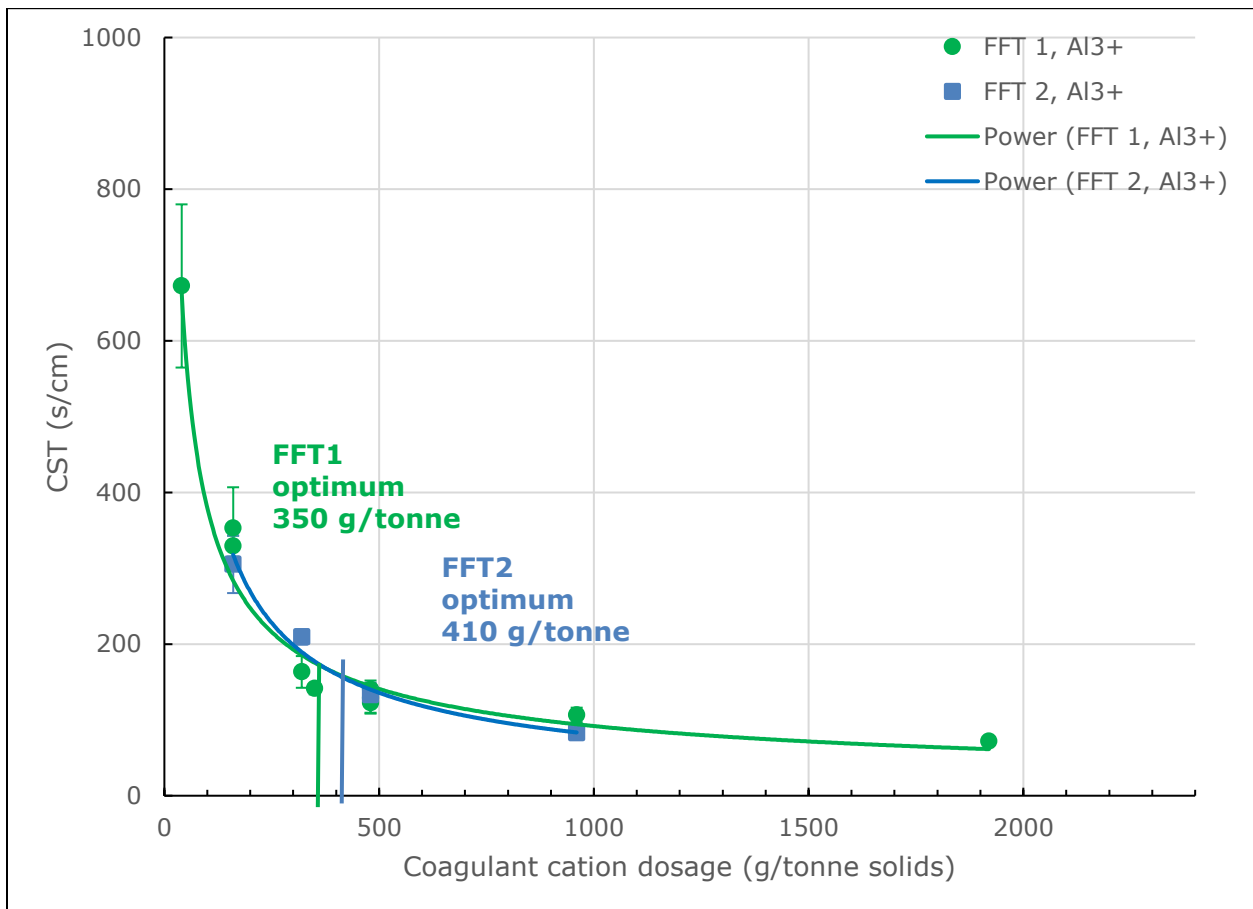


Figure 4-4 – Capillary suction time for different K-alum (Al<sup>3+</sup>) dosages for FFT-1 and FFT-2 where the error bars represent the standard deviation of multiple CST measurements

Presented below in Figure 4-5 is the response of capillary suction time to increases in gypsum dosage tested on FFT-1 and FFT-2. Optimum dosages were found using the technique described in Section 3.2 and are labeled on the plot.

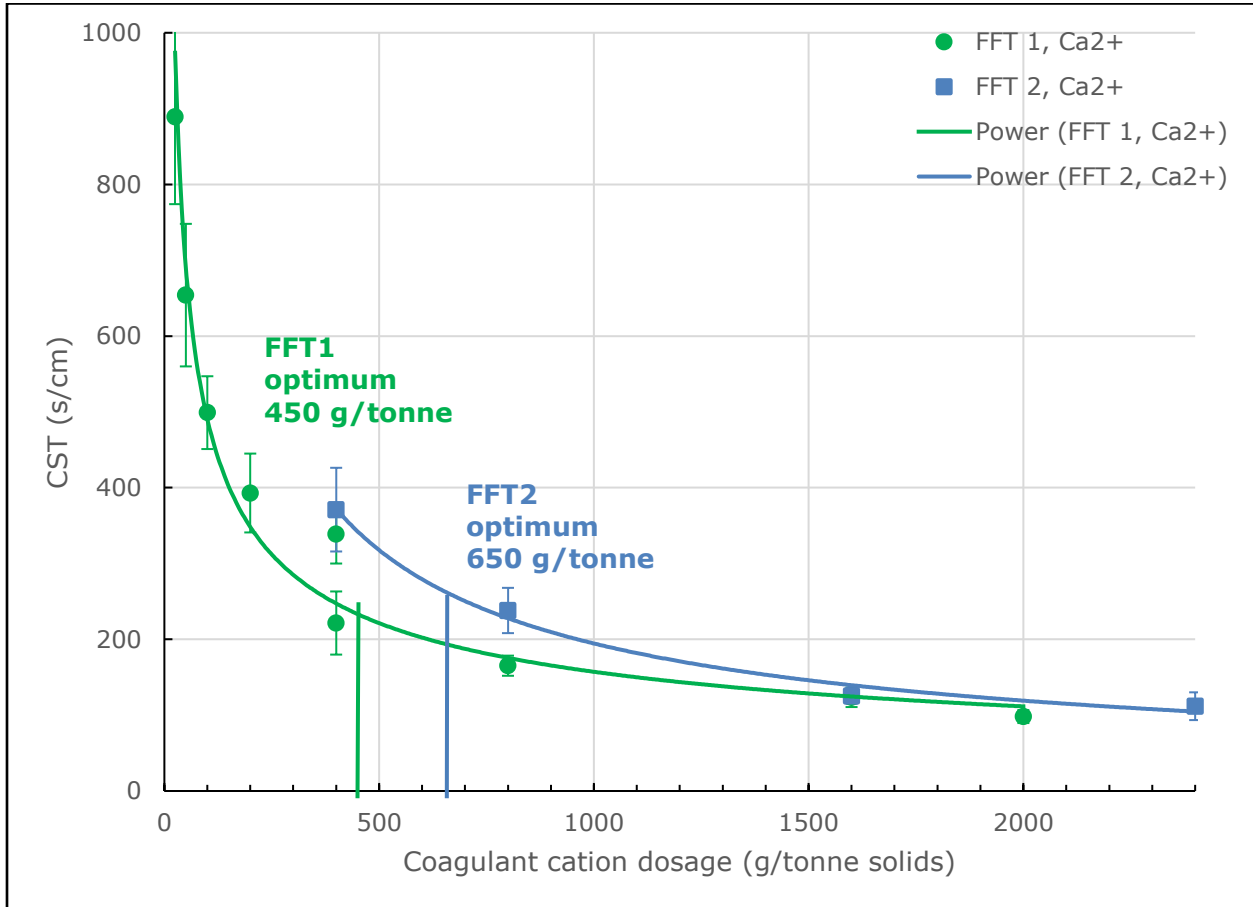


Figure 4-5 – Capillary suction time for different gypsum (Ca<sup>2+</sup>) dosages for FFT-1 and FFT-2 where the error bars represent the standard deviation of multiple CST measurements

Presented below in Figure 4-6 is the response of capillary suction time to increases in magnesium chloride dosage tested on FFT-1 and FFT-2. Optimum dosages were found using the technique described in Section 3.2 and are labeled on the plot. Note that the range of dosages for magnesium chloride is smaller than that of K-alum and gypsum. This is because once it was realized that the inflection point presented a good optimum dosage it was not necessary to test further once the inflection point on the plot was realized.

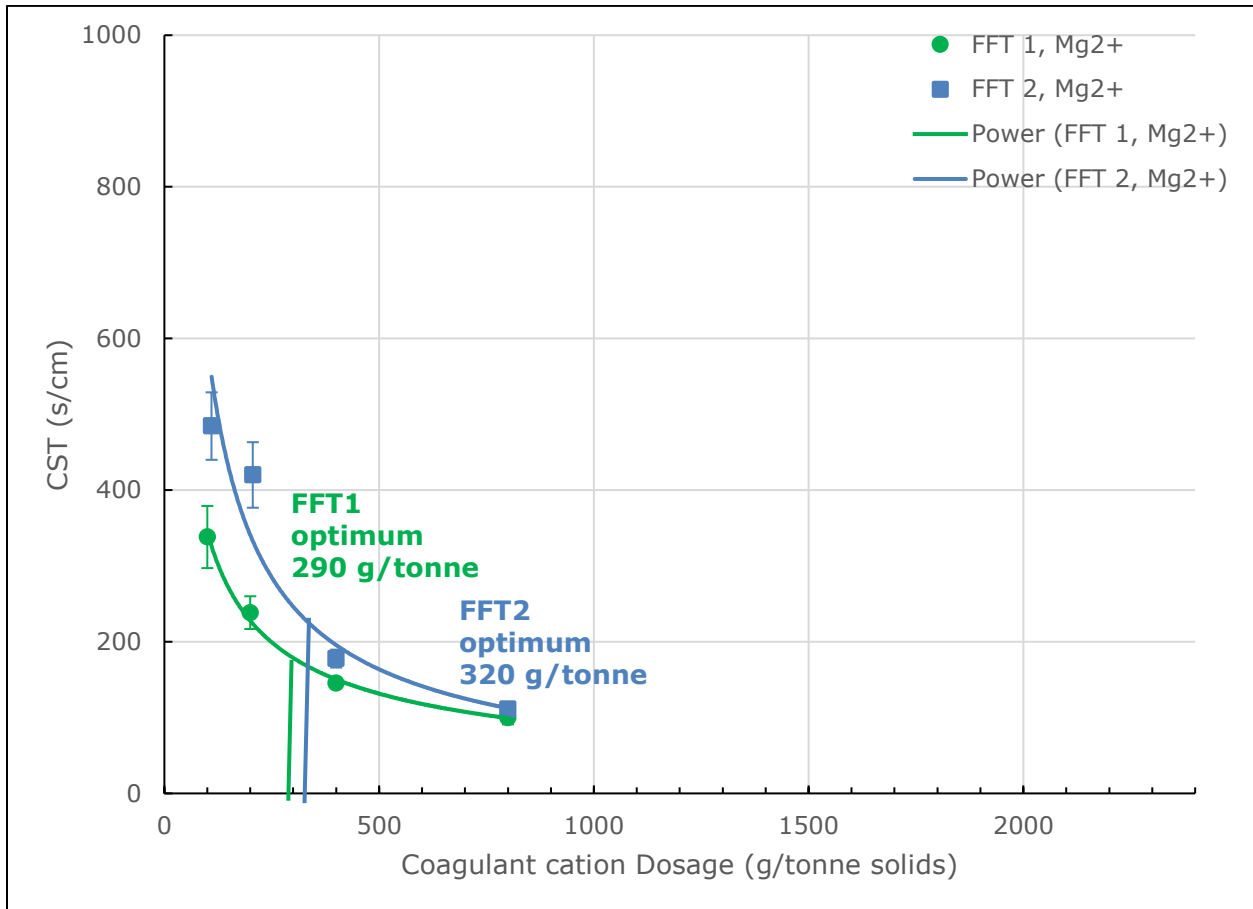
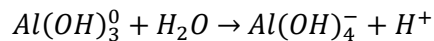
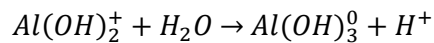
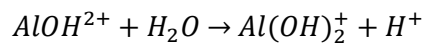
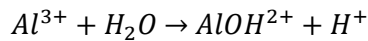


Figure 4-6 – Capillary suction time for different magnesium chloride (Mg<sup>2+</sup>) dosages for FFT-1 and FFT-2 where the error bars represent the standard deviation of multiple CST measurements

Water chemistry data for FFT treated with K-alum, gypsum, and magnesium chloride treatments are shown in Table 4-6, Table 4-7, and Table 4-8 respectively. For some of the FFT coagulation testing only a limited number of dosages were tested. This is because only enough dosages were tested to realize the inflection point on the plot of CST versus dosage for optimum dosage determination.

For the K-alum dosing shown in Table 4-6 note the increase in cation concentrations, in particular all cations aside from  $K^+$  and  $Al^{3+/2+}$ . The increasing concentration of  $K^+$  and  $Al^{3+/2+}$  is expected since these elements were added in the form of K-alum. The other cations increase with increasing K-alum dosing is because they are initially adsorbed to the clay surfaces and are subsequently released to the pore water after the addition of K-alum. This observation is important because changes in oil sand process water chemistry induced by coagulant addition can impact bitumen extraction, given that water released by treating tailings is recycled to extraction. In particular the increased calcium can form calcium carbonate scaling on piping. In depth study of the effect of water chemistry on extraction is beyond the scope of this project but it is recognized that water chemistry plays a large part on oil sands extraction efficiency.  $Al^{3+/2+}$  isn't present in solution until higher dosages of K-alum are added to the FFT which suggests that  $Al^{3+/2+}$  is in excess at dosages around 960 g/tonne for these FFT samples. The acidity of pore water tends to increase with increasing K-alum dosage. This is due to metal hydrolysis which for aluminum occurs by stepwise dissociation of the waters of hydration to yield protons. See chemical reactions below for metal hydrolysis (Essington 2004).



For the gypsum dosing of FFT in Table 4-7 the pH isn't affected by added gypsum but ion concentrations of course increase.  $HCO_3^-$  decreases slightly with increasing gypsum addition which suggests that the pH is maintained by the bicarbonate buffering system. Replicate CST testing was done around the suspected optimum dosages for K-alum and gypsum to ensure repeatability.

For magnesium chloride dosing of FFT the data in Table 4-8 show that the pH is unchanged with increases in dosage due to the bicarbonate buffering system. Slight increases in ion concentration are seen, with the exception of  $HCO_3^-$ .

Table 4-6 – Water chemistry for FFT coagulated with K-alum (Al<sup>3+</sup>)

FFT	Cation	M <sup>n+</sup> dosage (g/tonne of solids)	CST (s/cm)	Conductivity (mS/cm)	Aqueous Ion Concentration (mg/L)								
					Ca <sup>2+</sup>	Na <sup>+</sup>	K <sup>+</sup>	Mg <sup>2+</sup>	Al <sup>3+/2+</sup>	Cl <sup>-</sup>	SO <sub>4</sub> <sup>2-</sup>	HCO <sub>3</sub> <sup>-</sup>	pH
FFT-1	Control	0	-	0.66	7	134	10	3	0	55	20	273	8.32
FFT-1	Al <sup>3+</sup>	40	672	0.98	17	159	18	9	0	65	175	236	8.22
FFT-1	Al <sup>3+</sup>	160	353	1.20	31	173	39	14	0	63	358	130	7.97
FFT-1	Al <sup>3+</sup>	160	329	1.27	35	183	40	17	0	65	399	124	8.03
FFT-1	Al <sup>3+</sup>	320	163	1.64	73	196	81	31	0	61	621	107	7.46
FFT-1	Al <sup>3+</sup>	480	122	2.06	115	208	128	47	0	63	926	15	7.11
FFT-1	Al <sup>3+</sup>	480	129	2.02	102	212	124	47	0	63	908	20	7.09
FFT-1	Al <sup>3+</sup>	480	140	2.10	115	225	125	45	0	68	925	38	7.32
FFT-1	Al <sup>3+</sup>	960	107	3.37	272	274	311	116	1	70	1764	16	6.50
FFT-1	Al <sup>3+</sup>	1920	72	5.29	471	283	690	183	42	69	3221	0	4.41
FFT-2	Al <sup>3+</sup>	160	305	1.93	28	353	47	11	0	140	517	244	8.10
FFT-2	Al <sup>3+</sup>	320	209	2.36	71	384	88	19	0	139	831	126	7.90
FFT-2	Al <sup>3+</sup>	480	133	2.81	125	412	160	33	0	136	1157	64	7.52
FFT-2	Al <sup>3+</sup>	960	83	4.09	289	456	341	78	1	133	1980	2	5.54

Table 4-7 – Water chemistry for FFT coagulated with gypsum (Ca<sup>2+</sup>)

FFT	Cation	M <sup>n+</sup> dosage (g/tonne of solids)	CST (s/cm)	Conductivity (mS/cm)	Aqueous Ion Concentration (mg/L)								
					Ca <sup>2+</sup>	Na <sup>+</sup>	K <sup>+</sup>	Mg <sup>2+</sup>	Al <sup>3+/2+</sup>	Cl <sup>-</sup>	SO <sub>4</sub> <sup>2-</sup>	HCO <sub>3</sub> <sup>-</sup>	pH
FFT-1	Control	0	-	0.66	7	134	10	3	0	55	20	273	8.32
FFT-1	Ca <sup>2+</sup>	25	889	0.81	21	142	16	7	0	60	110	289	8.05
FFT-1	Ca <sup>2+</sup>	50	654	0.85	24	142	16	8	0	60	124	288	8.04
FFT-1	Ca <sup>2+</sup>	100	499	0.89	30	150	18	10	0	59	142	314	8.04
FFT-1	Ca <sup>2+</sup>	200	393	0.99	44	157	19	14	0	58	209	289	7.97
FFT-1	Ca <sup>2+</sup>	400	222	1.43	57	202	20	23	0	72	297	320	8.08
FFT-1	Ca <sup>2+</sup>	400	339	1.15	72	164	22	20	0	57	311	278	7.97
FFT-1	Ca <sup>2+</sup>	800	165	1.76	108	228	34	40	0	67	557	273	8.06
FFT-1	Ca <sup>2+</sup>	1600	124	2.30	247	244	29	57	0	69	1041	211	8.05
FFT-1	Ca <sup>2+</sup>	2000	98	2.66	327	250	56	70	0	71	1323	193	7.89
FFT-2	Ca <sup>2+</sup>	400	371	1.88	49	360	15	14	0	140	448	380	8.04
FFT-2	Ca <sup>2+</sup>	800	238	2.21	103	398	22	22	0	141	701	286	8.04
FFT-2	Ca <sup>2+</sup>	1600	125	2.91	280	407	26	39	0	141	1252	187	7.90
FFT-2	Ca <sup>2+</sup>	2400	112	3.21	375	434	28	45	0	141	1514	17	7.88

Table 4-8 – Water chemistry for FFT coagulated with magnesium chloride (Mg<sup>2+</sup>)

FFT	Cation	M <sup>n+</sup> dosage (g/tonne of solids)	CST (s/cm)	Conductivity (mS/cm)	Aqueous Ion Concentration (mg/L)								
					Ca <sup>2+</sup>	Na <sup>+</sup>	K <sup>+</sup>	Mg <sup>2+</sup>	Al <sup>3+/2+</sup>	Cl <sup>-</sup>	SO <sub>4</sub> <sup>2-</sup>	HCO <sub>3</sub> <sup>-</sup>	pH
FFT-1	Control	0	-	0.66	7	134	10	3	0	55	20	273	8.32
FFT-1	Mg <sup>2+</sup>	100	338	1.23	26	192	17	17	0	148	82	365	8.08
FFT-1	Mg <sup>2+</sup>	200	238	1.35	31	181	19	24	0	223	66	299	8.26
FFT-1	Mg <sup>2+</sup>	400	146	1.80	55	205	23	50	0	377	92	281	8.08
FFT-1	Mg <sup>2+</sup>	800	100	2.65	91	238	34	128	0	613	98	250	8.03
FFT-2	Mg <sup>2+</sup>	110	485	1.74	19	335	14	11	0	231	186	409	8.17
FFT-2	Mg <sup>2+</sup>	206	420	1.94	28	348	15	19	0	307	183	385	8.16
FFT-2	Mg <sup>2+</sup>	400	178	2.39	43	355	18	41	0	457	173	370	8.15
FFT-2	Mg <sup>2+</sup>	800	111	3.24	79	393	24	121	0	784	183	311	8.22

Tailings treatment in this project included optimization of the coagulation treatment using CST measurement on each of the test conditions. Pore water chemistry was analyzed to observe changes induced by coagulant addition. Tailings sample FFT-1 coagulated with either K-alum or gypsum was selected for the flocculation portion of this study. Magnesium chloride was ultimately excluded since it didn't stand out as a top performer and is not currently a coagulant used in oil sands tailings industry. Flocculant dosages were determined according to the method described in Section 3.2. The required flocculant dosage for FFT-1 coagulated with K-alum was 1250 g/tonne of solids. The required flocculant dosage for FFT-1 coagulated with gypsum was 900 g/tonne of solids. These two dosages were the optimum since they were the minimum amounts of polymer flocculant needed to obtain visible floc formation with low turbidity release water. Turbidity was not measured but was apparent when water was clear with no visible solids in suspension.

#### 4.3 Floc measurement

Floc measurements were made using photography with image analysis. One of the images that was analyzed for floc size distribution is shown in Figure 4-7 and the associated floc size distribution is shown in Figure 4-8. Between 10 and 20 images were used for each floc size distribution determination depending on the quality of images obtained. Images were captured during continuous sedimentation of the sample as flocs settled through water. All images captured, during the generation of the four samples, were analyzed in a similar fashion then compiled to get a representative floc-size distribution for each treatment condition. Error in this measurement is taken as the standard deviation determined for the test beads using the same image analysis procedure that was used for the floc size measurements. The floc size distributions for each test condition are presented in Figure 4-9. Note that the error bars on the plot are all the same value but appear to be different sizes due to the logarithmic scale on the x-axis. Table 4-9 shows the floc size distribution summary for each of the four FFT-1 treatment conditions.

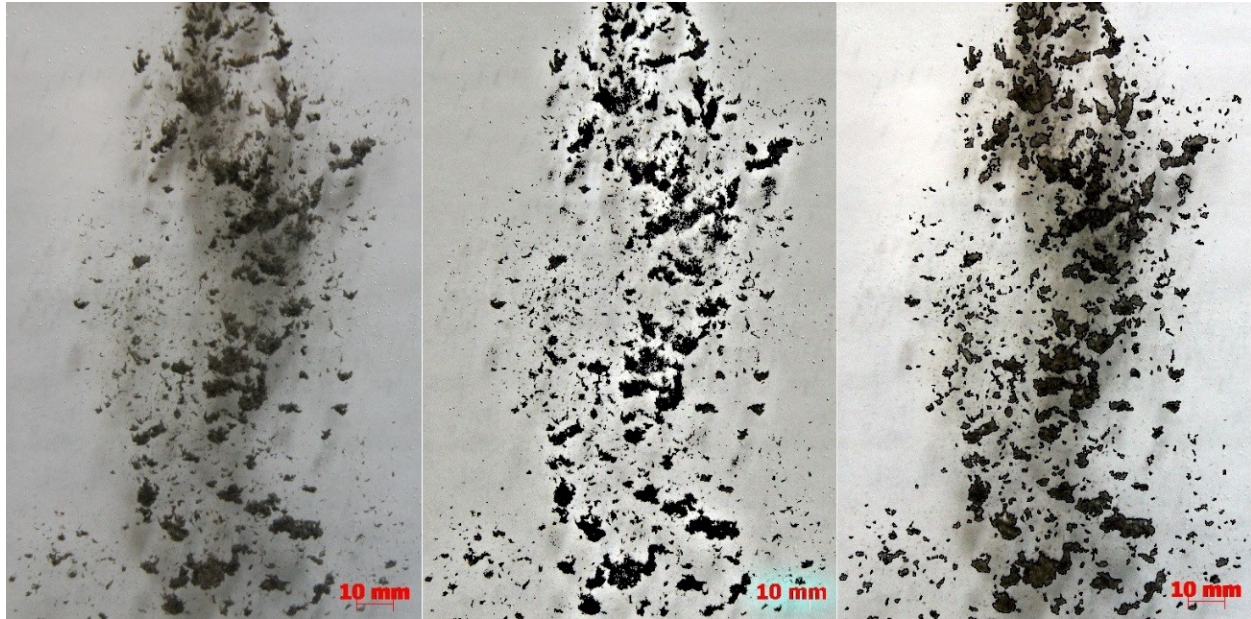


Figure 4-7 – Photos of flocs throughout image analysis process (1) raw image, (2) image after brightness adjustment and floc identification, (3) image of flocs surrounded by black border identifying flocs to be counted and sized

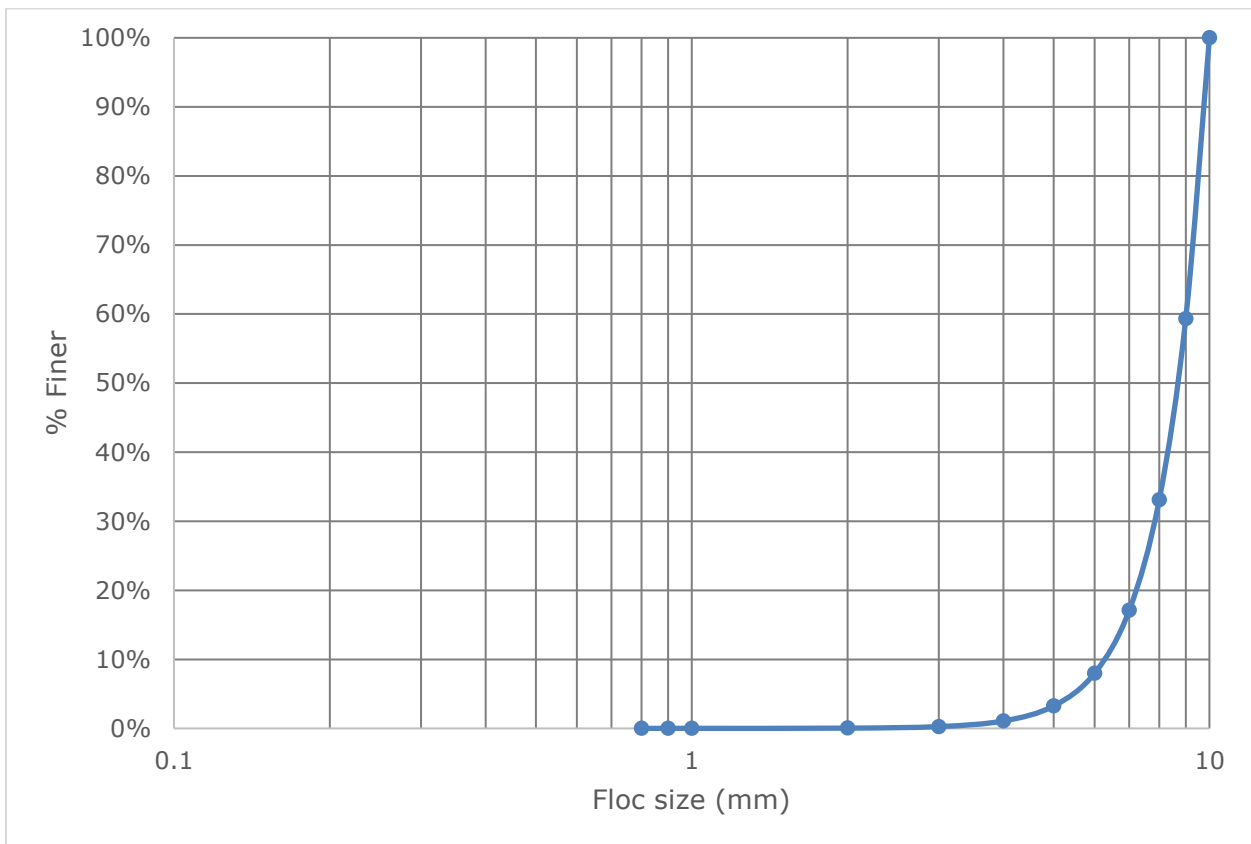


Figure 4-8 – Floc size distribution for above image (Figure 4-7)

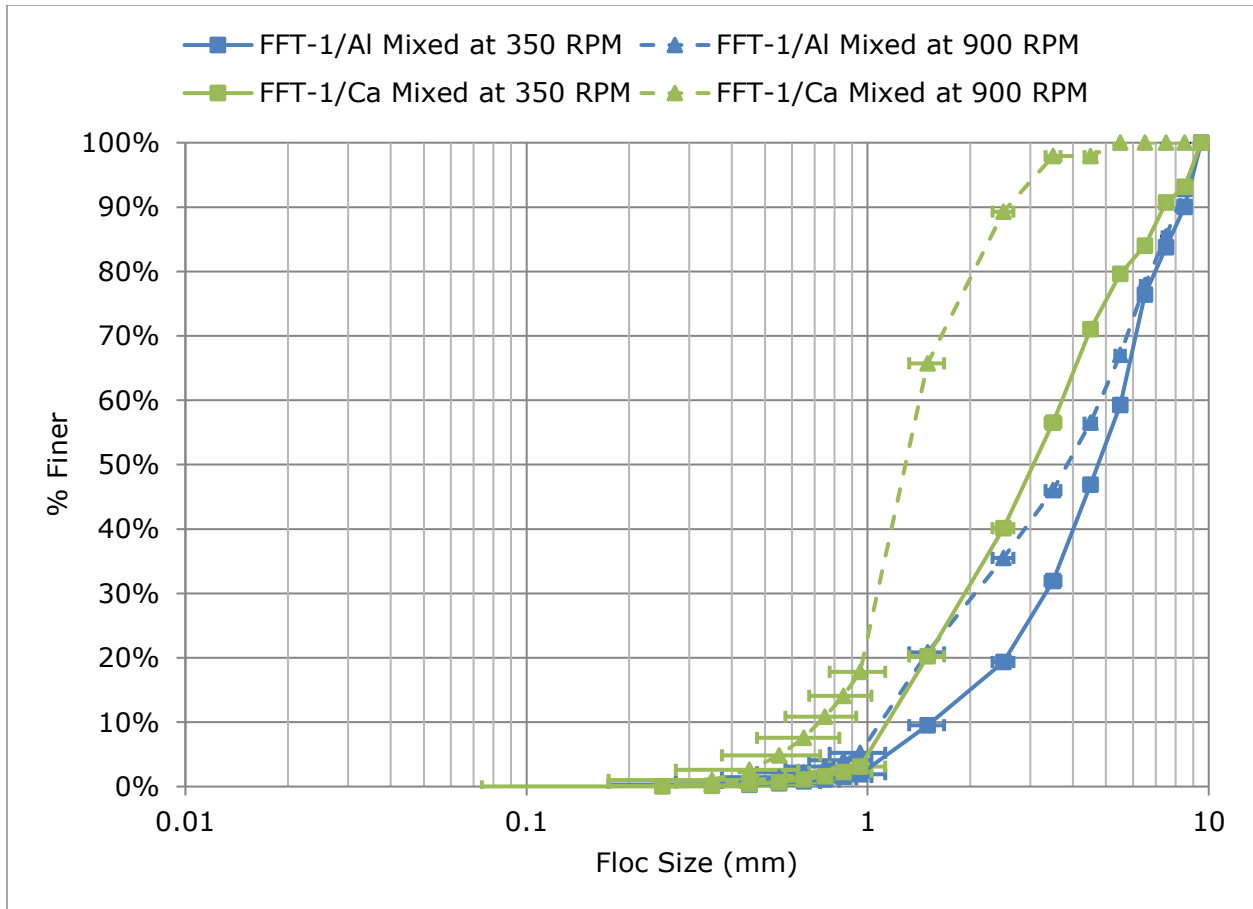


Figure 4-9 – Floc size distribution for FFT-1 treated with either K-alum (FFT-1/Al) or gypsum (FFT-1/Ca) and flocculated with A3338 at two different mixing speeds

Table 4-9 – Floc size distribution summary for FFT-1 treated with either K-alum (FFT-1/Al) or gypsum (FFT-1/Ca) and flocculated with A3338 at two different mixing speeds where  $D_{xx}$  is the floc diameter for which xx percentage are smaller than

	FFT-1/Al Mixed at 350 RPM	FFT-1/Al Mixed at 900 RPM	FFT-1/Ca Mixed at 350 RPM	FFT-1/Ca Mixed at 900 RPM
$D_{90}$ (mm)	8.5	8.1	7.4	2.6
$D_{75}$ (mm)	6.4	6.2	6.8	1.9
$D_{50}$ (mm)	4.8	3.9	3.1	1.3
$D_{25}$ (mm)	3.0	1.8	1.8	1.0
$D_{10}$ (mm)	1.5	1.1	1.1	0.7

Of the four FFT samples generated using FFT-1 only the two coagulated with K-alum were used for the remainder of the program. Specifically only these two samples were subjected to large strain consolidation testing then compared to results presented by (Jeeravipoolvarn 2010). The flocculated FFT-

1 samples coagulated with K-alum were selected over the gypsum treated samples because larger flocs were observed with the K-alum samples. Ideally all samples would have been subjected to consolidation testing but equipment availability was an issue. Figure 4-10 shows the floc size distribution of FFT-1 treated with K-alum and A3338 polymer as well as in-line thickened tailings (ILTT) treated with anionic flocculant Magnafloc 6260 and cationic coagulant Magnafloc 368 both sheared and non-sheared as reported by (Jeeravipoolvarn 2010).

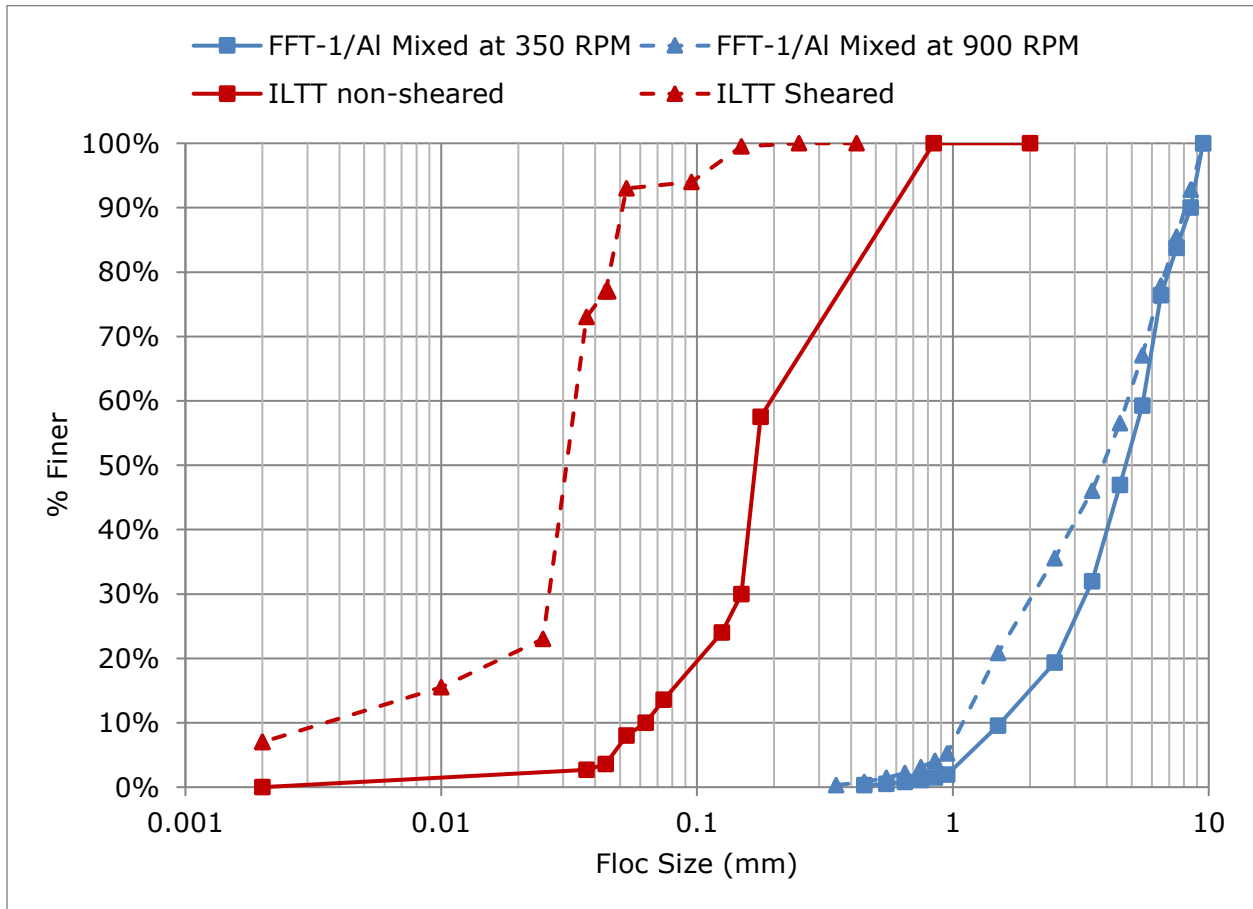


Figure 4-10 - Floc size distribution for FFT-1 treated with K-alum and flocculated with A3338 at two different mixing speeds compared to ILTT non-sheared and sheared samples by Jeeravipoolvarn (2010)

Tailings sample FFT-1 was coagulated with each of the two coagulants (K-alum and gypsum) then flocculated with A3338 polymer using two mixing speeds (350 RPM or 900 RPM). The floc size distribution was measured for each of the four conditions. The two samples coagulated with K-alum were selected for large strain consolidation testing and comparison to ILTT results from (Jeeravipoolvarn 2010).

#### 4.4 Geotechnical properties

Geotechnical testing on chemically amended tailings samples for this study include Atterberg limits, compressibility, hydraulic conductivity and vane shear strength. The Atterberg limits were determined for FFT-1 coagulated with either K-alum or gypsum and flocculated with A3338. Of the four samples generated during the flocculation portion of the project, only those coagulated with K-alum were subjected to consolidation testing, hydraulic conductivity measurement, and vane shear testing. The flocculated FFT-1 samples coagulated with K-alum were selected over the gypsum treated samples because larger flocs were observed with the K-alum samples. Atterberg limits included liquid and plastic limits. Compressibility and hydraulic conductivity was measured using the large strain consolidation (LSC) procedure. Vane shear strength was measured after each hydraulic conductivity measurement to document increases in shear strength with decreasing moisture content and void ratio.

##### 4.4.1 Atterberg limits

Fall cone testing for FFT-1, untreated and treated, yielded both the undrained shear strength as a function of moisture content and the liquid limit, as shown in Figure 4-11. For untreated FFT the liquid limit from fall cone measured 49% while plastic limit from hand rolling was 22%. FFT-1 treated with K-alum and A3338 the liquid limit measured 73% while plastic limit as 28%. FFT-1 treated with gypsum and A3338 the liquid limit measured 69% while plastic limit was 27%. The vane shear strength as a function of solids content is presented in Figure 4-12. This data is also shown in Figure 4-13 overlaid on a plot of shear strength as a function of solids content that was created by McKenna et al. (2016). Note in Figure 4-13 that the treated FFT samples move passed the liquid limit at lower solids contents than that of unammended FFT which means treatment permits trafficability at higher moisture contents.

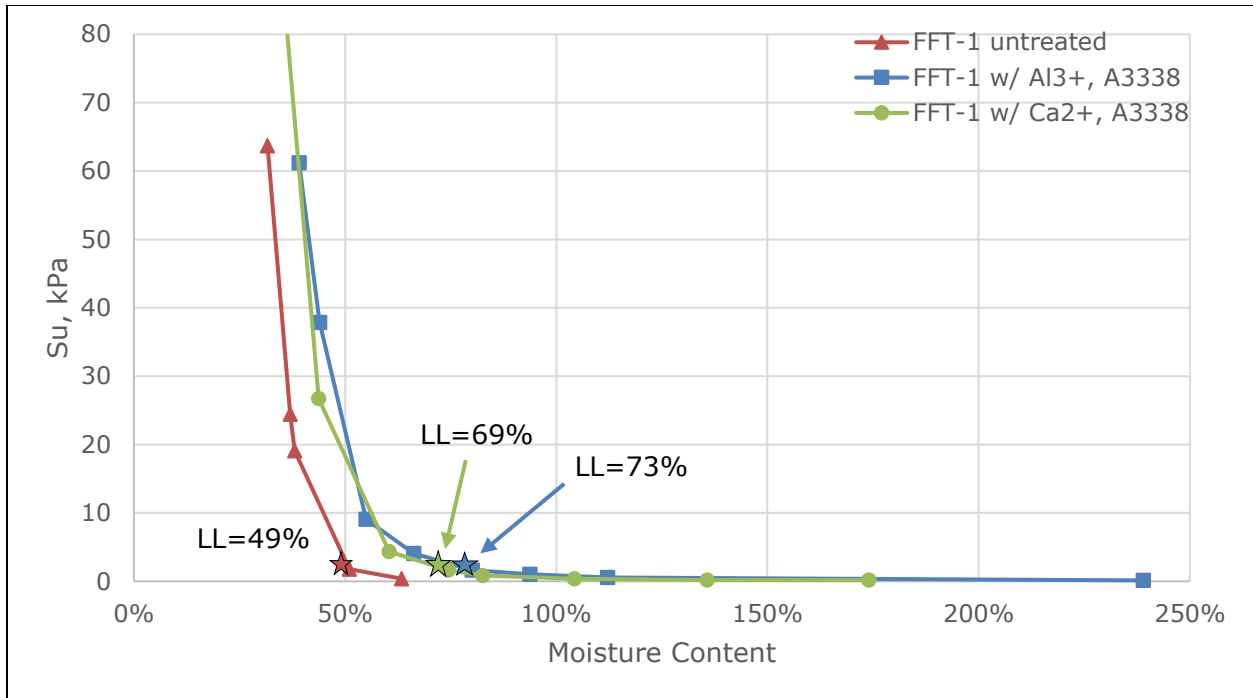


Figure 4-11 – Undrained shear strength as a function of moisture content ( $M_{\text{water}}/M_{\text{solids}}$ ) with liquid limit measured using fall cone for FFT-1 untreated and treated samples

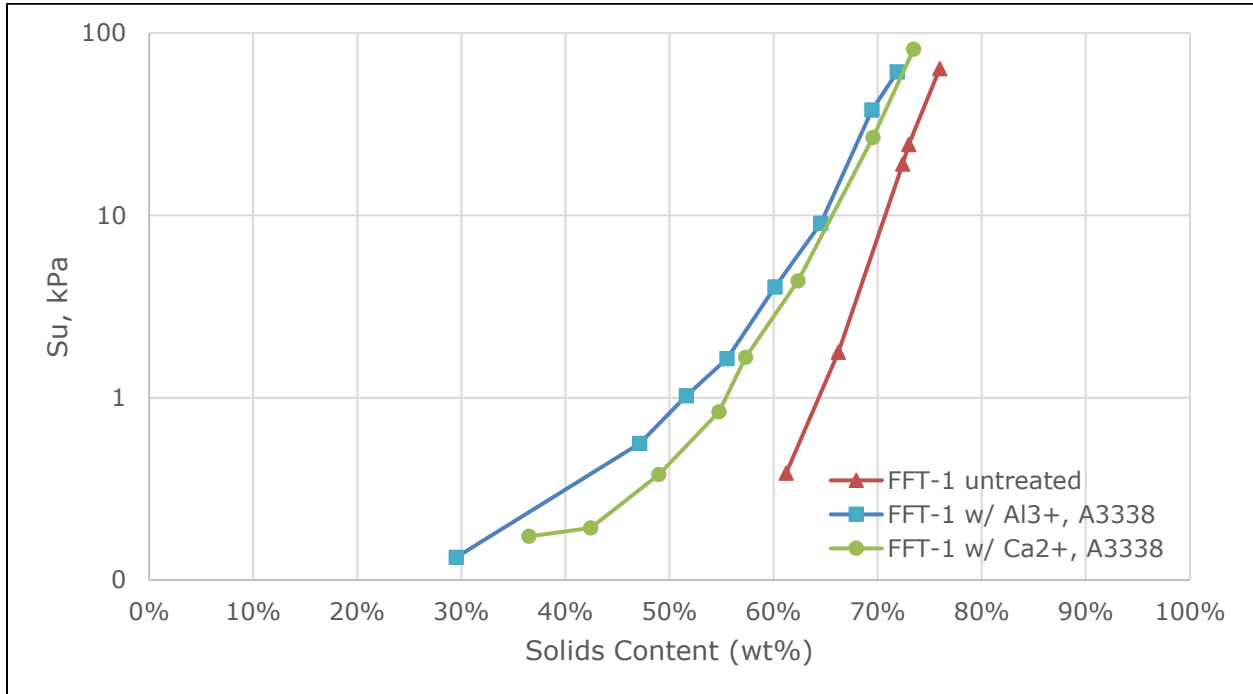


Figure 4-12 – Undrained shear strength as a function of solids content using fall cone for FFT-1 untreated and treated samples

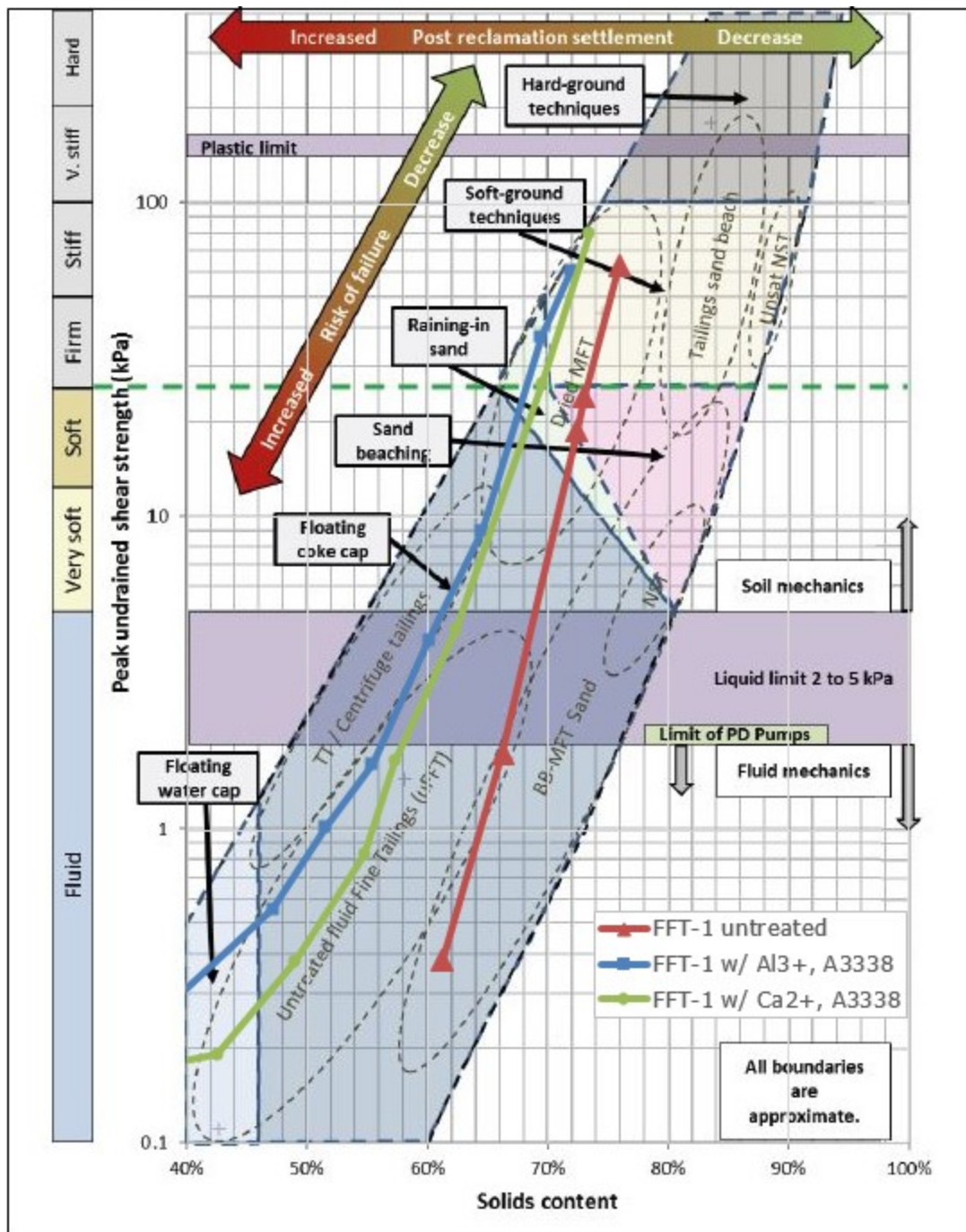


Figure 4-13 – Shear strength and solids content of oil sands fine tailings from McKenna et al. 2016 with strength data overlay from this project

#### 4.4.2 Large strain consolidation

Large strain consolidation testing was carried out on tailings sample FFT-1 coagulated with K-alum and flocculated with A3338 mixed at either 350 RPM or 900 RPM. Compressibility data for these samples are presented in Figure 4-14. In addition, compressibility data for in-line thickened tailings (ILTT), both sheared and non-sheared, are presented in Figure 4-14 for comparison (Jeeravipoolvarn 2010). It appears that shearing of flocculated tailings samples doesn't have a large impact on total settlement at higher void ratios but at lower void ratios there is a greater impact on compressibility. The differences in compressibility at lower void ratios is more prominent for FFT-1 samples than the ILTT samples.

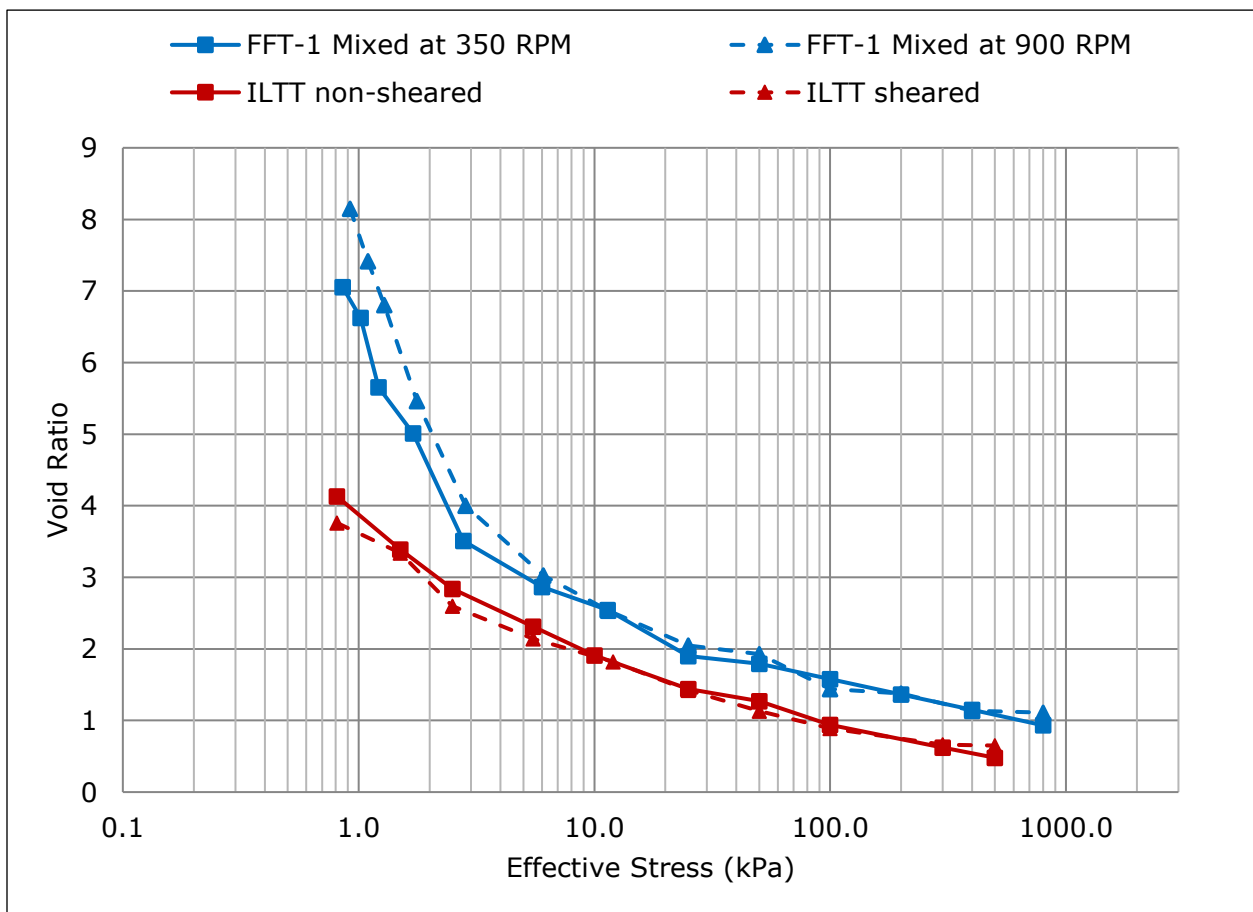


Figure 4-14 – Compressibility of FFT-1 coagulated with K-Alum and flocculated using two different mixing speeds compared to ILTT (Jeeravipoolvarn 2010)

#### 4.4.3 Hydraulic conductivity

Hydraulic conductivity testing was carried out on tailings sample FFT-1 coagulated with K-alum and flocculated with A3338 mixed at either 350 RPM or 900 RPM. Hydraulic conductivity data for these samples are presented in Figure 4-15. In addition, hydraulic conductivity data for in-line thickened tailings (ILTT), both sheared and non-sheared, are presented in Figure 4-15 for comparison (Jeeravipoolvarn 2010). At low void ratio there appears to be almost an order of magnitude difference between hydraulic conductivity for FFT-1 sheared at 350 RPM and 900 RPM, but due to the inherent error associated with this measurement these differences are minimal.

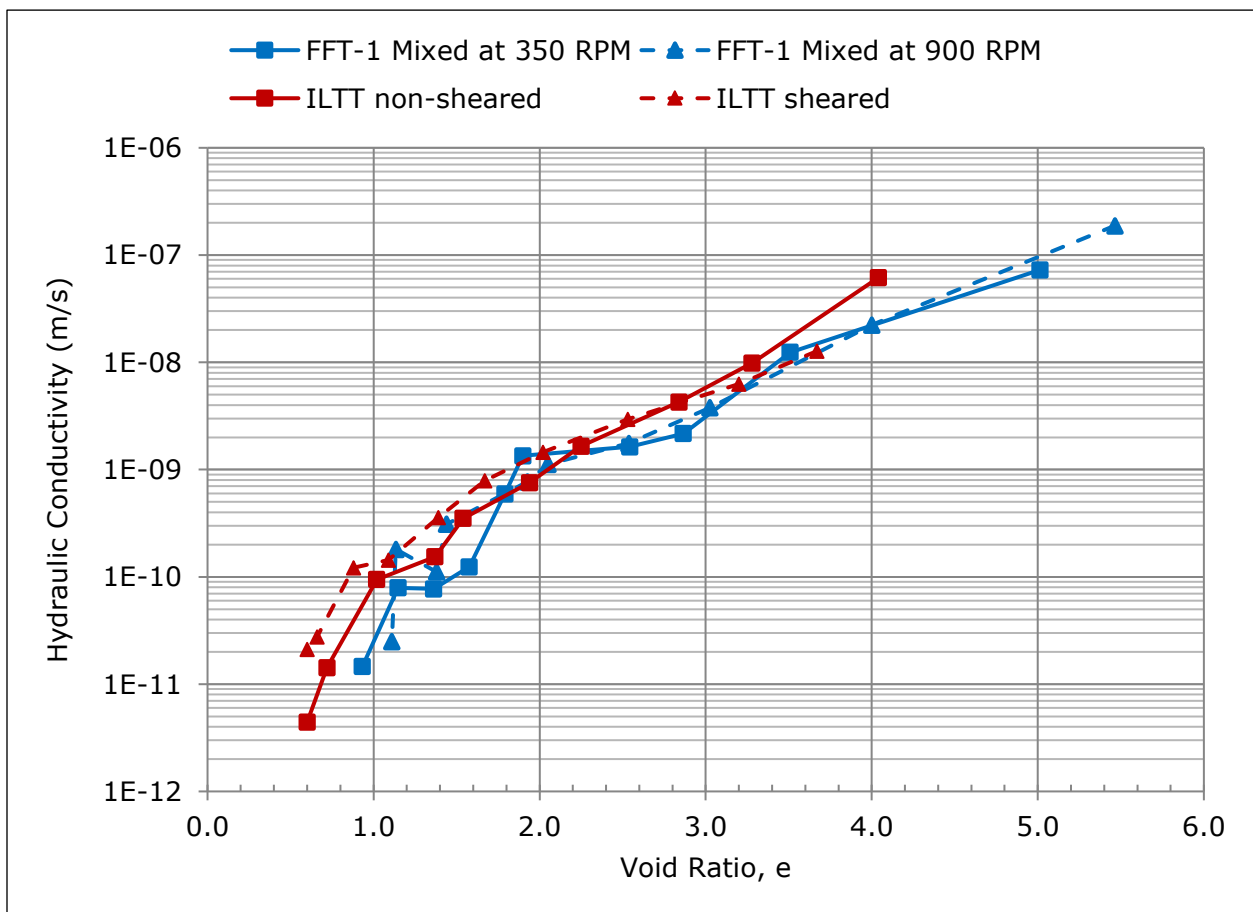


Figure 4-15 – Hydraulic conductivity of FFT-1 coagulated with K-Alum and flocculated using two different mixing speeds compared to ILTT (Jeeravipoolvarn 2010)

#### 4.4.4 Vane shear strength

Vane shear testing was carried out on tailings sample FFT-1 coagulated with K-alum and flocculated with A3338 mixed at either 350 RPM or 900 RPM. Vane shear strength data for these samples are presented in Figure 4-16. In addition, vane shear strength data for in-line thickened tailings (ILTT), both sheared and non-sheared, are presented in Figure 4-16 for comparison (Jeeravipoolvarn 2010). Differences in FFT-1 and ILTT vane shear strength at effective stress between 10 kPa and 100 kPa are evident.

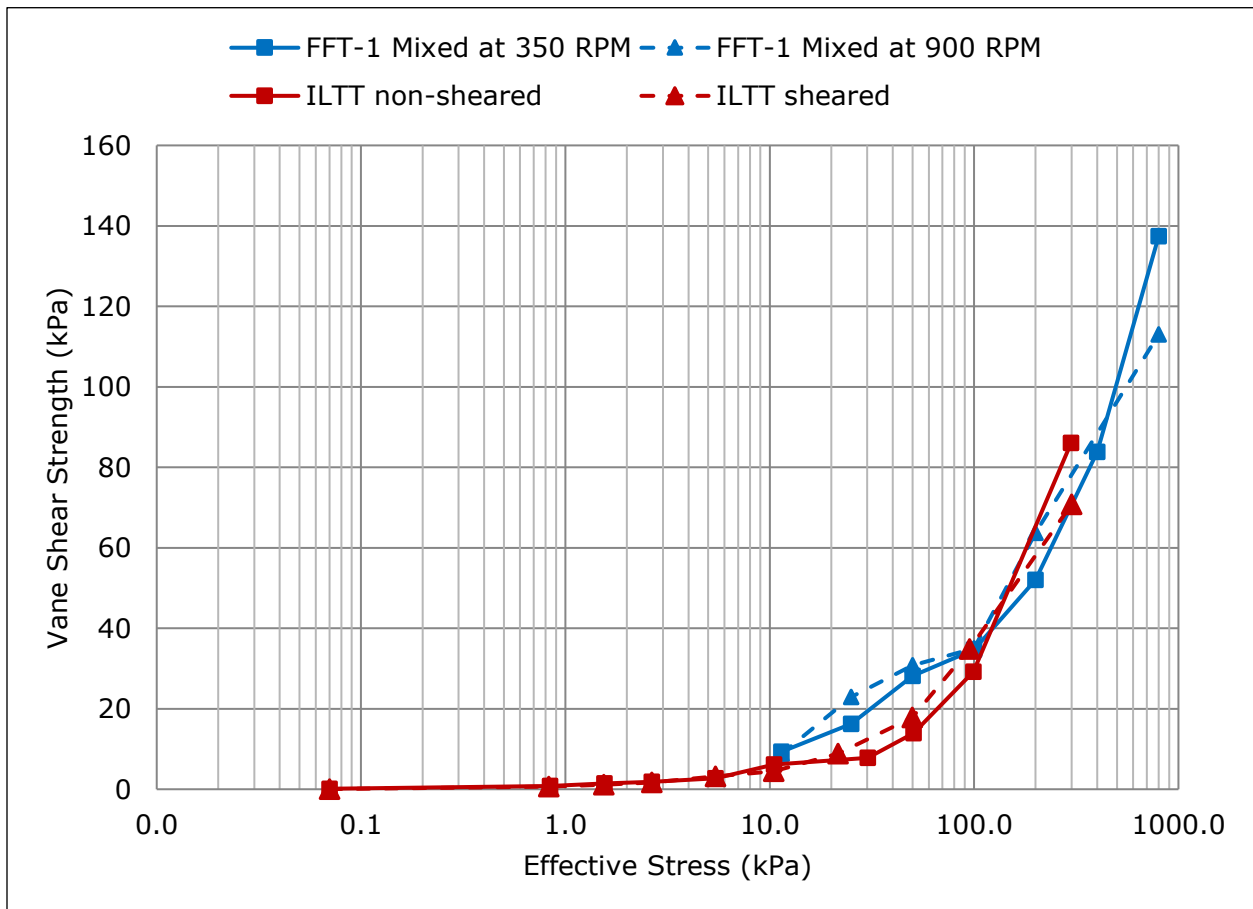


Figure 4-16 – Vane shear strength versus effective stress for FFT-1 coagulated with K-Alum and flocculated using two different mixing speeds compared to ILTT (Jeeravipoolvarn 2010)

Data obtained from large strain consolidation testing for this study are presented in Table 4-10 and Table 4-11.

Table 4-10 – Large strain consolidation test on FFT-1 coagulated with K-Alum and flocculated at mixing speed 350 RPM (un-sheared)

Effective Stress (kPa)	Void ratio, e	Water content, w	Hydraulic conductivity, k (m/s)	Hydraulic gradient, i	Vane shear strength (kPa)
0.9	7.1	321%	7.0E-09	0.12	-
1.0	6.6	301%	4.1E-09	0.13	-
1.2	5.7	257%	4.5E-09	0.11	-
1.7	5.0	228%	7.3E-08	0.23	-
2.8	3.5	160%	1.2E-08	0.31	-
6.0	2.9	130%	2.2E-09	0.36	-
11.4	2.5	116%	1.6E-09	0.82	9.3
25	1.9	86%	1.3E-09	0.96	16.2
50	1.8	81%	5.9E-10	1.00	28.2
100	1.6	72%	1.2E-10	1.33	34.7
200	1.4	62%	7.7E-11	4.59	52.0
400	1.1	52%	7.9E-11	5.05	83.8
800	0.9	42%	1.5E-11	28.11	137.4

Table 4-11 - Large strain consolidation test on FFT-1 coagulated with K-Alum and flocculated at mixing speed 900 RPM (sheared)

Effective Stress (kPa)	Void ratio, e	Water content, w	Hydraulic conductivity, k (m/s)	Hydraulic gradient, i	Vane shear strength (kPa)
0.9	8.1	370%	8.9E-09	0.13	-
1.1	7.4	337%	2.0E-08	0.12	-
1.3	6.8	309%	1.5E-08	0.09	-
1.8	5.5	248%	1.9E-07	0.25	-
2.8	4.0	182%	2.2E-08	0.34	-
6.1	3.0	138%	3.8E-09	0.42	-
11.4	2.5	115%	1.8E-09	0.48	8.8
25	2.0	93%	1.1E-09	0.96	22.9
50	1.9	88%	7.7E-10	0.96	30.8
100	1.4	65%	3.1E-10	1.05	35.0
200	1.4	63%	1.1E-10	2.00	63.7
400	1.13	52%	1.8E-10	2.29	-
800	1.11	50%	2.5E-11	27.86	113.0

Data for ILTT (Jeeravipoolvarn 2010), sheared and non-sheared, from large strain consolidation testing is presented in Table 4-12 and Table 4-13 respectively.

Table 4-12 – Large strain consolidation test results from ILTT non-sheared from Jeeravipoolvarn (2010)

Effective Stress (kPa)	Void ratio, e	Water content, w	Hydraulic conductivity, k (m/s)	Hydraulic gradient, i	Vane shear strength (kPa)
0.84	4.04	162%	6.2E-08	0.41	0.8
1.55	3.28	131%	9.8E-09	0.50	1.4
2.65	2.84	114%	4.3E-09	0.64	1.9
5.43	2.25	90%	1.7E-09	1.60	2.7
10.48	1.94	78%	7.6E-10	1.86	6.1
30.23	1.54	62%	3.5E-10	5.18	7.8
50.6	1.37	55%	1.5E-10	8.82	13.9
99.28	1.02	41%	9.5E-11	10.40	29.2
298.39	0.72	29%	1.4E-11	20.87	86.1
498.82	0.6	24%	4.4E-12	23.30	-

Table 4-13 – Large strain consolidation test results from ILTT sheared from Jeeravipoolvarn (2010)

Effective Stress (kPa)	Void ratio, e	Water content, w	Hydraulic conductivity, k (m/s)	Hydraulic gradient, i	Vane shear strength (kPa)
0.83	3.67	147%	1.3E-08	1.52	0.66
1.54	3.2	128%	6.3E-09	2.40	1.13
2.65	2.53	101%	2.9E-09	2.83	1.66
5.43	2.02	81%	1.5E-09	3.28	3.18
10.47	1.67	67%	7.9E-10	4.24	4.43
21.61	1.39	56%	3.6E-10	5.34	8.85
49.74	1.09	44%	1.4E-10	9.98	17.84
94.9	0.88	35%	1.2E-10	13.72	34.86
299.64	0.66	26%	2.8E-11	15.68	70.77
498.82	0.6	24%	2.1E-11	24.09	-

Geotechnical properties were measured for FFT-1 treated with K-alum and A3338. Two different mixing speeds were used to generate these samples. Atterberg limits, compressibility, hydraulic conductivity, and vane shear strength was assessed for both samples. Results from geotechnical testing was compared to a previous study on ILTT (Jeeravipoolvarn 2010). These results and comparisons will be discussed in the next chapter.

## 5 DISCUSSION

Dewatering of FFT can be done by a variety of methods, many of which include the addition of inorganic coagulants and polymer flocculants to promote solid-liquid separation through flocculation. Flocs are porous aggregates formed from smaller particles and are generated by the addition of these coagulants and flocculants. Neelakantan et al. (2018) studied the effect of different polymers and pH values on yield stress and floc size of kaolinite. Several studies on oil sands tailings flocs and effects of shear have been done previously (Jeeravipoolvarn 2010, Bajwa and Simms 2013, Jeeravipoolvarn et al. 2014, Derakhshandeh et al. 2016). Neelakantan et al. (2018) showed that floc size, presented as chord length, is largely affected by shear. Their study showed a shift from a unimodal distribution with larger flocs to a bimodal distribution of both smaller and large flocs. The current body of work found a similar shift from larger flocs to smaller flocs after being sheared but a shift to a bimodal floc size distribution was not observed. Neelakantan et al. (2018) found that yield stress of flocculated kaolinite suspension decreased upon shearing. This reduction in slurry yield stress due to shear was not measured in the current study which looked only at the shear strength of the dewatered deposit. Work by Jeeravipoolvarn (2010) with ILTT, both sheared and non-sheared, involved assessment of floc size by wet sieve and hydrometer. Since this floc measurement method is different than the protocol used for the current body of work it must be considered as a source of error when comparing the floc size distributions of both studies. Although different methods were used for floc measurement, the differences in floc size distribution between treated FFT-1 and ILTT are large enough to show that much larger flocs were produced for this study than for the ILTT study. Compressibility of ILTT was assessed for both sheared and non-sheared samples and little difference in compressibility was found between samples. For FFT-1 samples treated with K-alum and polymer it was found that the compressibility was slightly affected at higher void ratios. Jeeravipoolvarn (2010) found that shearing ILTT had no effect on the hydraulic conductivity which is what was found in this study with FFT-1. Jeeravipoolvarn (2010) measured vane shear strength throughout large strain consolidation testing like the current study and it was found that at higher void ratios the sheared ILTT had lower shear strength compared to non-sheared ILTT. The current study found that vane shear strength was not greatly impacted by the different mixing conditions although the vane shear strength was greater than that reported by Jeeravipoolvarn (2010) between 10 kPa and 100 kPa effective stress. The differences in vane shear strength may be attributed to the differences in floc sizes but may also be due to differences in tailings properties, chemical amendments, and mixing conditions. Bajwa and Simms (2013) used wet sieve and hydrometer for apparent particle size determination and found that the

distribution is affected by polymer dosage. Although changes in apparent particle size distribution were observed with increases in polymer dosage, there were minimal differences in undrained shear strength. The results presented by Bajwa and Simms (2013) cannot be directly compared to the current body of work because floc size changes were induced by varying polymer dosage and not by shear. It is important to note though that polymer dosage affects floc size distribution. Derakhshandeh et al. (2016) looked at the effects of pipelining shear on flocculated MFT and it was found that there was a reduction in yield stress due to shear. This yield stress is measured on the flocculated tailings and not of the dewatered deposit so a comparison with vane shear results is not possible.

Although there are many ways to measure flocs, as described in Chapter 2, the selected technique was photography with image analysis. This technique minimizes disturbance of flocs and allows measurement of macroscopic flocs which were expected in this project. Although this was the most suitable measurement technique for this project there are several instances for errors both in the images and the analyses. For the images, there are instances where two or more flocs overlap and end up appearing as one large floc. To minimize overlapping of flocs it was helpful to have a dilute flocculated system. Additionally, a thin tank was used (5 cm) to have flocs in the plane of view although flocs still had the opportunity to overlap. During image analysis, if overlapping flocs were observed they were manually removed from the analysis although overlapping was not always apparent. The main cause for error with overlapping flocs is that some flocs are not accounted for. Aside from the removal of overlapping flocs from images, attempts were made to take as many images as possible to have many flocs to measure. For the image capture and analysis technique it was critical to be able to obtain high quality images exhibiting good contrast between flocs and water. This made image analysis simpler since the software could easily discern flocs from water. High quality images could be obtained with a high-resolution camera and use of a treatment recipe exhibiting low turbidity release water. Low turbidity release water is required for recycling of process water and allows high contrast between flocs and water. In addition to error associated with images of flocs there is an error associated with the image analysis portion. To get a sense of the image analysis error, images of test beads having known sizes of either 3 mm or 4.5 mm were used for image analysis. Since all beads were of known size it was possible to use the software to measure the sizes and determine how different the measured values were from the actual values. The difference between actual and measured values was used to determine the error associated with image analysis. This error in test bead measurement was used for the error in floc measurement and the maximum error associated with test beads is used for error bars in Figure 4-9. The error bars shown in Figure 4-9 appear larger for smaller floc measurements but this is deceiving since the x-axis has a

logarithmic scale. So even though the error bars appear different sizes, they are all represented by the same value. It is important to note that since the calibration using test beads used only 3 mm and 4.5 mm sizes there is uncertainty in the error for flocs that measure outside this range.

With the floc measurement protocol in place it was necessary to develop an appropriate tailings treatment recipe. The recipe needed to exhibit clear solid-liquid separation with low turbidity release water for high contrast images. To develop the recipe, three different coagulants (K-alum, gypsum, and magnesium chloride) and a single flocculant (A3338) were selected. Coagulants were tested over a range of dosages on two different FFT samples. The coagulant assessment included testing each coagulated FFT using capillary suction time (CST). CST represents the rates of water removal from slurry so low values are conducive of good dewaterability. CST testing proved useful to assess coagulation because low CST values was indicative of increased coagulation. For coagulation screening, a plot of CST versus coagulant dosage was generated for each FFT/coagulant combination. For each of these plots a clear inflection point was evident which was selected as the optimum coagulant dosage. Once the trend of the data was apparent with the FFT/Al<sup>3+</sup> testing it was not necessary to test as many dosages for subsequent coagulants. Only enough dosages needed to be tested to recognize the inflection point on the CST versus dosage plot. Note that the optimum dosage does not represent the point at which the lowest CST time is observed but a point where further increases in dosage do not yield substantial benefits in terms of CST reduction. Following coagulation screening, only K-alum and gypsum were selected as coagulants. Magnesium chloride did not offer any benefit to coagulation and it is not currently used in industry while both alum and gypsum are. If magnesium chloride had performed better then it may have justified being included in flocculation testing. Additionally, only FFT-1 was selected for flocculation study because it required lower dosages of coagulant and had material properties more similar to the cyclone overflow used by Jeeravipoolvarn (2010) which was used for comparison later on. Optimum coagulant dosages for FFT-1 are 350 g/tonne and 450 g/tonne for Al<sup>3+</sup> (K-alum) and Ca<sup>2+</sup> (gypsum) respectively. These coagulant dosages are rather high since they are greater than those suggested for use in CT (Matthews et al. 2002) which suggests dosages of 68 g/tonne for Al<sup>3+</sup> and 140 g/tonne for Ca<sup>2+</sup>. Polymer dosages were assessed by incrementally adding small amounts of polymer and gently mixing until good flocculation was observed. Once an apparent optimal dosage was obtained, the flocculation test was repeated with polymer being added in a single step then mixed gently to confirm the optimum dosage. The required flocculant dosage for FFT-1 coagulated with K-alum was 1250 g/tonne of solids. The required flocculant dosage for FFT-1 coagulated with gypsum was 900 g/tonne of solids. These two dosages were the optimum since they were the minimum amounts of polymer flocculant needed to obtain visible floc

formation with low turbidity release water. These polymer dosages are within the expected range for this type of polymer and tailings.

With the treatment recipes determined, a treatment system was necessary to allow for images of flocs to be obtained. This was done by assembly of an in-line treatment system with flocs ultimately being deposited into a glass tank full of water. As flocs settled through the water, images of flocs could be obtained for subsequent size determination. The treatment system was designed so that as flocs were deposited to the glass tank, a second stream was diverted to a sample container. The importance of this was to have a sample with the same floc size distribution as that deposited to the glass tank.

With the treatment system developed, the image analysis technique needed to be established. The deposition system described above was used, and images were captured of flocs as they settled through water. Images were captured throughout the flocculation process until the sample container was filled. Pictures were taken manually every 30 to 60 seconds so between 10 and 20 images were obtained and used for each floc size distribution determination. All images captured, during the generation of the four samples, were analyzed in a similar fashion then compiled to get a representative floc-size distribution for each treatment condition. FFT-1 coagulated with gypsum showed a large difference in floc size distribution with increased shear while FFT-1 coagulated with K-alum had larger flocs. Since the K-alum samples had larger floc sizes it was selected for consolidation testing. Ideally all samples would have been subjected to consolidation testing but due to limited equipment availability only the two FFT-1 samples coagulated with K-alum were tested. Although the gypsum treated samples were not tested for consolidation, they were still tested to see how their undrained shear strength responded to changes in moisture content. Both K-alum and gypsum treated samples responded similarly to changes in moisture content. The liquid limit of K-alum and gypsum treated FFT-1 samples were 69% and 73% respectively. These liquid limits are similar to those found with other polymer treated FFT (Yao et al. 2012) which ranged from 65% to 69% depending on polymer dosage.

Large strain consolidation testing was carried out on tailings sample FFT-1 coagulated with K-alum and flocculated with A3338 mixed at either 350 RPM or 900 RPM. These mixing speeds were used because below 350 RPM mixing was insufficient to flocculate the FFT and for mixing speeds greater than 900 RPM too much shear was introduced to the sample and floc measurements could not be made. These mixing speeds are not necessarily representative of field mixing conditions but represent the limits of the laboratory setup.

It appears that shearing of flocculated tailings samples doesn't have a large impact on total settlement since each sample (FFT-1 and ILTT) consolidates to the same void ratio regardless of shear. For the hydraulic conductivity, at low void ratio there is almost an order of magnitude difference between samples flocculated at 350 RPM and 900 RPM for FFT-1 suggesting that the sample mixed at 900 RPM may consolidate slightly faster at this void ratio. Comparing hydraulic conductivity of FFT-1 to ILTT, ILTT has slightly higher hydraulic conductivity than FFT-1. These differences however are minimal since the error in measurements can produce scatter of one order of magnitude like seen in Figure 2-1. Vane shear strength for FFT-1 with K-alum compared to ILTT shows similar values with the exception of the strength at effective stresses 10 kPa to 100 kPa. Between these points the FFT-1 samples both exhibit higher vane shear strength than both the non-sheared and sheared ILTT samples. Shear strength at effective stresses between 10 kPa and 100 kPa may be important because these ranges of effective stress can be expected during dry landscape reclamation. Even though floc size may have an effect on the shear strength, the differences in shear strength may be attributed to samples differences such as mineralogy and chemical treatments. Also, since the coagulant dosage is extremely high, it may be the source of added shear strength.

## 6 CONCLUSIONS

Given the work that has already been done, the goal of this research was to determine if increasing the average floc size of chemically amended FFT would positively affect the geotechnical properties of the resulting soil-like material. To achieve this research goal the following objectives were pursued:

1. Develop method to characterize floc size distribution;
2. Develop treatment process to create flocculated tailings suitable for floc measurement;
3. Evaluate impact of treatment process on floc size;
4. Evaluate floc size impact on geotechnical behavior including compressibility, hydraulic conductivity, and vane shear strength.

The floc size measurement protocol developed in this study was effective at determining floc sizes and in producing bulk samples for further testing. Limitations to the flocculation setup were that a low solids content and high coagulant dosage were required to allow for the necessary contrast for image analysis. This protocol is better for the creation and analysis of larger floc sizes; study of smaller flocs (less than about 0.3 mm) was problematic because of limitations of the imaging system.

The treatment process consisted of both the method for determining coagulant dosages and for pumping treated tailings to the glass tank for acquisition of images of flocs. Pre-treatment with coagulant followed by in-line mixing of polymer followed by dynamic mixing served well to adjust mixing conditions. Coagulant screening using CST worked well as a method to select a suitable dosage to minimize turbidity and avoid unnecessary overdosing of coagulant. The high coagulant dosages used were suitable for this study but are not necessarily optimal or economical for field application, especially since they are higher than those recommended for CT (Matthews et al. 2002). From the floc size data it was apparent that both coagulant type and mixing conditions affected the floc size distribution.

Large strain consolidation testing with hydraulic conductivity and vane shear testing was carried out on tailings sample FFT-1 coagulated with K-alum and flocculated with A3338 mixed at either 350 RPM or 900 RPM. From the consolidation data it appears that shearing of flocculated tailings samples does not have a large impact on total settlement since each sample (FFT-1 and ILTT) consolidates to the same void ratio regardless of shear. Hydraulic conductivity, at low void ratio there is almost an order of magnitude difference between samples flocculated at 350 RPM and 900 RPM for FFT-1 but this difference is within the range of error for this measurement. This could however suggest that the sample mixed at 900 RPM may consolidate slightly faster at lower void ratios. Comparing hydraulic conductivity of FFT-1 to ILTT,

ILTT has slightly higher hydraulic conductivity than FFT-1. Vane shear strength for FFT-1 with K-alum compared to ILTT shows similar values with the exception of the strength at effective stresses 10 kPa to 100 kPa. Between these points the FFT-1 samples both exhibit higher vane shear strength than both the non-sheared and sheared ILTT samples. Shear strength at effective stresses between 10 kPa and 100 kPa may be important because these ranges of stress can be expected during dry landscape reclamation. Additionally, the shear strength values expected for this range of stresses is what is required to make soil trafficable. Within the range of parameters used in this study, it can be concluded that increased floc sizes, such as may be generated with low mixing speeds, may have a significant impact on the evolution of the topography of the reclaimed areas since treated FFT may be trafficable at lower moisture contents.

#### 6.1 Recommendations for future work

The objectives of this research were to develop a floc measurement system and procedure and to evaluate the impact of tailings treatment and floc size on geotechnical properties. These objectives were completed although several new questions arose. These questions may be topics for further study and include:

1. Use the setup for floc size measurement to obtain video and get settling rates of individual flocs to obtain floc density. This would still require floc size determination but would then be combined with Stokes Law.
2. Assess the use of in-line systems for measuring floc/particle size directly so more measurements can be made, in order to expand the scope of the study.
3. Assess the use of release water for oil sands extraction to observe effect on extraction efficiency.
4. Compare floc measurements made with image analysis directly with those made by hydrometer and wet sieve.

## 7 REFERENCES

- Addai-Mensah, J. and Prestidge, C. 2005. Structure formation in dispersed systems. *In Coagulation and Flocculation 2nd Ed. Edited by H. Stechemesser and B. Dobias.* Taylor & Francis, Boca Raton, FL, pp. 135-216.
- ASTM International. 2017a. D4318 standard test methods for liquid limit, plastic limit, and plasticity index of soils.
- ASTM International. 2017b. D1140 standard test methods for determining the amount of material finer than 75- $\mu\text{m}$  (no. 200) sieve in soils by washing.
- ASTM International. 2016. D4648-16 standard test method for laboratory miniature vane shear test for saturated fine-grained clayey soil. ASTM International.
- Bajwa, T. and Simms, P. 2013. Influence of dewatering and desiccation on microstructure and vane strength of polymer amended oil sand fine tailings. *In GeoMontreal 2013* , pp. 8.
- Beier, N., Wilson, W., Dunmola, A., and Segó, D. 2013. Impact of flocculation-based dewatering on the shear strength of oil sands fine tailings, *Canadian Geotechnical Journal*, **50**(9): 1001-1007.
- BGC Engineering Inc. 2010. Oil sands tailings technology review. Oil Sands Research and Information Network, University of Alberta, School of Energy and the Environment, Edmonton, Alberta.
- Biggs, C.A. and Lant, P.A. 2000. Activated sludge flocculation: On-line determination of floc size and the effect of shear, *Water research*, **34**: 2542-2550.
- Camp, T.R. and Stein, P.C. 1943. Velocity gradients and internal work in fluid motion, *Journal of the Boston Society of Civil Engineers*, **30**: 219-237.
- Consortium of Tailings Management Consultants, (CTMC). 2012. Oil sands tailings technology deployment roadmaps: Project report. Report prepared for AI-EES and the Oil Sands Tailings Consortium (OSTC).

COSIA. 2016. Unified fines method for minus 44 micron material and for particle size distribution. COSIA, Canada's Oil Sands Innovation Alliance, Calgary, Alberta.

Currie, R., Bansal, S., Khan, I., and Mian, H. 2014. An investigation of the methylene blue titration method for clay activity of oil sands samples. Edmonton, Alberta.

Derakhshandeh, B., Junaid, A., and Freeman, G. 2016. Effects of shearing and shearing time on dewatering and yield characteristics of oil sands flocculated tailings. *In International Oil Sands Tailings Conference*, pp. 6.

Essington, M.E. 2004. Soil and water chemistry. CRC Press, Boca Raton [u.a.].

Fine Tailings Fundamentals Consortium, (FTFC). 1995. Advances in oil sands tailings research. Edmonton, Alta. : Alberta Dept. of Energy, 1995, .

Fitria, D., Scholz, M., Swift, G.M., and Hutchinson, S.M. 2014. Impact of sludge floc size and water composition on dewaterability, *Chemical Engineering & Technology*, **37**(3): 471-477.

Francois, R.J. 1987. Strength of aluminium hydroxide flocs, *Water research*, **21**(9): 1023.

Hansbo, S. 1957. A new approach to the determination of the shear strength of clay by the fall-cone test. Stockholm.

Hogg, R. 2005. Flocculation and dewatering of fine-particle suspensions. *In Coagulation and Flocculation 2nd Ed. Edited by H. Stechemesser and B. Dobias*. Taylor & Francis, Boca Raton, FL, pp. 805-850.

Jarvis, P., Jefferson, B., Gregory, J., and Parsons, S.A. 2005a. Review: A review of floc strength and breakage, *Water research*, **39**: 3121-3137.

Jarvis, P., Jefferson, B., and Parsons, S. 2005b. Measuring floc structural characteristics, *Reviews in Environmental Science & Biotechnology*, **4**(1): 1-18.

Jeeravipoolvarn, S., Scott, J.D., Chalaturnyk, R., and Shaw, B. 2014. Effect of pipelining shear on consolidation properties of oil sands fine tailings. *In Tailings and Mine Waste '14*, pp. 495-506.

Jeeravipoolvarn, S. 2010. Geotechnical behavior of in-line thickened oil sands tailings. [electronic resource]. 2010.

Jeeravipoolvarn, S. 2005. Compression behaviour of thixotropic oil sands tailings. 2005.

Kaminsky, H.A.W., Etsell, T.H., Ivey, D.G., and Omotoso, O. 2009. Distribution of clay minerals in the process streams produced by the extraction of bitumen from athabasca oil sands, *The Canadian Journal of Chemical Engineering*, **87**(1): 85-93.

Karlsson, R. 1961. Suggested improvements in the liquid limit test, with reference to flow properties of remolded clays. *In Proceedings of the 5th International Conference on Soil Mechanics and Foundation Engineering*, Vol. 1, pp. 171-184.

Kasperski, K. 1992. A review of properties and treatment of oil sands tailings, *AOSTRA Journal of Research*, **8**(11).

Leung, W.W. 2016. Inferring in-situ floc size, predicting solids recovery, and scaling-up using the leung number in separating flocculated suspension in decanter centrifuges, *Separation and Purification Technology*, **171**: 69-79.

Liang, L., Peng, Y., Tan, J., and Xie, G. 2015. A review of the modern characterization techniques for flocs in mineral processing. .

Matthews, J.G., Shaw, W.H., MacKinnon, M.D., and Cuddy, R.G. 2002. Development of composite tailings technology at syncrude, *International Journal of Surface Mining, Reclamation and Environment*, **16**(1): 24-39.

McKenna, G., Mooder, B., Burton, B., and Jamieson, A. 2016. Shear strength and density of oil sands fine tailings for reclamation to a boreal forest landscape. *In Fifth International Oil Sands Tailings Conference*, pp. 130-153.

Miller, W.G. 2010. Comparison of geoenvironmental properties of caustic and noncaustic oil sand fine tailings. .

- Neelakantan, R., Vaezi G, F., and Sanders, R.S. 2018. Effect of shear on the yield stress and aggregate structure of flocculant-dosed, concentrated kaolinite suspensions, *Minerals Engineering*, **123**: 95-103.
- Omotoso, O. and Morin, M. 2008. AST methylene blue procedure: Dean-stark solids. *In Edited by Natural Resources Canada, CanmetENERGY-Devon, Extraction & Tailings*, , pp. 122-127.
- OSTC. 2012. Technical guide for fluid fine tailings management. Oil Sands Tailings Consortium (OSTC), Calgary, Alberta.
- Ray, D.T. and Hogg, R. 1987. Agglomerate breakage in polymer-flocculated suspensions, *Journal of colloid and interface science*, **116**: 256-268.
- Scholz, M. 2005. Review of recent trends in capillary suction time (CST) dewaterability testing research, *Industrial & Engineering Chemistry Research*, **44**(22): 8157-8163.
- Scott, J.D., Jeeravipoolvarn, S., and Chalaturnyk, R.J. 2008. Tests for wide range of compressibility and hydraulic conductivity of flocculated tailings. *In GeoEdmonton '08*, pp. 738-745.
- Sedgwick, A. and Fair, A. 2014. Furthering tailings R & D via the COSIA tailings EPA and the research working group. *In International Oil Sands Tailings Conference 2014*, pp. 257.
- Sobkowicz, J. 2012. The oil sands tailings technology roadmap and action plan: Introduction and key recommendations. *In International Oil Sands Tailings Conference 2012*, pp. 13-23.
- Sobkowicz, J. 2010. History and developments in the treatment of oil sands fine tailings. Boca Raton, CRC Press.
- Suthaker, N.N. 1995. Geotechnics of oil sand fine tailings. 1995.
- Wang, D., Wu, R., Jiang, Y., and Chow, C.W.K. 2011. Characterization of floc structure and strength: Role of changing shear rates under various coagulation mechanisms, *Colloids and surfaces*, (1-3).
- Watson, P., Fenderson, T., Mahmoudkhani, A., Nair, M., Patel, A., and Roberts, G. 2011. Breakage and reformation of flocs in oil sands tailings slurries. *In Tailings and Mine Waste 2011*.

Yao, Y., van Tol, A.F., and van Paassen, L. 2012. The effect of flocculant on the geotechnical properties of mature fine tailings: An experimental study. *In* International Oil Sands Tailings Conference.

8 APPENDIX

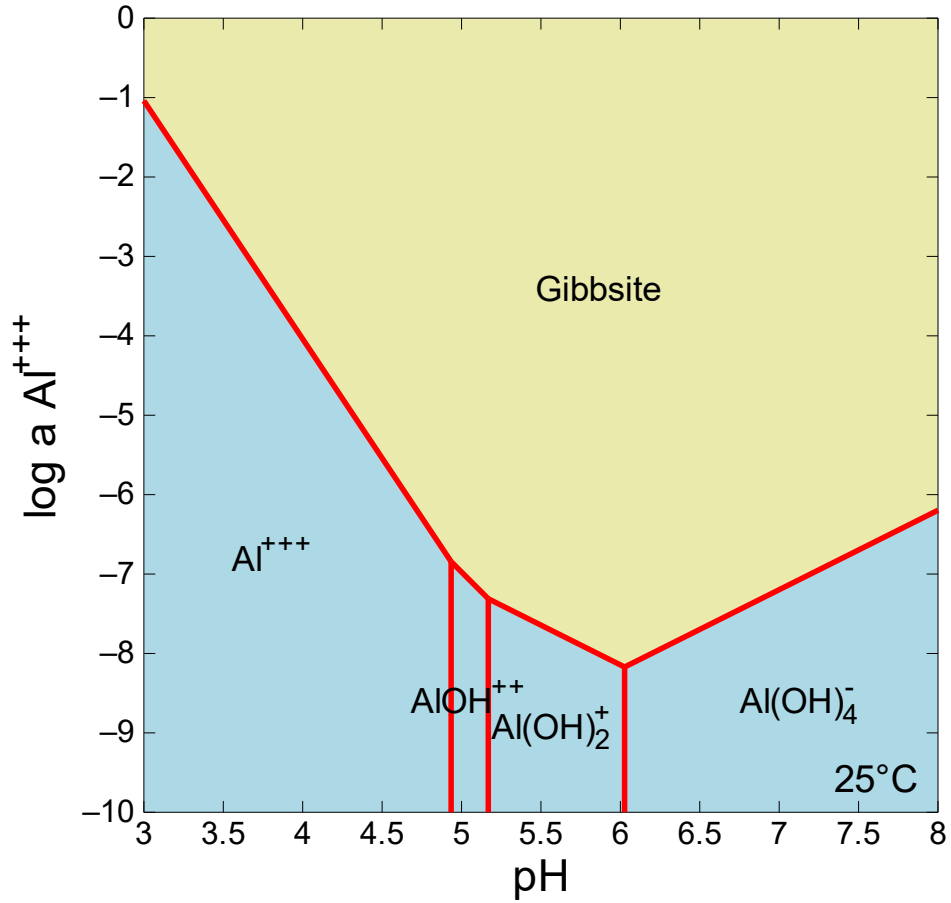


Figure 8-1 – Activity diagram showing aluminum species in aqueous and solid phases as a function of pH at 25°C

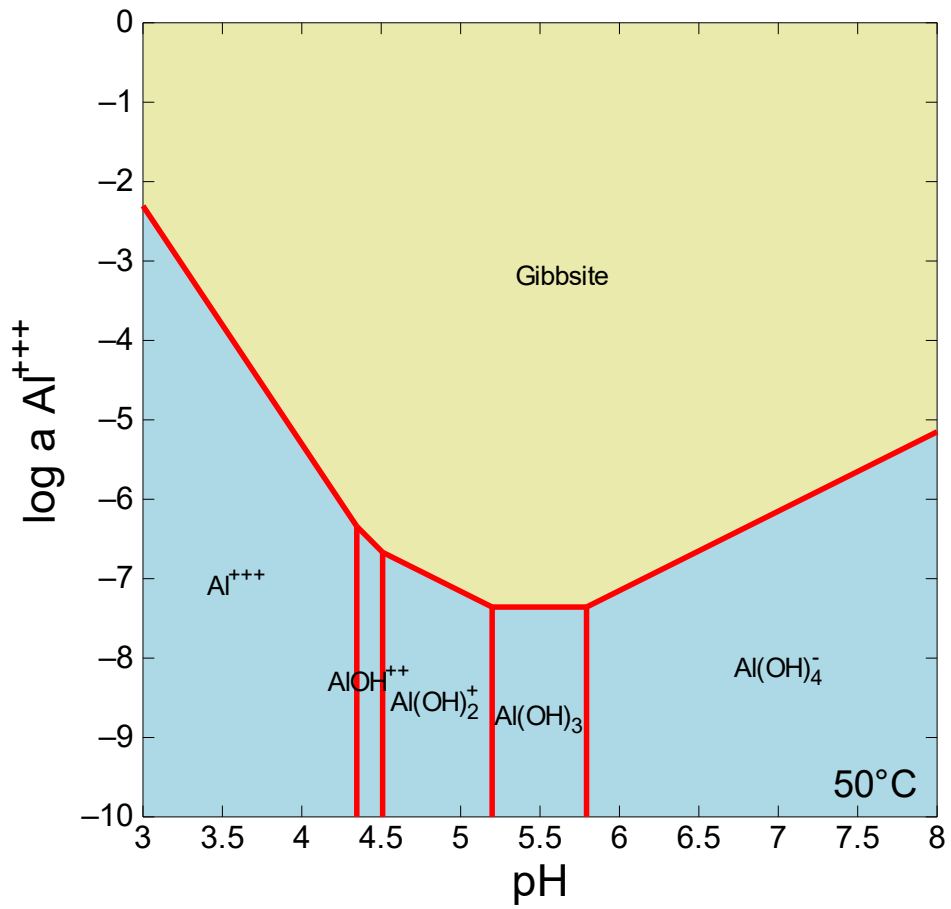


Diagram  $\text{Al}^{+++}$ , T = 50°C, P = 1.013 bars,  $a[\text{H}_2\text{O}] = 1$

Figure 8-2 - Activity diagram showing aluminum species in aqueous and solid phases as a function of pH at 50°C